Faculdade de Engenharia da Universidade do Porto
Instituto de Ciências Biomédicas Abel Salazar

Instituto de Investigação e Inovação em Saúde

Targeted Delivery of Spermine-Modified Acetalated Dextran Nanoparticles in a Spheroid-based Cancer Model

André João da Silva Silveira Gonçalves

Master's Degree in Bioengineering

Supervisor: Professor Bruno Sarmento, PhD

Acknowledgements

Em primeiro lugar, gostaria de agradecer ao meu supervisor, o Professor Bruno Sarmento, pela oportunidade de integrar a sua equipa e o presente projeto, bem como por toda a dedicação, disponibilidade e preocupação com que orientou este trabalho. Agradeço ainda a autonomia científica e o espírito crítico que me ensinou a desenvolver no decurso deste estágio, os quais considero vitais acima de tudo para o meu próprio crescimento pessoal.

Em segundo lugar, estendo também este agradecimento aos restantes membros do grupo Nanomedicines & Translational Drug Delivery, por me acolherem de modo imediato (ainda que a troco de bolo), e por toda a ajuda, ensinamentos e conselhos valiosos que me transmitiram ao longo do ano. Em particular, agradeço ao Tomás Ramos, meu mentor e amigo, pelo rigor em todas as dicas, críticas e instruções que me possibilitaram executar este trabalho, e mais ainda pela inexorável paciência que demonstrou diariamente, tanto em virtude dos meus erros como das minhas reclamações sobre a oitava temporada de Game of Thrones. Desejo-lhe, a longo prazo, um excelente e promissor futuro, e a curto, uma defesa de Doutoramento indolor.

Seguidamente, agradeço ainda o contributo do grupo do Professor Hélder Santos, da Universidade de Helsínquia pela cedência do polímero utilizado neste trabalho, e do grupo da Professora Maria José Oliveira, do i3S, pelo fornecimento dos monócitos utilizados nos ensaios celulares. Estendo ainda este agradecimento à Cláudia Machado, pela ajuda valiosa no processamento histológico das amostras biológicas, à Ana Rita Malheiro e ao Rui Fernandes, por toda a assistência durante os ensaios de microscopia eletrónica de transmissão, e a todas as equipas e investigadores do i3S que ao longo do semestre me cederam materiais e equipamentos ou me ajudaram em alturas de necessidade.

Noutro registo, quero também agradecer o apoio a todos os meus amigos e família, nomeadamente àqueles que sempre se lembraram de mim durante meio ano de absentismo, e especialmente aos meus pais e à minha irmã, pelo incondicional apoio que transmitido no dia-a-dia, mesmo perante as mais adversas das circunstâncias. Estou ciente de que nunca teria chegado aonde estou hoje sem o seu contributo, e devo sobretudo a eles todo o percurso académico e pessoal que construí até agora. Espero que estejam orgulhosos.

Contents

List of Figures

List of Tables

List of Abbreviations

AcDEX	Acetalated Dextran
ATCC	American Type Culture Collection
BAI-1	Brain angiogenesis inhibitor 1
CAF	Cancer-Associated Fibroblasts
CD44	Cluster of Differentiation 44
CIMP	Cpg Island Methylator Phenotype
CIN	Chromosomal Instability
CrC	Colorectal Cancer
CSC	Cancer Stem Cells
CTL	Cytotoxic T-lymphocytes
DC	Dendritic Cell
DCM	Dichloromethane
DLS	Dynamic Light Scattering
DR5	Death Receptor 5
DTS	Dispersion Technology Software
ECM	Extracellular Matrix
EDC	1-ethyl-3-(3-dimethylaminopropyl)carbodiimide hydrochloride
EGF	Epidermal Growth Factor
EGFR	Epidermal Growth Factor Receptor
EMT	Epithelial to Mesenchymal Transition
EPR	Enhanced Permeability and Retention
FACS	Fluorescence-Activated Cell Sorting
FBS	Foetal Bovine Serum
FGS	Fibroblast Growth Supplement
FITC	Fluorescein Isothiocyanate
GD-AIF	Glioma-derived Angiogenesis Inhibitory Factor
GM-CSF	Granulocyte-Macrophage Colony-Stimulating Factor
H&E	Hematoxylin and Eosin
HA	Hyaluronic Acid
HA:Sp-AcDEX	Hyaluronic Acid-functionalized Spermine-modified Acetalated Dextran
HEPES	4-(2-Hydroxyethyl)-1-piperazine ethanesulfonic acid
HI	Heat-Inactivated

HIF	Human Intestinal Fibroblasts
IFN	Interferon
IL	Interleukin
LPS	Lipopolysaccharide
M-CSF	Macrophage-Colony Stimulating Factor
MCTS	Multicellular Tumour Spheroids
MES	(Morpholino)Ethanesulfonic Acid
MHC	Major Histocompatibility Complex
MSI	Microsatellite Instability
MSNs	Mesoporous Silica Nanoparticles
N.D.	Not Determined
NHS	N-Hydroxysuccinimide
NK	Natural Killer
NP	Nanoparticle
Nut-3a	Nutlin-3a
PIG3	p53-inducible Gene 3
P/S	Penicillin/Streptomycin
PBS	Phosphate Buffer Saline
PdI	Polydispersity Index
PVA	Poly(Vinyl) Alcohol
RFU	Relative Fluorescence Units
RH	Relative Humidity
RPMI	Roswell Park Memorial Institute
SD	Standard Deviation
Sp-AcDEX	Spermine-Modified Acetalated Dextran
TAA	Tumour-Associated Antigens
TAM	Tumour Associated Macrophages
TEM	Transmission Electron Microscopy
TME	Tumour Microenvironment
TP53	Tumour Protein p53
TSP-1	Thrombospondin-1
VEGF	Vascular Endothelium Growth Factor
WHO	World Health Organization

Abstract

Colorectal cancer (CrC) is one of the most incident forms of cancer worldwide, commonly showing unfavourable prognostics despite the wide range of available anticancer therapies. With the current paradigm for cancer treatment gradually shifting to contemplate the synergistic combination of different approaches (namely in the form of chemoimmunotherapeutic strategies), our group previously developed an antitumour nanosystem based on spermine modified acetalated dextran nanoparticles (Sp-AcDEX NPs), capable of co-encapsulating the hydrophobic drug nutlin-3a (Nut-3a) and the hydrophilic immune mediator granulocyte-macrophage colony-stimulating factor (GM-CSF). In the current work, these particles were further functionalized with hyaluronic acid (HA), a natural biocompatible polymer with affinity for CD44 receptors in tumour cells and macrophages, resulting in a targeted nanosystem for specialized cancer drug delivery. The NPs were characterized through dynamic light scattering (DLS) and zeta potential measurements, revealing similar size and polydispersity index (PdI) but lower surface charge in respect to the original NPs. In parallel, a triple cell based co-culture spheroid model of CrC, entailing an epithelial cancer cell line, human intestinal fibroblasts and human monocytes, was utilized along flat monocultures of each of these cell types to comparatively assess the cytotoxicity and antiproliferative effect of the developed NPs. Results showed these NPs to be non-toxic in 2D cultures of cancer cells and macrophages at concentrations up to 200 μg/mL, despite exhibiting concentration-dependant toxicity towards fibroblasts during the first 24 h post-incubation. HA inclusion did not result in increased toxicity in respect to bare NPs. Contrarywise, the same NPs seemed to severely impair the survival of cells in triple-culture spheroids at all concentrations and regardless of their loading with Nut-3a, although these cells displayed a percentage of association towards bare NPs no higher than 10% after 24 h of incubation. Overall, the developed NPs showed to be a promising concept to promote targeted delivery in the context of CrC, but their therapeutic potential requires additional *in vitro* validation following further optimization of experimental procedures and refinement of spheroid-based assays.

I. Introduction

1.1. Colorectal Cancer

Cancer is a major public health problem worldwide, posing as the first or second leading cause of death before age 70 years in at least 91 countries according to 2015 estimates from the World Health Organization (WHO) (Figure 1). Its incidence and mortality rates are increasing on a global scale and reflect not only the aging and growth of the population resulting from declines in the number of deaths caused by stroke and heart disease in developed countries (Bray et al., 2018; Siegel, Miller, & Jemal, 2018), but also the so-called "epidemiologic transition" – a region-wide shift in predominance from infectious to degenerative diseases, frequently driven by healthcare and lifestyle improvements coupled to socioeconomic and political changes - that is taking place in third-world countries. With developing countries adopting a more *westernized* lifestyle (OMRAN, 2005), the global cancer burden rose to 18.1 million cases last year, resulting in 9.6 million deaths according to estimates from GLOBOCAN2018 (Ferlay et al., 2019). Of these, CrC places third in terms of incidence and second in terms of mortality, representing 9.4% of all incident cancer in men and 10.1% in women. It shows three-folded incidence rates across developed countries in respect to transitioning ones (Bray et al., 2018), in a direct correlation with the Human Development Index associated with these countries (Fidler, Soerjomataram, & Bray, 2016).

Several risk factors are linked with the incidence of CrC. While aspects like old age, genetic predisposition and personal/familiar history of diseases like adenomatous polyps or inflammatory bowel diseases have been connected to CrC occurrences on multiple occasions (Jackson-Thompson, Ahmed, German, Lai, & Friedman, 2006), environmental and lifestyle factors seem to play a larger role in the manifestation of the disease than in other types of cancer (Johnson & Lund, 2007); in fact, according to some observational evidence, incidence rates of CrC among individuals migrating from low-risk to high-risk countries tend to increasingly match those typical of the host country (Haenszel & Kurihara, 1968; Janout & Kollárová, 2001). More specifically, various studies have positively identified high intakes of fat (primarily of animal origin) (Willett, Stampfer, Colditz, Rosner, & Speizer, 1990), physical inactivity, cigarette smoking and heavy alcohol consumption, among other factors (Haggar & Boushey, 2009) as preventable causes associated with the development of colorectal cancer. Nevertheless, such correlations are not uniform, and manifest differently in terms of patient's gender

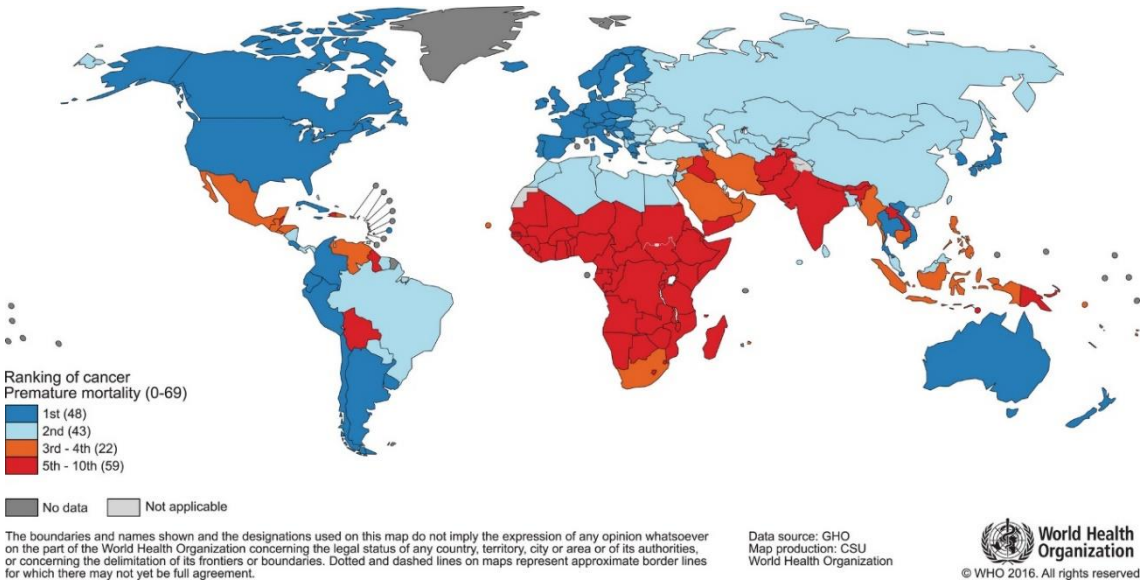

Figure 1 - Worldwide rankings of premature mortality attributed to cancer. Source: World Health Organization.

(Wei et al., 2005; Willett et al., 1990), geographic location (Haggar & Boushey, 2009) and affected intestinal section (Johnson & Lund, 2007).

1.1.1. A brief look into the tumour's microenvironment

According to Hanahan & Weinberg, tumours have increasingly been recognized as organs whose complexity approaches and may even exceed that of normal healthy tissues (Hanahan & Weinberg, 2011). As such, and opposingly to earlier portrayals of tumours as large masses of proliferating cells, cancer biology is nowadays contemplating the intricacies and interactions within the tumour microenvironment (TME), in order to properly assess and understand the cellular and molecular mechanisms underlying tumorigenesis (Figure 2). In the year 2000, Douglas Hanahan and Robert Weinberg (Hanahan & Weinberg, 2000) postulated the main features explaining cancer survival and proliferation (termed "the Hallmarks of Cancer"), in an article which framed the stage for cancer research in the ensuing decade, until its renewal in 2011 (Hanahan & Weinberg, 2011). In short, the main cellular mechanisms ensuring tumour progression include unlimited cancer cell replication, evasion from growth suppressors, promotion of invasion and metastasis, resistance to apoptosis, angiogenesis stimulation, preservation of proliferative signalling, evasion of immune destruction, genome instability and mutation, and tumour enhanced inflammation (Hanahan & Weinberg, 2011; Wang et al.,

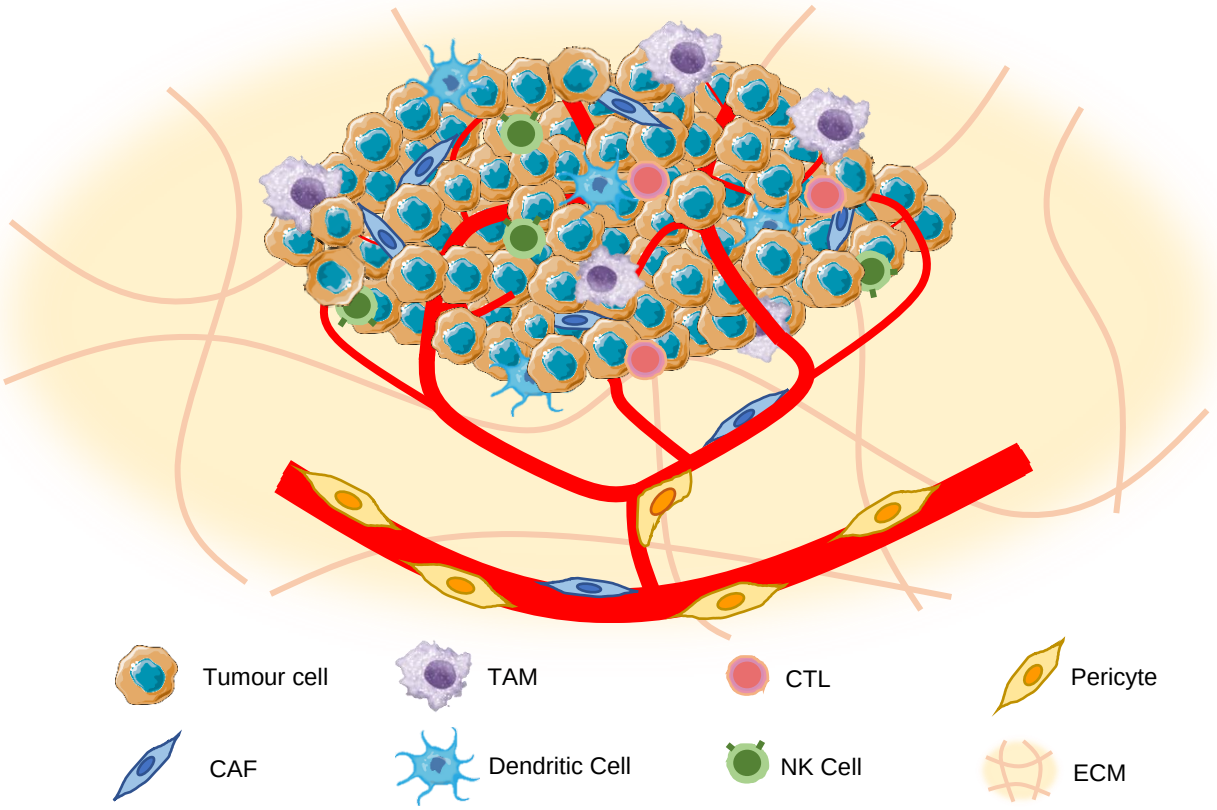

Figure 2 – Schematic representation of the TME.

2017). Such characteristics are attained in part due to the different sets of cell types that make up the TME (cancer cells, stromal cells, resident immune cells, etc.) as well as to the wide range of interactions and signalling pathways that determine their individual and collective functions (Hanahan & Weinberg, 2011).

Cancer Cells

The most evident constituent of the tumour microenvironment are the cancer cells themselves, as they make up the foundation of the disease. These cells generically harbour mutations in oncogenes (genes that promote cell growth under normal conditions) or tumour suppressor genes (genes that inhibit cellular replication or promote apoptosis) (Vogelstein, Lane, & Levine, 2000), causing a malignant overproliferation tied to an increased genetic instability (Reya, Morrison, Clarke, & Weissman, 2001). After some rounds of division, the accumulation of mutations eventually leads to the establishment of a genetically polyclonal population, with different levels of differentiation and tendency to form metastasis (Hanahan & Weinberg, 2011). Moreover, recent evidence points to the existence of a particular subtype of cancer cells, the cancer stem cells (CSC), which make up a small (and often resistant to therapy) self-renewing

population, prone to aberrant differentiation and with tumour and metastasis-initiating capabilities (Reya et al., 2001).

Cancer-Associated Fibroblasts (CAF)

The term “cancer-associated fibroblasts’’ may encompass cells like the fibroblasts that create the structural foundation supporting most normal epithelial tissues (Hanahan & Weinberg, 2011), but mostly refers to perpetually activated myofibroblasts; these are similar to the fibroblasts consistently found in wounds and sites of chronic inflammation, and are identifiable by their expression of α-smooth muscle actin (Franco, Shaw, Strand, & Hayward, 2010). These mutagenic CAFs are either derived from bone marrow precursors or epithelial cells undergoing epithelial to mesenchymal transition (EMT), and significantly contribute to cancer progression by remodelling the extracellular matrix (ECM), inducing angiogenesis, enhancing metastasis and directly stimulating cell proliferation via the secretion of growth factors, chemokines and immune suppressive cytokines (Östman & Augsten, 2009).

Immune Cells

The immune system can be both beneficial and detrimental for tumour proliferation (de Visser, Eichten, & Coussens, 2006). On the one hand, through combined action of the innate and adaptive systems, it can specifically identify and eliminate malignant cells after detecting abnormalities in their surface antigens or type I major histocompatibility complex (MHC) molecules. One of the main events during the initiation of an anticancer immune response is the specific detection of tumour-associated antigens (TAA) by cells of the innate immune system. A subset of these innate leucocytes, the dendritic cells (DC), constitute the most important type of antigen presenting cells in the organism, bridging the action of the innate and the adaptive immune systems by specializing on the cross-presentation of said TAA to cytotoxic T-lymphocytes (CTL) (Wculek et al., 2019). These lymphocytes, along with the innate Natural Killer (NK) cells, are the main effector agents directly responsible for the antagonization of tumour progression, and are in turn further stimulated and supported by the pro-inflammatory cytokines released by classically-activated M1 macrophages (such as interleukin-1 (IL-1), IL-6, IL-12 and tumour necrosis factor-α (TNF-α)), in what is described as a T_H1 type immune response (Coulie, Van den Eynde, van der Bruggen, & Boon, 2014; Lewis & Pollard, 2006; O'Sullivan et al., 2012; Sica et al., 2008). Conversely, the innate immune system is involved in wound healing processes that entail angiogenesis, ECM remodelling and release of growth factors, which often facilitate the survival and proliferation of cancer cells (de Visser et al., 2006). Importantly, a specific subset of macrophages that is present in the environment (termed Tumour Associated Macrophages, TAM) (Noy & Pollard, 2014) and continuously exposed to tumour-derived cytokines such as IL-4, IL-10, IL-13, transforming growth factor-β1 (TGF-

β1) and prostaglandin E_2 tend to develop into alternatively activated M2 macrophages (Elgert, Alleva, & Mullins, 1998; Mantovani, Sozzani, Locati, Allavena, & Sica, 2002; Petty & Yang, 2017). These phenotypical variants are responsible for the generation of a permissive immune environment that sustains tumour growth and dissemination, promoting angiogenesis and repairing wounded tissues, due to their poor antigen-presenting capability and general proficiency at suppressing T-cell proliferation (Goswami et al., 2017; Lewis & Pollard, 2006; Petty & Yang, 2017; Zhong, Chen, & Yang, 2018).

Overall, the interactions between immune cells and the remaining cells within the tumour are diverse, complex and not fully disclosed. Nevertheless, it is generally accepted that the immune system represents the strongest intrinsic force opposing tumour growth and dissemination (Schuster, Nechansky, & Kircheis, 2006). In 2004, Dunn *et al*. (Dunn, Old, & Schreiber, 2004) defined the three E's of Cancer Immunoediting - a concept that has been used to describe the process by which the interaction between tumour and immune cells and cells either Eliminates the tumour, holds it in a state of dormancy (Equilibrium), or allows its Escape and proliferation. Collectively, these three stages summarize the paradigm for cancer progression over time: in the elimination phase, taking place after the tumour sprouts, the immune system clears most of the malignant cells, leaving yet behind some of the least immunogenic ones including CSCs. This leads to an equilibrium between the two populations, that can be maintained for years or even decades, and in which tumours do not grow. Finally, by accumulating mutations and epigenetic changes, cancer cells eventually gain the ability to evade and subvert the immune system, leading to their escape, proliferation, and the generation of a tumour cell repertoire capable of expanding and eventually form metastasis in immune-competent individuals (Budhu, Wolchok, & Merghoub, 2014; Dunn et al., 2004).

Endothelial cells, pericytes and other cells

A number of different cell populations play key supportive roles in sustaining tumour growth and development. For instance, endothelial cells, which make up the inner walls of blood and lymph vessels, are essential to provide cancer cells with nutrients and oxygen necessary for tumour survival, and may even cause these cells to become metastatic through specific interactions (Maishi & Hida, 2017). Pericytes provide important support for blood vessel formation and function and are capable of tumour homing, enhancing angiogenesis at these sites and cooperating with malignant cells to induce a local regenerative phenotype, facilitating tumour growth and metastasis (Matos

et al., 2019). Other types of cells with relevant functions at the TME include adipocytes and neuroendocrine cells (Wang et al., 2017).

ECM

The ECM is a non-cellular component of tissue whose main components include collagen, proteoglycans, laminin and fibronectin, in varying percentages and subtypes according to the tissue's structure and function (Walker, Mojares, & Del Río Hernández, 2018). While ECM remodelling is usually tightly controlled to ensure organ homeostasis and functions, its structure and composition become disorganized during cancer progression. Importantly, the ECM normally plays a key role in conducting a dense network of molecular and mechanical signals that affects the dynamics of nearby cells, conditioning their behaviour according to different stimuli (Crotti et al., 2017). Cancer-induced alterations in the properties of the ECM, such as increased substrate stiffness, can limit the access of the host's own defences to the tumour and trigger over-expression of transcription factors that induce tumour cell proliferation, checkpoint blockade and EMT. These hence exacerbate the tumorigenic environment, and facilitate the process of oncogenic transformation, tissue invasion and metastasis during cancer initiation and progression (Crotti et al., 2017; Lu, Weaver, & Werb, 2012).

1.1.2. Mutational mechanisms leading to CrC

Overall, CrC formation follows a transformation of normal colonic epithelium to an adenomatous intermediate and ultimately to adenocarcinoma, in the so-called "adenoma-carcinoma sequence" (as depicted in Figure 3) (Morson, 1974; Pino & Chung, 2010). Mechanistically, the genomic interactions leading up to tumour development are intricate and complex but can usually be categorized into one or a combination of three different sources: CpG island methylator phenotype (CIMP), microsatellite instability (MSI) and chromosomal instability (CIN). CIMP is an epigenetic instability pathway characterized by vast hypermethylation of promoter CpG island sites, resulting in the inactivation of several tumour suppressor genes or other tumour-related genes (Nazemalhosseini Mojarad, Kuppen, Aghdaei, & Zali, 2013). MSI consists in a particular form of genetic instability generated by a deficient DNA mismatch repair, resulting in accumulation of indels at simple repeated sequences known as microsatellites (Dolcetti

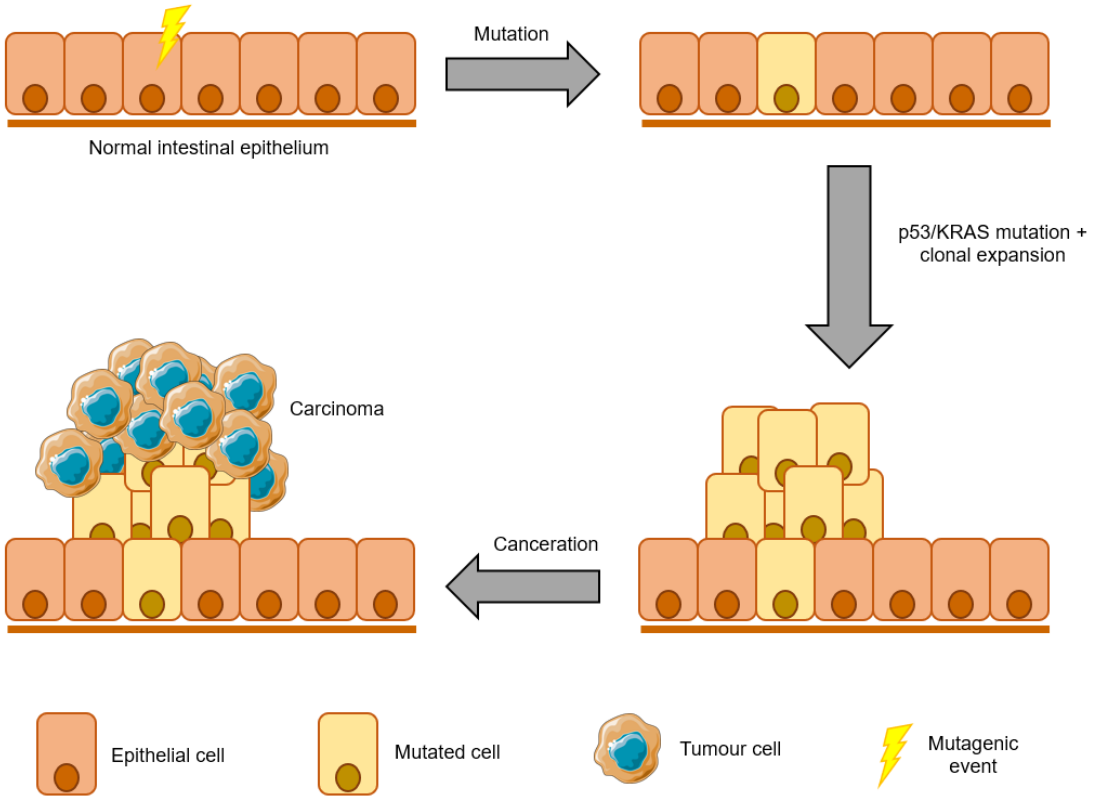

Figure 3 - Different stages in the progression and development of a colorectal carcinoma.

et al., 1999). However, while these are important mechanisms underlying tumorigenic mutagenesis, they will not be extensively discussed in this section.

CIN is associated with 65%-70% of sporadic CrCs and relates to an accelerated rate of gains/losses of large portions of chromosomes that results in intercellular karyotypic variability – culminating in the phenomena of aneuploidy (a disparity in the number of chromosomes) and frequent loss of heterozygosity. These abnormalities observed in CIN-derived tumours often bring about a characteristic set of mutations in specific tumour suppressor genes and oncogenes, the most important of which being Adenomatous Polyposis Coli, KRAS and TP53 (Tumour Protein p53) (Fearon, 2011). The Adenomatous Polyposis Coli gene product is a large protein with different functional domains that regulates differentiation, adhesion, polarity, migration, apoptosis and chromosomal segregation (Fearon, 2011). Mutagenesis in this gene increases the levels of β-catenin, which activates the Wnt signalling pathway to enhance the transcription of various oncogenes with T-cell factor transcription factors (Komiya & Habas, 2008; Mann et al., 1999; Tariq & Ghias, 2016). KRAS mutation is associated with a constitutive activation of the Ras-signalling pathway, which regulates different cellular functions through a number of known effector pathways; examples are the Raf-MEK-ERK pathway, which inhibits enzymes involved in cell cycle control and arrest, and the PI3K/AKT/PKB pathway, which enhances tumour growth by promoting EMT – even

though these pathways often converge and result in overlapping effects (Fearon, 2011; Porru, Pompili, Caruso, Biroccio, & Leonetti, 2018). TP53 is thought to be the most commonly mutated gene in human cancers (Kandoth et al., 2013), and its carcinogenesis is reviewed in the next section.

1.1.3. The role of p53

TP53 is located in the short arm of chromosome 17, consists of 11 exons and 10 introns and is responsive to several cellular stresses including DNA damage, or even the activation of certain oncogenes (H. Janouskova et al., 2013; Saha, Qiu, & Chang, 2013; Vogelstein et al., 2000). Once activated, its product, p53, plays a central role in the coordination of cell cycle arrest, DNA repair, apoptosis (via both the intrinsic and extrinsic pathways), senescence and autophagy (Arnold J. Levine, 1997). Some of the best-studied targets of p53 are (i) p21 and Rb (cell cycle inhibitors monitoring the G1 checkpoint) (el-Deiry et al., 1993); (ii) GADD45, 14-3-3α and Reprimo, which contribute to cell cycle arrest in G2 (Vogelstein et al., 2000); (iii) Bax, Fas, p53-inducible Gene 3 (PIG3) and Death Receptor 5 (DR5), which regulate caspase activation and apoptosis (Pino & Chung, 2010; Toshiyuki & Reed, 1995; Vogelstein & Kinzler, 2004); and (iv) thrombospondin-1 (TSP-1), brain angiogenesis inhibitor 1 (BAI-1) and glioma-derived angiogenesis inhibitory factor (GD-AIF), which prevent the formation of new blood vessels (Teodoro, Evans, & Green, 2007). p53 is degraded via ubiquitin-mediated proteolysis, a process where enzymes like E3-ubiquitin ligase, MDM4 and more importantly MDM2 bind to its transactivation domain, effectively flagging it for degradation in the proteasome by ubiquitination (X.-L. Li, Zhou, Chen, & Chng, 2015b; Senturk & Manfredi, 2012).

Development of CrC is a multifactorial process involving the activation of oncogenes and inactivation of tumour suppressor genes (A. J. Levine & Oren, 2009). p53 is a key tumour suppressor gene whose mutations are reported to occur in around 50% of sporadic CrC cases (X.-L. Li et al., 2015b; Lopez et al., 2012). The levels of p53 in normal cells are usually kept in check through a negative feedback loop that employs MDM2 and selective activity-regulating modifications to p53 (in the form of acetylation, glycosylation, etc.) - allowing cells to properly mature in normal circumstances (Vogelstein et al., 2000). This balance is broken when cells are put under stress, enabling a rise in p53 levels and prompting cells to undergo DNA repair or apoptosis following cell cycle inhibition (Figure 4). Point mutations in highly conserved regions of TP53 that lead

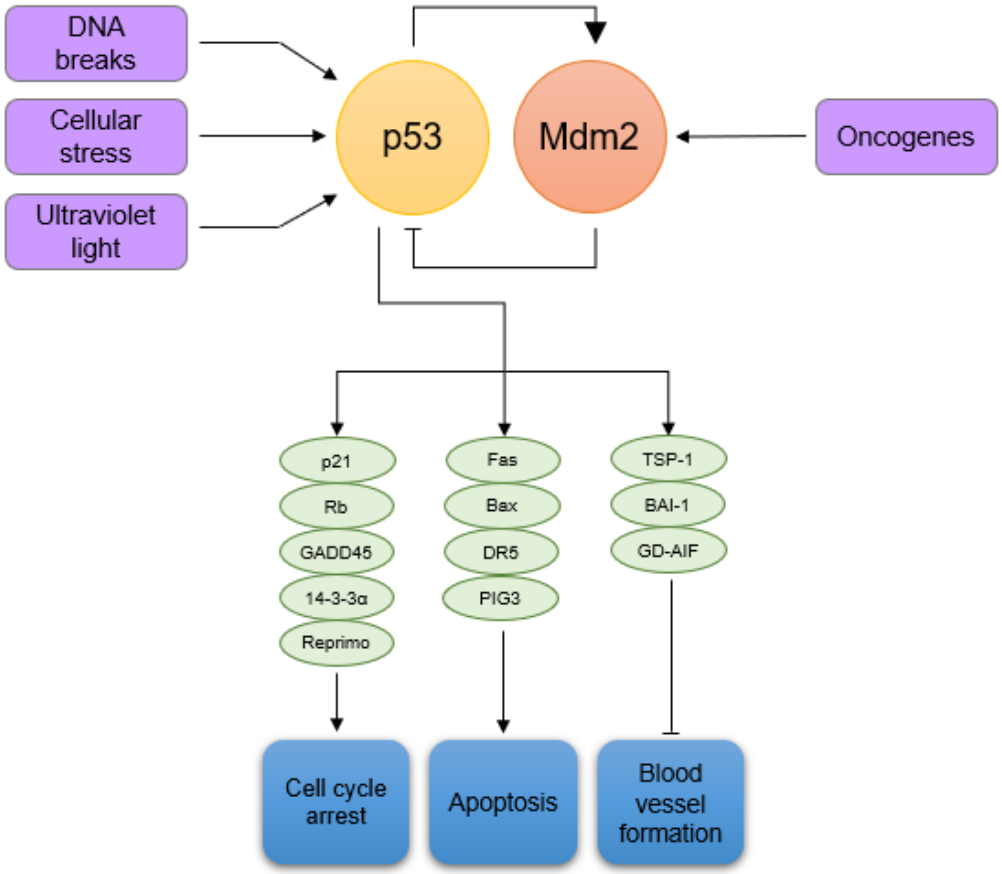

Figure 4 - Schematic summary of the stimuli leading to p53 stimulation and downstream mediators responsible for cell cycle arrest. Following its upregulation by the detection of cellular stress or DNA damage, activated p53 binds the regulatory region of a multitude of tumour related genes to coordinate their expression and activity; these genes command an intricate network of interactions that regulate cell cycle progression, angiogenesis and induction of programmed cell death. The regulatory feedback relation between p53 and its main inhibitor MDM2 is highlighted.

to loss of p53 function are thus a key event in carcinogenesis, enabling erroneous cell cycles to proceed unchecked and resulting in malignant cell growth and proliferation with increased tumour angiogenesis (Fearon, 2011; Arnold J. Levine, 1997; Vogelstein et al., 2000). Notwithstanding, other sets of alterations in important mediators of p53 activity, including for example the overexpression of MDM2 (which excessively binds and sequesters p53, inhibiting its tumour supressing activity), have also been reported as driving forces of tumorigenesis in cases where p53 mutations do not take place (Senturk & Manfredi, 2012).

1.1.4. CrC treatments and therapeutic targets

For many years, the backbone of therapeutic approaches for CrC has been based on chemotherapy, namely on fluoropyrimidines and more specifically fluorouracil - a fluorinated pyrimidine which is thought to act primarily by inhibiting thymidylate synthase (Edler et al., 2002; Meyerhardt & Mayer, 2005). This enzyme is the rate limiting mediator in pyrimidine nucleotide synthesis, and its inhibition greatly hampers the process of DNA synthesis (Edler et al., 2002; Salonga et al., 2000), which is vital for tumour proliferation. Recent chemotherapeutic approaches have thus coupled the use of fluorouracil to cytotoxic drugs (namely irinotecan and oxaliplatin), as well as conjugated these strategies with administration of antibody-mediated targeted therapies. The latter exist in the form of epidermal growth factor receptor antagonists like cetuximab (which targets the ligand-binding domain of the epidermal growth factor receptor, EGFR) (Baselga, 2002; Lenz, 2007) and angiogenesis inhibitors such as bevacizumab (that selectively binds to human vascular endothelium growth factor, VEGF, and is used in KRAS wild-type CrC patients) (Ferrara, Hillan, & Novotny, 2005; Kabbinavar et al., 2003; Koido et al., 2013; Sousa, Cruz, Pinto, & Sarmento, 2018). Combinational therapy using fluorouracil is currently considered the gold standard for CrC therapy (Passardi et al., 2015), although a considerable portion of patients eventually end up developing resistance to this agent (Bajetta et al., 1997).

More recently, pharmacologic reactivation of p53 has also become a chemotherapeutic target due to its pivotal role in tumour development and suppression (Ventura et al., 2007). As such, and in order to restore normal p53 function in cancer cells, pharmacological inhibitors of MDM2 have already been extensively researched for their anti-cancer activities through stabilization of p53 protein. One of these MDM2 antagonists is Nut-3a, a hydrophobic, non-genotoxic cis-imidazoline analogue, which occupies the binding pocket of this protein, disrupting the MDM2-p53 interaction. Since its discovery, Nutlin has been one of the most investigated small molecules in the field of cancer therapy (Saha et al., 2013), and while it is still undergoing early-stage clinical trials, it poses as a potential candidate for combinational chemotherapy against CrC, with simultaneous applications along other drugs (Hana Janouskova et al., 2013; X.-L. Li, Zhou, Chen, & Chng, 2015a).

On a different note, immunotherapy entails an emerging range of active therapeutic approaches which aim at eradicating cancer by mounting a tumour-driven immune response against malignant cells (Xiang, Snook, Magee, & Waldman, 2013). As

previously mentioned, it has been well established that tumour sites often sprout amidst extremely immunosuppressive microenvironments (Zhong et al., 2018), whose nature is partially perpetuated by the action of TAMs exhibiting an M2 phenotype and continuously secreting anti-inflammatory cytokines (Goswami et al., 2017; Petty & Yang, 2017; Zhong et al., 2018). Therefore, emerging strategies targeting this macrophage population strive to subvert their polarization status and promote a shift to an M1 pro-inflammatory state (Parayath, Parikh, & Amiji, 2018), which drives normal immune effector functions against malignant cells (Xiang Zheng et al., 2017) and has been positively correlated with patients' survival time (Parayath et al., 2018). M1 differentiation can be induced either by administration of cytokines, namely in the form of GM-CSF (Bauleth-Ramos et al., 2017; Matos et al., 2019), IL-12 (Q. Wang et al., 2016) or interferon-gamma (IFN-γ) (Duluc et al., 2009) (possibly in combination with TNF-α, or bacterial lipopolysaccharide, LPS) (Biswas & Mantovani, 2010), or macrophagic microRNAs that contribute to and are associated with the M1 phenotype, as is the case of miR-155 (Cai et al., 2012). In sum, by promoting leukocytes' survival, proliferation and activation (Bauleth-Ramos et al., 2017), enabling the generation of pro-inflammatory mediators like IL-1, IL-6, IL-12 and TNF-α, as well as reactive oxygen and nitrogen species, and enhancing antigen presentation to T cells via incremental expression of major histocompatibility complex II (MHC-II) molecules (X. Zheng et al., 2017), M1 macrophages are considered strongly microbicidal and antitumoral, and their phenotypic repolarization a potential candidate for investigation in the scope of anticancer therapies (Singh et al., 2017).

Additionally, different immunotherapies targeting CrC aim at promoting the identification of specific TAA, thereby activating and increasing the number of effector T cells, which are able to generate an effective cytotoxic response against malignant cells. Recent progress in these strategies lead to the ongoing development of cancer vaccines or adoptive cell transfer therapy (Matos et al., 2019). Cancer vaccines prime the immune system against one or more TAA, prompting it to specifically attack cancer cells bearing said molecules. While the main challenges in such procedure lie in selecting a suitable antigen target candidate and designing an efficient vaccine mechanism, different kinds of cancer vaccines (employing either antigenic peptides (Goydos, Elder, Whiteside, Finn, & Lotze, 1996; Okuno et al., 2011), activated dendritic cells (Morse et al., 1999), whole tumour cells (Jocham et al., 2004) or TAA-coding viral vectors (Horig et al., 2000; Larocca & Schlom, 2011)) have already been submitted to clinical trials. Therapies involving adoptive cell transfer, on the other hand, see that autologous T cells are removed from patients, activated and expanded to large quantities *in vitro* and transferred back into the patients (Koido et al., 2013). The newly inserted CTLs are highly

reactive, present specificity against malignant cells and can be further stimulated upon administration of adjuvant cytokines such as IFN molecules, which augment the expression of MHC class I on the cell surface (Koido et al., 2013).

The need for new solutions

Despite the current availability of widespread types of cancer therapies, the average outcomes of the disease are still unfavourable, often owing to the general aggressiveness and considerable side effects of most treatments (Fernandes et al., 2015). In truth, on the one hand, the majority of chemotherapies undergo a rather homogeneous drug biodistribution across tissues and unselectively exert their cytotoxicity on both normal cells and malignant cells, while often severely compromising the quality of life of the patients (Jones et al., 2006; Kline et al., 2014). On the other, the potential of immunotherapy is currently limited by the restricted amount of TAA that are truly tumour-specific, tied to the risk of triggering autoimmune toxicities against healthy tissues from which said TAA are derived (Xiang et al., 2013). Furthermore, mechanisms of self-tolerance may also constrain the instigation of the desired immune responses against these antigens (Xiang et al., 2013). Lastly, differing cancer profiles are observable across a wide range of patients, and each individual's genetic and environmental backgrounds affect how he responds to a given treatment - making certain strategies less effective in particular sets of patients and also less predictable in terms of clinical outcome (Senft, Leiserson, Ruppin, & Ronai, 2017) .

In the specific case of CrC, most deaths are due to their systemic dissemination and metastasis to lung and liver, rather than from the primary tumour itself (which may be eradicated by surgery and standard chemotherapy) (Hana Janouskova et al., 2013; X.-L. Li et al., 2015a). Besides, with cancer being such a complex, multifactorial and widely variable disease, it has become generally accepted that it is unlikely for a singular monotherapy to provide cancer patients with satisfactory prognostics (Bauleth-Ramos et al., 2017; Zugazagoitia et al., 2016). Consequently, the ever-evolving paradigm for cancer treatment is nowadays striving to contemplate the global landscape of interconnected interactions between cells, genes, biochemical mediators and drugs, so as to strategically integrate distinct treatment modalities in order to optimize the chance of cure (Emens, 2010).

It is now well understood that targeting one aspect of tumour biology will bring consequences for other elements involved in the TME (Emens, 2010). Apoptosis, for instance, which is induced by numerous chemotherapeutics, has proven to be highly immunogenic under certain circumstances by leading to increased immune presentation

of TAA derived from tumour cells debris (Zitvogel et al., 2010). Besides, other drugs indirectly enhance intrinsic tumour cell immunogenicity through modulation and downregulation of a variety of immunoregulatory cells and pathways (Chen & Emens, 2013). Overall, accumulating evidence suggests that several chemotherapeutic drugs are more efficient against tumours that are implanted in immunocompetent hosts, in comparison to immunodeficient ones (Emens, 2010). A handful of current strategies are therefore turning towards the synergistic combination of different therapeutics into a sort of chemoimmunotherapy that at its core induces targeted cytotoxicity in cancer cells while prompting an effective restoration of antitumor immune mechanisms (Chen & Emens, 2013). These new multifunctional combinational systems that are able to simultaneously target cancer cells, release chemotherapeutics at the tumour site, stimulate tumour-driven immune responses and minimize collateral damage in host tissues are of utmost importance in the new generation of medicines (Hull, Farrell, & Grodzinski, 2014).

1.2. *In vitro* models for cancer therapy screening

For some time, one of the major hurdles in cancer research has been the collection and interpretation of data from *in vitro* assays that would provide pertinent insights and valid conclusions regarding the real manifestations of the disease (Cox, Reese, Bickford, & Verbridge, 2015). In fact, approximately 90% of the cancer drugs that enter clinical trials fail during the course of the tests, and the 10% that do succeed often only add weeks or months to the patients' life expectancy (rather than years) (Gevaert, 2013). When adding the fact that cancer drug development carries a financial burden of approximately 1 billion dollars for each drug that succeeds through all stages of clinical trials, with the cost substantially increasing between each subsequent phase, it becomes evident that the screening for new drugs or novel anticancer therapies currently has its efficiency hindered by a poor translation of pre-clinical results and limited accuracy of testing models to predict human responses (Cox et al., 2015).

For many years, two-dimensional (2D) cell culture models have been the mainstay for cancer research in terms of assessing *in vitro* cellular responses to diverse biophysical and biochemical cues (Duval et al., 2017). These models, typically relying on flat surfaces of glass or polystyrene as mechanical support for the cells, are simple, inexpensive, efficient and provide a practical way to observe and analyse cells cultures – allowing homogenous cell growth and proliferation due to its inherent (non-

physiological) uniform distribution of nutrients and growth factors in the medium (Duval et al., 2017). However, said models fail to recapitulate the shape and fundamentally deterministic morphology of cells that drive some important aspects such as cell behaviour, signal transduction, cell-cell and protein-protein interaction, and responsiveness to external stimuli (Gevaert, 2013). Features like these can instead be replicated in tri-dimensional (3D) models, in which biological cells are permitted to grow and interact with its surroundings in all three dimensions (Antoni, Burckel, Josset, & Noël, 2015). 3D cell models have therefore gained popularity in the last few years as a more realistic alternative to mimic *in vivo* conditions in terms of cell viability, morphology, physiology, differentiation, response to stimuli, migration, gene expression and protein synthesis, cell polarization and communication with the ECM and other cells (Antoni et al., 2015). Furthermore, the cell aggregation that is formed in 3D avoids the "monolayer morphology", which is not natural for all cell types (Antoni et al., 2015), and creates a gradient of nutrient access and waste build-up that is not possible to simulate in 2D (Duval et al., 2017). Accordingly, comparative transcriptomic studies showed that numerous genes tied to cell survival, proliferation, differentiation and resistance to therapy were differentially expressed in cells grown in 3D configurations versus 2D cultures (Zietarska et al., 2007). Altogether, these finding make 3D cultures an attractive platform for a more effective screening of the drug candidates that move onto animal studies, reducing the number of required animals and preventing a significant loss of time and resources (Cox et al., 2015).

Given cancer's high complexity and variability (Breitenbach & Hoffmann, 2018), with convoluted processes and widespread phenotypes across different patients and populations (Maule & Merletti, 2012; OMRAN, 2005), it became increasingly clear that the classical 2D in vitro cell assays were not sufficiently accurate to portray the intricate mechanisms underlying phenomena like tumour metastasis, dormancy, extravasation and ECM remodelling, along with the extensive myriad of interactions that take place between the different elements within the TME (Katt, Placone, Wong, Xu, & Searson, 2016). Thus, following recent technological advances in materials science, cell biology and bioreactor design, a growing number of 3D tumour models are currently being adopted and implemented in cancer research (Antoni et al., 2015), as well as simultaneously improved in complexity and diversity, alongside anticancer therapies themselves (Katt et al., 2016).

Many design choices can be contemplated when creating a 3D model for cancer. Variables like the provenience of the cells (commercial cell lines, patient cells, stem cell-derivates, etc.), biophysical properties (partial gas pressure, relative humidity, pH, etc.),

availability of nutrients and ECM composition/architecture are among the most important features to consider (Wirtz, Konstantopoulos, & Searson, 2011), since each of them will have a unique impact over how the system responds to the stimuli under test. In the end, the elements that compose the model and its overall complexity are largely dependent on the purpose it intends to fulfil (Katt et al., 2016).

Despite the current widespread usage of 2D models in cellular assays, the application of 3D models to mimic cancer is not new. The use of Transwells, for example, has been reported since the 90s for a multitude of studies evaluating cancer cell migration and invasion (Esparis-Ogando, Zurzolo, & Rodriguez-Boulan, 1994; Ferreira, Gaspar, & Mano, 2018; Tang, Chikhale, Shah, & Borchardt, 1993; Walsh, Ueda, Nakanishi, & Yoshida, 1992). In short, Transwell methods are used for drug screening and to study the translocation of cancer cells across porous membranes under experimental conditions such as the presence of different chemoattractants, silencing agents, soluble factors or even other cell types (Justus, Leffler, Ruiz-Echevarria, & Yang, 2014). Other 3D models include tumour microvessels and the so-called “hybrid models”. Microvessels are generally fabricated by seeding endothelial cells onto predefined ECM scaffolds or self-assembling the vessels through matrix remodelling, and are used to study interactions between the tumour and its vasculature (Bogorad et al., 2015). On the other hand, hybrid models focus more on the interaction between cancer cells and the ECM, and may refer to whole tumour sections embedded in a synthetic matrix (Nguyen-Ngoc et al., 2012), 3D invasion models based on the seeding of clusters of cancer cells (or even individual cells) in an ECM material (Liu et al., 2010), or avascular microfluidic devices that mimic the confined migration of tumour cells through thin fibres in the ECM (Konstantopoulos, Wu, & Wirtz, 2013).

Another important class of 3D models for cancer, spheroids (or Multicellular Tumour Spheroids, MCTS) are aggregates of cells grown in suspension by self-assembly or embedded in a three-dimensional matrix using 3D culture methods and represent avascular clusters of cancer cells or even small-scale metastasis (Hirschhaeuser et al., 2010). While more expensive and cumbersome to operate than normal 2D cultures (Friedrich, Seidel, Ebner, & Kunz-Schughart, 2009), MCTS do represent a huge leap in fidelity towards the in vivo setting, highlighting the importance of cell-cell and cell-matrix interactions in a way that cannot be replicated in 2D conditions (Cattin, Ramont, & Ruegg, 2018; Virgone-Carlotta et al., 2017). By adapting the method for spheroid formation and tuning its size, it is possible to control the establishment of oxygen and nutrients gradients, culminating (or not) in the formation of a necrotic core reminiscent of poorly vascularized tumours (Friedrich et al., 2009; Katt et al., 2016). An

important factor resulting of these interactions is that MCTS present much different profiles in terms of protein and gene expression when compared to equivalent cultures outside of the three-dimensional setting – thus bridging yet another empiric gap between the in vitro model and the clinical reality (Friedrich et al., 2009; Hirschhaeuser et al., 2010). Moreover, the utility of MCTS can be further expanded by including more than one cellular type in its composition, allowing for the screening of interactions between different cell types in the microenvironment along with the response of the global system to a certain drug or other stimuli under testing (Devi, Mishra, Roy, Ghosh, & Maiti, 2015; Lazzari et al., 2018). Overall, MCTS currently pose as very pertinent models to study cellular functions (in terms of cell growth, proliferation, invasiveness, tendency to form metastasis, etc.) and interactions at the TME, along with the response/sensitivity of the whole tumour to chemotherapeutics, targeted therapies and specific delivery vehicles (Figure 5) (Mikhail, Eetezadi, & Allen, 2013; Perche, Patel, & Torchilin, 2012).

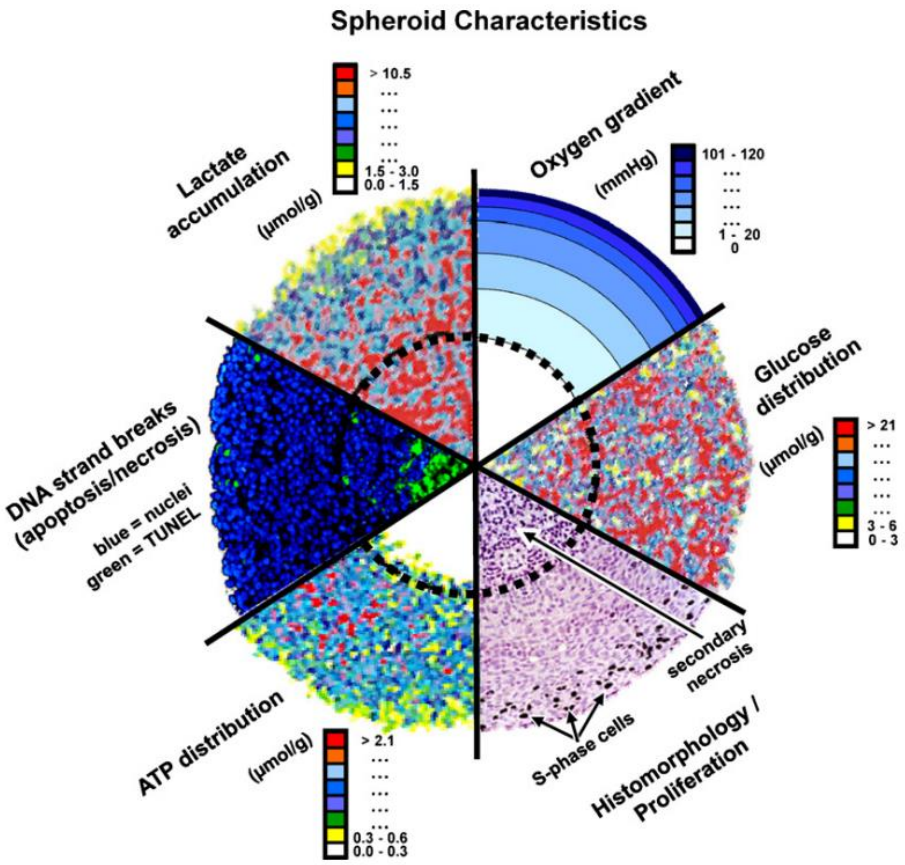

Figure 5 – Analytical data regarding the distribution gradients of lactate, oxygen, glucose, ATP, DNA breaks and proliferative cells, measured across the body of a monoculture tumour spheroid. A concentric disposition surrounding a necrotic core displaying intensive cell death can be observed. Adapted from (Hirschhaeuser et al., 2010) with the permission of Elsevier.

1.3. The promise of Nanotechnology

Most current anticancer strategies have evolved to not only rely on the combination of different synergistic therapies, but also to bridge different fields of scientific knowledge like nanotechnology, biology and materials' science, which brought about some unconventional tools for Medicine that are nowadays still revolutionizing the paradigm of cancer research (Irvine, Hanson, Rakhra, & Tokatlian, 2015).

The application of nanotechnology in Medicine offers valuable tools for the diagnosis and treatment of various diseases (Rezvantalab et al., 2018). In particular, nanotherapeutics and particularly nanoparticles (NPs) have emerged as the foundation of powerful and versatile drug delivery systems that can administer a wide range of chemotherapeutics, target specific cells and exert tuneable immunomodulatory effects (Bauleth-Ramos et al., 2017; Fontana, Figueiredo, Bauleth-Ramos, Correia, & Santos, 2018). Furthermore, existing biomaterials have gone beyond their traditional application in medical devices to become the basis of various drug delivery, cell targeting and tissue engineering applications, while new ones are currently being assessed in regard to their safety, chemical properties, biocompatibility and mechanisms of interaction with the organism (namely with the immune system) (W. A. Li & Mooney, 2013). Over the past years, NPs have gained widespread popularity as vehicles for anticancer therapy, with an ever-increasing number of nanoformulations being approved for clinical trials (Robert, Wilson, Venuta, Ferrari, & Arreto, 2017). Owing to their size and shape tuneability, biocompatibility and biodegradability, along with their ability to incorporate higher drug payloads, enhance their stability and circulation time and decrease toxicity, NPs have the potential to overcome some of the main obstacles currently hindering classical drug administration for cancer treatment (Matos et al., 2019). In particular, polymeric NPs can serve as especially powerful delivery systems, as they are able to undergo chemical modifications (making them more suitable for given applications), co-load different molecules, protect and release their cargos in a controlled/sustained manner and target specific cells through functionalization (Bauleth-Ramos et al., 2017). Depending on the preparation method, polymeric nanoparticles can form two types of structures: nanospheres, which consist of a matrix system in which the drug is uniformly dispersed, and nanocapsules, wherein the drug is contained in a cavity surrounded by a polymeric membrane (Sharma, 2019). This preparation protocol, along with the selected polymer, are the capital forces governing the fundamental properties of the final nanosystem.

Acetalated dextran (AcDEX), for instance, is a biocompatible polymer that can be prepared in a single step by reversibly modifying dextran (a biocompatible, biodegradable, Food and Drug Administration-approved, homopolysaccharide of glucose) with acetal-protecting groups, which renders the polymer completely hydrophobic, as opposite to its hydrophilic parent dextran (K. E. Broaders, J. A. Cohen, T. T. Beaudette, E. M. Bachelder, & J. M. J. Fréchet, 2009). Likewise, AcDEX can be processed into NPs via standard nanoemulsion techniques (K. E. Broaders, J. A. Cohen, T. T. Beaudette, E. M. Bachelder, & J. M. Fréchet, 2009), and encapsulate both hydrophilic and hydrophobic drugs upon double-emulsion (Bauleth-Ramos et al., 2017), and even undergo further functionalization for different biomedical applications (E. M. Bachelder, Pino, & Ainslie, 2017). Importantly, as a pH-sensitive polymer, AcDEX gradually degrades in acidic environments while being protected in physiological conditions (pH ≈ 7.4) (Eric M Bachelder, Pino, & Ainslie, 2016). As a result, the polymer has shown confirmed, promising immunotherapeutic potential for cancer-based applications (Bauleth-Ramos et al., 2017; Fontana et al., 2017).

1.3.1. NP targeting systems in CrC

One of the main factors potentiating the application of nanostructured devices in cancer drug delivery is the possibility to adapt the system in order to promote a privileged, localized delivery of chemotherapeutics at the tumour site, thereby ensuring that a higher drug amount reaches its designated destination and negating eventual hazardous side effects towards the patient's own healthy cells (Davis, Chen, & Shin, 2008; Peer et al., 2007).

Strategies for targeted delivery can be categorized as either passive or active. Passive targeting exploits particular aspects of the disease or its affected site to promote non-specific drug accumulation at said site, hence boosting its therapeutic effects locally (Danhier, Feron, & Préat, 2010). Conversely, the principle of active targeting entails the existence of a driving force that specifically and unequivocally directs the cargo to its target, being usually based on the interaction between a given ligand that is incorporated (such as an antibody or carbohydrate) into the system and its overexpressed receptor at the site of interest (Langer, 1998). Despite its enhanced effectiveness however, the active targeting process cannot be dissociated from the passive one because it can only take place after passive accumulation occurs (Bae, 2009; Danhier et al., 2010).

Generally, tumours present a number of characteristics that facilitate both passive and active targeting strategies (Danhier et al., 2010). The intense angiogenesis that takes place at tumour site is often rapid and defective, leading to an increased permeability of the blood vessels due to the endothelium's lack of integrity that facilitates the escape of NPs (Peer et al., 2007). Furthermore, the dysfunctional lymphatic drainage in tumours causes retention of the administered nanocarriers, allowing the release of payloads into the vicinity of the tumour cells in what is known as the enhanced permeability and retention (EPR) effect (Maeda, Wu, Sawa, Matsumura, & Hori, 2000). Another remarkable characteristic of tumour sites that can be highly exploitable for drug delivery is their intrinsically acidic pH (ranging between 6.0 and 7.0), which arises from the accumulation of acidic metabolites generated by glycolysis – an alternate ATP-generating source that is explored by tumour cells even when oxygen is available (Feron, 2009). The application of biodegradable pH-sensitive materials for NP production (as the aforementioned AcDEX, for example), can take advantage of this acidity gradient to normally carry their cargo through the body under physiological pH, and release it by degradation upon contacting with the more acidic vicinities of the tumour site (Bauleth-Ramos et al., 2017; Peer et al., 2007). These tumour features make up the basis for most of the currently existent passive routes of drug delivery (Langer, 1998).

Active targeting in cancer drug delivery hinges on identifying specific molecules that are overexpressed in the surface of cancer cells, and coupling their cognate ligands to NPs in order to promote molecular binding interactions between the two, usually followed by internalization of the latter (Danhier et al., 2010). Some of the most studied overexpressed receptors in cancer include (i) the transferrin receptor, which internalizes transferrin - a serum glycoprotein that transports iron through the blood and into cells - via receptor-mediated endocytosis (Daniels, Delgado, Helguera, & Penichet, 2006), (ii) the folate receptor, a well-known tumour marker that binds and internalizes the vitamin folate, which is normally required for DNA biosynthesis, repair and methylation in fast proliferating cells (Cheung et al., 2016), and (iii) the EGFR, which binds members of the Epidermal Growth Factor (EGF) family and stimulates processes involved in tumour growth and progression such as proliferation, angiogenesis, and metastasis, namely in CrC (Danhier et al., 2010; Lurje & Lenz, 2009).

One other receptor that merits attention is the cluster of differentiation 44 (CD44). This class of transmembrane glycoproteins is involved in processes of extracellular adhesion, cell migration and signal transduction and functions as a common biomarker for a range of stem cells, including CSCs, and some noncancer, tumour-associated cells, such as macrophages (Mattheolabakis, Milane, Singh, & Amiji, 2015). Its best-known

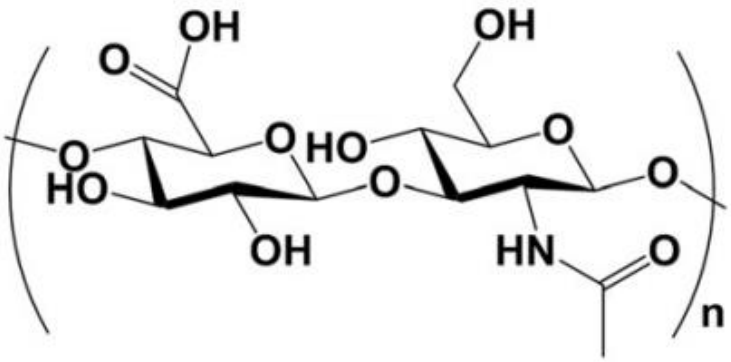

Figure 6 - Molecular structure of hyaluronic acid.

ligand is hyaluronic acid (HA), a biodegradable, biocompatible mucopolysaccharide composed of repeating disaccharide units of D-glucuronic acid and N-acetyl-D-glucosamine (Figure 6), that naturally exists as a major component in the ECM. By exhibiting very high hydration ratio, negative charge and viscoelasticity, HA plays a significant role in maintaining tissue hydration and conferring elasticity and resistance to the ECM, namely in connective tissues (Necas, Bartosikova, Brauner, & Kolář, 2008).

Upon binding of HA with the CD44 receptor, the complex is internalized and leads to the eventual degradation of the polymer. Being over-expressed in a large number of solid tumours, CD44-like receptors have become an important tool in cancer diagnostics (by serving as an early biomarker) and cancer treatment, due to their cognate affinity for HA, which showed great promise as a tumour targeting moiety bearing minimal toxicity in drug carriers (Mattheolabakis et al., 2015). On the field of Nanomedicines, anticancer nanoformulations employing the HA:CD44 interaction have surfaced in the forms of doxorubicin-carrying Mesoporous Silica NPs (MSNs) (Park et al., 2019), siRNA-loaded chitosan NPs (Zhang et al., 2019) and even self-assembled HA NPs bearing amphiphilic conjugates (Choi et al., 2009), among other formulations.

1.4. Context and outline of the thesis

As previously stated, chemoimmunotherapies are becoming emergingly attractive as anticancer strategies due to their combined potential to both promote cancer cell death through the action of cytotoxic drugs, and stimulate resident immune cells to enhance the presentation of TAA derived from these cells (Chen & Emens, 2013). By consequently activating an effective immune response and attenuating the

immunosuppressive environment of the tumour, these strategies should convert the TME into a sort of “endogenous vaccine”, making it possible to attain powerful anticancer effects on multiple fronts (Bauleth-Ramos et al., 2017; Bracci, Schiavoni, Sistigu, & Belardelli, 2014).

Due to their small size and biochemical versatility, NPs also pose as attractive candidates for vehicles of drug delivery in such therapies. Recently, our group utilized polymeric AcDEX harbouring chemical modifications with spermine molecules to produce a multifunctional nanocarrier for anticancer chemoimmunotherapy. These spermine-modified acetalated dextran (Sp-AcDEX) NPs were successfully loaded with the hydrophobic drug Nut-3a and the hydrophilic cytokine GM-CSF, and showed promising in vitro results (Bauleth-Ramos et al., 2017). Moreover, a triple culture spheroid-based model, encompassing colorectal epithelium cancer cells, intestinal fibroblasts and human monocytes, was also explored as a testing platform for anticancer nanotherapies in the context of CrC. Therefore, the present work purports to incorporate into these NPs an active targeting system governed by the interaction of HA with the CD44 receptor, and utilize said MCTS to perform a comparative study between the biological responses towards these NPs in 2D and 3D.

Likewise, the main objectives of this dissertation are (i) to develop and optimize a viable strategy to functionalize Sp-AcDEX NPs with HA in order to promote CD44 targeting; (ii) to assess the therapeutic efficacy of HA-functionalized Sp-AcDEX (HA:Sp-AcDEX) NPs in vitro, particularly when loaded with Nut-3a; (iii) to address the effects of the optimized NPs in the developed CrC co-culture spheroid model, in order to evaluate its biological significance in comparison to 2D cultures.

This dissertation is organized in four chapters: Chapter 1 consists of a general introduction. Chapter 2 describes the methodology utilized to carry out the experiments. Chapter 3 reports the obtained results; here, at first, the iterative process leading up to Sp-AcDEX NPs functionalization is documented, followed by the main observations regarding their performance in 2D and 3D cellular assays; the characterization of the utilized spheroid model is also presented. Chapter 4 consists of a global discussion of the experimental results. Finally, Chapter 5 presents the main conclusions and final insights on the developed work, whilst future proposals are also suggested.

II. Materials and Methods

2.1. Materials and reagents

Sp-AcDEX was synthetized and kindly provided by Professor Hélder A. Santos' group, Nanomedicines and Biomedical Engineering group, at the Faculty of Pharmacy of the University of Helsinki. HA (PRIMALHYAL20, 20,000 Da) was obtained from Givaudan (Vernier, Switzerland) and kindly offered by the University of Minho. 3D Petri Dishes® for spheroid casting (Z764019-6EA) were purchased from Sigma-Aldrich (USA) and kindly provided to us by the research group of Professor Cristina Barrias, Bioengineered 3D Microenvironments, at i3S, Porto, Portugal. The following materials and reagents were also purchased from Sigma-Aldrich: Agarose powder (A9539); Dichloromethane (DCM; anhydrous, 99.8%); 2-(4-(2-hydroxyethyl) piperazin-1-yl) ethanesulfonic acid (HEPES); Poly(vinyl) alcohol (PVA) 98-99% hydrolysed; 2-(N-Morpholino)ethanesulfonic acid (MES); fluorescein isothiocyanate (FITC); Sodium Chloride anhydrous (NaCl, 58.44 g/mol); Monosodium phosphate (NaH_2PO_4, 119.98 g/mol); Disodium phosphate anhydrous (HNa_2PO_4, 141.96 g/mol). 1-ethyl-3-(3-dimethylaminopropyl)carbodiimide hydrochloride (EDC) was obtained from ThermoScientific (USA). N-Hydroxysuccinimide (NHS) was purchased from Merck Millipore (USA). Nutlin-3a (Nut-3a) was purchased from ApexBio (USA). Macrophage-Colony Stimulating Factor (M-CSF) was obtained from ImmunoTools (Friesoythe, Germany). Ultrapure water characterized by 0.055 $\mu S\ cm^{-1}$ of conductivity and 18.2 $M\Omega.cm$ of resistivity was prepared in-house using Milli-Q station from Millipore Corp. (Madrid, Spain).

HCT116 human colorectal cancer cells were obtained from American Type Culture Collection (ATCC, USA) and kindly provided to our group by the research team of Professor Maria José Oliveira, Tumour and Microenvironment Interactions, at i3S, Porto, Portugal. Roswell Park Memorial Institute (RPMI-1640) medium was purchased from ThermoFisher Scientific. Human Intestinal Fibroblasts (HIF) and Fibroblast Medium were purchased from ScienCell Research Laboratories (San Diego, California, USA). Human monocytes were isolated from leukocyte-enriched buffy coats provided by Hospital S. João, Porto, Portugal, as described elsewhere (Oliveira, Santos, Oliveira, Torres, & Barbosa, 2012), and also kindly provided to us by the research group of Professor Maria José Oliveira.

2.2. Preparation of Sp-AcDEX NPs

Synthesis of AcDEX and spermine modification were performed by the Nanomedicines and Biomedical Engineering group at the Faculty of Pharmacy of the University of Helsinki, through reductive amination chemistry as described elsewhere (E. M. Bachelder, Beaudette, Broaders, Dashe, & Frechet, 2008; Cohen et al., 2011).

Preparation of Sp-AcDEX NPs was achieved via a water-in-oil-in-water double emulsion by evaporation method as described elsewhere (Bilati, Allemann, & Doelker, 2003; Cohen et al., 2011). First, 12.5 mg of the Sp-AcDEX were dissolved in 0.25 mL of DCM and cooled down on ice before sonication; for particles containing Nut-3a, 400 µg of this drug were previously dissolved in the same amount of DCM.

Afterwards, 25 µL of phosphate buffer saline (PBS) 1x, pH 7.4, were added drop-by-drop to the polymer-DCM solution, followed by a 30 second pulsed sonication (10 seconds ON, 5 seconds OFF) with 50% amplitude on an ice bath, using a Vibra-Cell™ ultrasonic processor (Sonics and Materials, Inc., USA). 0.5 mL of PVA aqueous solution (2% w/v) were then added to the resulting solution, and the mixture was sonicated under the same conditions to yield the final double-emulsion; this solution was promptly transferred into a second PVA aqueous solution (2.5 mL, 0.2% w/v) and stirred for 3 h at 300 rpm to evaporate the organic solvent. Finally, the NPs were collected, separated by centrifugation (19 000 rcf, 5 min, 10 °C), washed twice with 10 millimolar (mM) HEPES at pH 8.0 (with centrifugations under the same conditions) and stored in the same solution at a final volume of 1 mL, at room temperature (RT).

In order to incorporate FITC into the NPs, the compound was previously dissolved in DCM and the particles were produced by double-emulsion as described above. In order to remove all external and unbound FITC remaining in the final solution, the NPs were collected by centrifugation and washed five more times with 10 mM HEPES at pH 8.0.

2.2.1. HA functionalization of Sp-AcDEX NPs

Previously prepared NPs were redispersed in 10 mM MES buffer solution containing an amount of sodium hyaluronate ranging between 0.01% and 10% of the utilized mass of Sp-AcDEX (m/m of NPs); the resulting solution was stirred at 300 rpm for two hours at a concentration of 1 mg/mL. Particles were then collected by centrifugation (11000 rcf; 5 min; 10 °C), washed twice with 10 mM HEPES at pH 8.0 (with centrifugations under the same conditions) and stored in the same solution at a

final volume of 1 mL, at RT. For functionalization through carbodiimide conjugation, NPs were initially incubated in 10 mM MES with the previous amount of sodium hyaluronate, along with EDC and NHS at a 10-folded concentration in respect to that of HA, with the rest of the procedure being carried out as described above.

2.2.2. Physicochemical properties of NPs

The produced nanoparticles were dispersed in 10 mM HEPES buffer at pH 7.4 and transferred to magnetic cuvettes before being submitted to DLS analysis The average diameter (Z-average), PdI and surface Zeta (ζ)-Potential of all NP samples were measured at 25 °C using a Zetasizer Nano ZS instrument (Malvern Ltd., UK). The Malvern Dispersion Technology Software (DTS) was used with monoclonal data processing mode to determine the average abovementioned parameters and error values. All measurements were performed in triplicate.

2.2.3. Negative-staining transmission electron microscopy (TEM)

For negative staining transmission electron microscopy, 5 µL of samples were mounted on Formvar/carbon film-coated mesh nickel grids (Electron Microscopy Sciences, Hatfield, PA, USA) and left standing for 1 min. The liquid in excess was removed with filter paper, and 5 µL of 1% uranyl acetate were added on to the grids and left standing for 10 seconds, after which the excess liquid was removed with filter paper. Visualization was carried out on a JEOL JEM 1400 TEM at 120 kV (Tokyo, Japan). Images were digitally recorded using a CCD digital camera Orious 1100W Tokyo, Japan, at HEMS / i3S of the University of Porto. The transmission electronic microscopy was performed at the HEMS core facility at i3S, University of Porto, Portugal.

2.3. Cell culture

HCT116 human colorectal cancer cells were cultured in RPMI supplemented with 10% heat-inactivated (HI) Foetal Bovine Serum (FBS), penicillin (100 IU/mL) and streptomycin (100 mg/mL); HIF were cultured in Fibroblast Medium supplemented with 2% FBS, 1% Fibroblast Growth Supplement (FGS) and 1% penicillin/streptomycin solution (P/S). All cultures were incubated at 37 °C in 5% CO_2 / 95% relative humidity (RH), and subculturing was done according to instructions provided by ATCC and ScienCell Research Laboratories.

2.3.1. 2D cell viability

Briefly, HCT116 and HIF cells were seeded in 96-well plates at a cell density of 10000 cells/well and allowed to attach for 24 hours. The medium was then removed, and 100 µL of NPs suspensions in the corresponding cell culture medium were added to the cells at the concentrations of 0 (control), 50, 100, 200, and 500 µg/mL. Free HA was also incubated with HCT116 cells and human macrophages, at a total final mass of 0.01/0.02/0.04/0.1 µg. Plates were incubated at 37 °C under 5% CO_2 and 95% of RH for 24, 48 and 72 hours, after which the medium was removed and the viability was assessed through a resazurin reduction assay. In the case of human monocytes, cells were seeded at a density of 40000 cells/well and incubated for 7 days in RPMI supplemented with 5 ng/mL of M-CSF (37 °C / 5% CO_2 / 95% RH), to allow macrophage differentiation prior to NP addition.

2.3.2. Resazurin reduction assays

Resazurin reduction assays were used to assess cell viability as described elsewhere (Prabst, Engelhardt, Ringgeler, & Hubner, 2017). Briefly, 100 µL of cell culture medium containing 20% resazurin (v/v) were added to cells (or spheroids where noted) previously seeded in a 96-well plate; the plate was then incubated for 2h in a cell culture incubator at 37 °C / 5% CO_2 / 95% RH, protected from light, and fluorescence intensity was measured in a 96 black well plate with SynergyMx™ MultiMode Microplate Reader (BioTek™, USA), with of 530 nm excitation/590 nm emission wavelengths.

2.3.3. Casting of 3D Petri Dish® agarose molds

In order to generate similar spheroids, 3D Petri Dishes® with 81-wells (Sigma-Aldrich, St. Louis, MO, USA) were used according to the manufacturer's instructions, as illustrated in Figure 7 ("Casting, Equilibrating and Seeding the 3D Petri Dish®,"). Briefly, an aqueous solution of 2% agarose in 0.9% (w/v) NaCl was prepared in a sterile environment and heated to boil and completely dissolve the agarose. The molten solution was then flushed through a 0.2 micron-pore filter and 500 µL were transferred into 3D Petri Dishes® micro-molds and allowed to gel. Afterwards, the resulting 3D Petri Dishes®

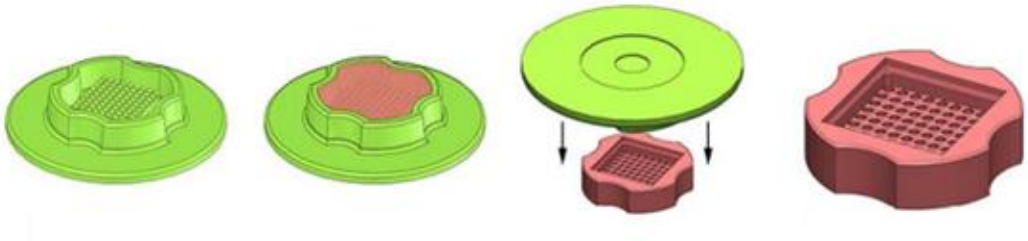

Figure 7 - Schematic procedure of the casting of 3D Petri Dish® molds with 2% agarose (w/v).

were carefully transferred to a 12-well tissue culture plate and incubated overnight in RPMI medium.

2.3.4. Preparation and characterization of the 3D triple cell co-culture spheroids

Upon reaching 80% confluence, HCT116 cells and HIF were collected and counted in a haemocytometer. The appropriate volume of each cell suspension, along with freshly isolated peripheral blood monocytes, were collected and mixed to yield a cell ratio of 4:1:4 (monocytes: HCT116: HIF). The mixture was then centrifuged (1200 rpm; 21 °C; 5 min) and cells were resuspended in RPMI supplemented with M-CSF at 50 ng/mL; the suspension was then seeded atop the agarose 3D Petri Dishes® inside a 12-well tissue culture plate, at a final cell density of 5000 cells per spheroid. After a 30 min incubation period for cells to settle into the micro-molds, 2 mL of medium were added to the wells and the growing spheroids were incubated for 7 days to allow monocyte differentiation, with medium renewal every two days.

Characterization of the triple-culture model was carried out in triplicate or higher at days 1, 4, 7 and 10 post-seeding. To this end, approximately 40 spheroids were carefully transferred to a 96-well plate (10 spheroids per well) and their metabolic activity was assessed through a resazurin reduction assay. Spheroid images were obtained using a ZOE Fluorescent Cell Imager (Bio-Rad) with BRIGHTFIELD mode, and spheroid diameter was measured using the ImageJ software. The remaining spheroid-containing micro-molds were fixated for 30 minutes in a paraformaldehyde aqueous solution (4% w/v) and stored in PBS 1x, pH 7.4, at 4 °C, for posterior histological processing.

2.3.5. Spheroid histological analysis

Spheroid-containing micro-mold samples from days 1, 4, 7 and 10 post-seeding were collected and embedded in paraffin for Hematoxylin and Eosin (H&E) staining.

Tissue sections 3 µm thick were mounted on glass slides and dried overnight at 37 °C prior to the staining procedure. The sections were first deparaffinized in xylol (3 x 5 minutes) and rehydrated via a decreasing ethanol series (100% ethanol, 96% ethanol, 70% ethanol, 50% ethanol and distilled water, 3 minutes each) before being stained with haematoxylin for 3 minutes and eosin for 1 minute. The final histological preparations were observed under a light microscope (Zeiss Axioscope 2).

2.3.6. Spheroid viability/antiproliferation assays

Triple-culture spheroids were collected after 7 days of culturing and seeded in 96-well plates previously coated with 2% (w/v) agarose, at the concentration of one spheroid per well; 100 µL of RPMI were added to each well, and spheroids were allowed to settle onto the agarose beds. Afterwards, the medium was removed and 100 µL of NPs at the concentrations of 0 (control), 50, 100 and 200 µg mL^{-1} were added to the wells. Plates were incubated at 37 °C under 5% CO_2 and 95% of RH for 24, 48 and 72 hours, after which the medium was removed and the viability was assessed through a resazurin reduction assay.

2.3.7. Quantitative NP uptake by spheroids

Prior to spheroid seeding, all wells containing agarose 3D Petri Dishes® in the 12-well plates were blocked with molten 2% agarose and allowed to gel, in order to concentrate the NPs on top of the spheroids. At the 7^{th} day post-spheroid seeding, the medium was removed and 2mL of FITC-labelled NPs dispersed in RPMI (at 50 µg/mL) were added to each mold and incubated for 3 or 24 h at 37 °C; a control condition without NPs was included for each time point. Afterwards, 40 spheroids were collected from each mold into Eppendorf tubes, washed twice with PBS (pH 7.4) by centrifugation (300 rcf, 5 minutes, 4 °C) and incubated in trypsin for 25 minutes at 37 °C in 5% CO_2/ 95% RH to allow spheroid dissociation. RPMI medium was then added to the tubes to inactivate trypsin, and the resulting cell suspension was centrifuged again at the same conditions, washed two more times with PBS, resuspended in fluorescence-activated cell sorting (FACS) buffer (PBS with 5% FBS) and transferred to polystyrene tubes after filtration through a 70 µm-pore membrane filter. Finally, samples were measured using a BD FACSCanto II flow cytometer (BD Biosciences, USA). All data was analysed using FlowJo software (Tree Star, Inc., USA).

2.4. Statistical analysis

All experiments were performed in triplicate or higher (n≥3). Measurement values are expressed as mean ± standard deviation (SD) unless stated otherwise. All data was treated by One-way ANOVA or Two-way multivariable ANOVA with Bonferroni post-Hoc test using GraphPad Prism (v. 7.00, GraphPad Software, San Diego, CA). Statistically significant results were defined as follows: *P<0.05, **P<0.01, ***P<0.001, and ****P<0.0001.

III. Results

3.1. Production and characterization of bare Sp-AcDEX NPs

The physicochemical properties of the bare Sp-AcDEX NPs that served as the basis of this study were determined via analysis in a Zetasizer Nano ZS instrument, and are summarized in Table 1. These NPs presented a size of around 200 nm in diameter and a PdI close to 0.1, indicating adequate and uniform dispersity in solution (Clayton, Salameh, Wereley, & Kinzer-Ursem, 2016). The highly positive surface zeta potential of 42 mV suggests a high degree of stability in solution (Vinothini & Rajan, 2019), and is an expected value owing to the cationic nature of the spermine groups.

The size and morphology of the NPs were further evaluated by TEM, as depicted in Figure 8. The particles showed homogeneous size of around 160 nm and spherical shape, validating the results obtained by DLS. A slight decrease of approximately 40 nm in the average NP diameter can be observed in the captured images, which may be explained by the fact that DLS measures particles in an aqueous environment, while this assay does so in a dried state (Prabha, Zhou, Panyam, & Labhasetwar, 2002). Bearing these properties in mind as a starting point for the development of a viable functionalization protocol, the rationale behind the iterative strategies to stably coat these NPs sought to generate the lowest possible increase in particle size and PdI, coupled to a decrease in the surface charge (in the intent of simultaneously maximizing the effectiveness of HA adsorption and the stability of the final product).

Table 1 - Physicochemical characterization of the bare Sp-AcDEX NPs used in this study. Measurements are displayed as means ± SD (n=9).

	Size (nm)	PdI	Zeta Potential (mV)
Bare NPs	195 ± 12	0.109 ± 0.043	42.5 ± 5.1

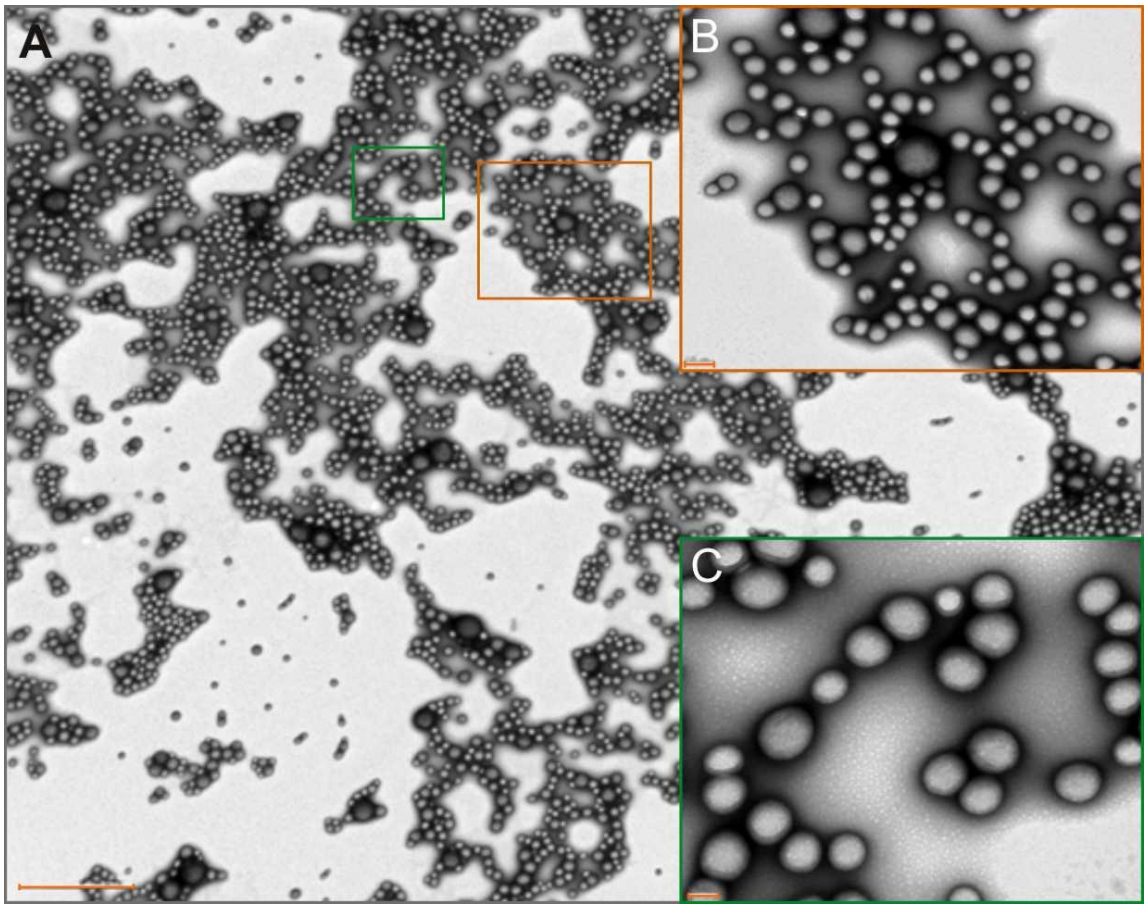

Figure 8 - TEM image of bare Sp-AcDEX NPs. A) Coloured squares represent areas magnified in subsequent pictures. Scale bar is 2 µm. B) Magnification of bare Sp-AcDEX NPs. Scale bar is 200 nm. C) Magnification of bare Sp-AcDEX NPs. Scale bar is 100 nm.

3.2. Production and optimization of HA:Sp-AcDEX NPs

The first and main approach to functionalize Sp-AcDEX NPs consisted on adsorption of HA to the NPs by electrostatic interaction. By stirring said NPs in an appropriate reaction buffer containing HA, it is possible to promote an ionic-driven attraction of the negative backbone of HA towards the globally positive bulk of the particles. Firstly, previously prepared NPs were stirred for 3 hours in HA-containing HEPES buffer at pH 8.0. However, upon stirring and washing, densely aggregated pellets impossible to redisperse were formed. Moreover, the same aggregation could be observed in similar control conditions not containing HA. Therefore, to overcome this issue, a set of parameters potentially affecting the stability of the NPs were optimized prior to the inclusion of HA in the system, as described below.

3.2.1. Reaction pH

In light of the nature of the molecules being used in this system, the working pH quickly became one of the first addressed variables in terms of optimization. Being a pH-sensitive polymer, AcDEX degrades below pH 7.0 (E. M. Bachelder et al., 2017) while retaining some stability in alkaline conditions; on the other hand, although more tolerant, HA functionalization reactions usually present higher yield and efficacy at acidic pH (Chua, Neoh, Kang, & Wang, 2008; Z. Wang et al., 2016). Therefore, the working pH was thoroughly controlled throughout the procedures.

In order to first assess the impact of pH on the overall stability of the particles, bare Sp-AcDEX NPs were stirred for 3 hours in two different buffers (100 mM Phosphate buffer and 10 mM HEPES), at pH 8.0 and 7.4, followed by two washes with HEPES buffer at pH 8.0; their physicochemical properties are presented in Table 2. The NPs experienced intense aggregation in all tested conditions, as shown by the high values of size and PdI, along with the quasi-neutral surface charge.

Table 2 - Physicochemical characterization of bare Sp-AcDEX NPs stirred in 10 mM HEPES and 100 mM phosphate buffer at different pH conditions, followed by washing in 10 mM HEPES (19000 rcf, 5 min, 10 °C). Measurements are displayed as means ± SD (n=3).

Coupling buffer	Buffer pH	Size (nm)	PdI	Zeta Potential (mV)
10 mM HEPES	8.0	992 ± 591	0.426 ± 0.108	-1.0 ± 2.5
	7.4	672 ± 307	0.459 ± 0.116	-5.6 ± 1.9
100 mM Phosphate buffer	8.0	565 ± 372	0.324 ± 0.077	6.6 ± 7.4
	7.4	535 ± 37	0.426 ± 0.039	-2.6 ± 1.5

3.2.2. Coupling buffer and stirring time

Since different reaction buffers for HA adsorption have been reported in the literature, a comparative assay ensued so as to evaluate their effect on NP stability. Following up the previous experiment, the previous protocol was reproduced with the reaction pH further lowered to 7.2 in order to fall into the buffering range of MES (which was included in this study), and the stirring time reduced to 2 hours. A successful reduction of size and PdI was achieved in regard to the previous assay (Table 3). Additionally, by providing bare NPs with physicochemical properties deemed suitable for the system, 10 mM MES at pH 7.2 was herein selected as the coupling buffer to carry out HA adsorption.

Table 3 - Physicochemical characterization of bare Sp-AcDEX NPs stirred in various buffers at pH 7.2, followed by washing in 10 mM HEPES (19000 rcf, 5 min, 10 °C). Measurements are displayed as means ± SD (n=3).

Coupling buffer	Size (nm)	PdI	Zeta Potential (mV)
10 mM HEPES (pH 7.2)	421 ± 166	0.264 ± 0.066	18.1 ± 13.6
100 mM Phosphate buffer (pH 7.2)	352 ± 9	0.303 ± 0.033	33.6 ± 1.9
10 mM MES (pH 7.2)	259 ± 15	0.221 ± 0.038	33.7 ± 3.2

3.2.3. HA Molecular Weight and NP washing conditions

Following the optimization of the reaction buffer, HA was finally included in the system. 20 kDa HA was chosen over 1000 kDa HA, given the latter's proclivity to form insoluble precipitates when mixed with any of the aforementioned buffers. Nevertheless, the new HA-bearing particles repeatedly underwent intense aggregation during the washing steps, resulting once again in insoluble clusters.

The amount of HA included in the particles is discussed in the next section. Meanwhile, it was deemed necessary to mitigate the inherent aggressiveness of the washing procedure in order to overcome the aggregation problem. To this end, in three different days, newly prepared NPs were stirred in MES containing 0.1% HA (m/m of NPs) under the previously defined conditions, and washed using Amicon filters according to the manufacturer's instructions (14000 rcf, 10 min, 10 °C); in parallel, similarly prepared HA:NPs were washed normally by ultracentrifugation under these same settings, as a control condition. The obtained particles are described in Table 4.

Table 4 - Physicochemical characterization of bare Sp-AcDEX NPs stirred in 10 mM MES at pH 7.2, followed by washing in 10 mM HEPES (14000 rcf, 10 min, 10 °C) using Amicon filters, on three different days. The same filters were washed and reused between experiments; a control condition with washes performed by ultracentrifugation under the same conditions was included. Measurements are displayed as means ± SD (n=3).

Washing protocol	Size (nm)	PdI	Zeta Potential (mV)
Amicon wash, Test #1	364 ± 67	0.254 ± 0.053	14.3 ± 3.5
Amicon wash, Test #2	964 ± 531	0.385 ± 0.118	-7.1 ± 16.9
Amicon wash, Test #3	1303 ± 292	0.726 ± 0.098	-21.5 ± 5.6
Ultracentrifugation	311 ± 52	0.274 ± 0.043	29.2 ± 2.5

Although the final properties of the NPs seemed acceptable after the first test, the aggregation increased exponentially in subsequent attempts, as denoted by the poor results in all three parameters. Moreover, upon inspecting the Amicon filters after each

wash, it was observed that high levels of NPs were ultimately retained in the membranes and could not be recovered; likewise, it was unviable to successfully replicate the functionalization procedure using Amicon filters.

Nevertheless, the assay also revealed that washes by ultracentrifugation at lower speed reduced particle aggregation in regard to previous tests, while still allowing for the recovery of a significant amount of NPs. Therefore, washes were henceforth performed by ultracentrifugation, and the washing speed reduced to 14000 rcf in subsequent tests, and later to 11000 rcf.

3.2.4. Percentage of HA

In order to devise a suitable HA ratio to produce stable and efficiently functionalized NPs, previously prepared NPs were stirred in the presence of different concentrations of HA, followed by washing under the aforementioned conditions. The physicochemical properties of the particles were once again analysed in a Zetasizer instrument, with results presented in Table 5. As expected, increasing the concentration of adsorbed HA causes particles to grow in size and become more prone to aggregation, as evidenced by the increasing PdI values. HA adsorption also lowers the surface charge of the particles, which was equally expected due to the polymer's overall negative charge. Remarkably, there seems to be a sporadic increase in particle aggregation for HA concentrations above 0.3% (m/m of NPs), as evidenced by the monumental shifts in all three parameters. Particle size and morphology were further assessed by TEM (Figure 9), in order to inspect for differences along the increasing HA concentrations. The diameters and amounts of aggregation were consistent with those measured by DLS, with preparations above 0.3% HA showing dense clusters of NPs with high heterogeneity (Figure 9I-M). Subsequently, and since NP coating with 0.2% HA (m/m of NPs) showed little aggregation, coupled to a minor increase in size and a distinct decrease in surface charge, this concentration was deemed ideal for NP functionalization, being utilized from this point onward.

Table 5 - Physicochemical characterization of Sp-AcDEX NPs upon adsorption of HA at different concentrations. HA percentages are presented in respect to the original polymer's mass. HA was insoluble in the coupling buffer at 10% concentration (m/m of NPs). Measurements are displayed as means ± SD (n=3). N.D., not determined.

Washing protocol	Size (nm)	PdI	Zeta Potential (mV)
Bare NPs	252 ± 19	0.182 ± 0.035	36.1 ± 3.8
NPs + 0.01% HA	281 ± 21	0.239 ± 0.043	32.7 ± 4.2
NPs + 0.1% HA	317 ± 42	0.252 ± 0.044	26.6 ± 5.0
NPs + 0.2% HA	265 ± 29	0.195 ± 0.059	29.4 ± 3.6
NPs + 0.3% HA	2181 ± 586	0.599 ± 0.083	-3.7 ± 5.5
NPs + 0.5% HA	1567 ± 191	0.594 ± 0.152	-9.7 ± 9.5
NPs + 1% HA	2028 ± 269	0.761 ± 0.171	-13.5 ± 0.7
NPs + 2% HA	1734 ± 205	0.701 ± 0.035	-19.2 ± 0.6
NPs + 10% HA	N.D.	N.D.	N.D.

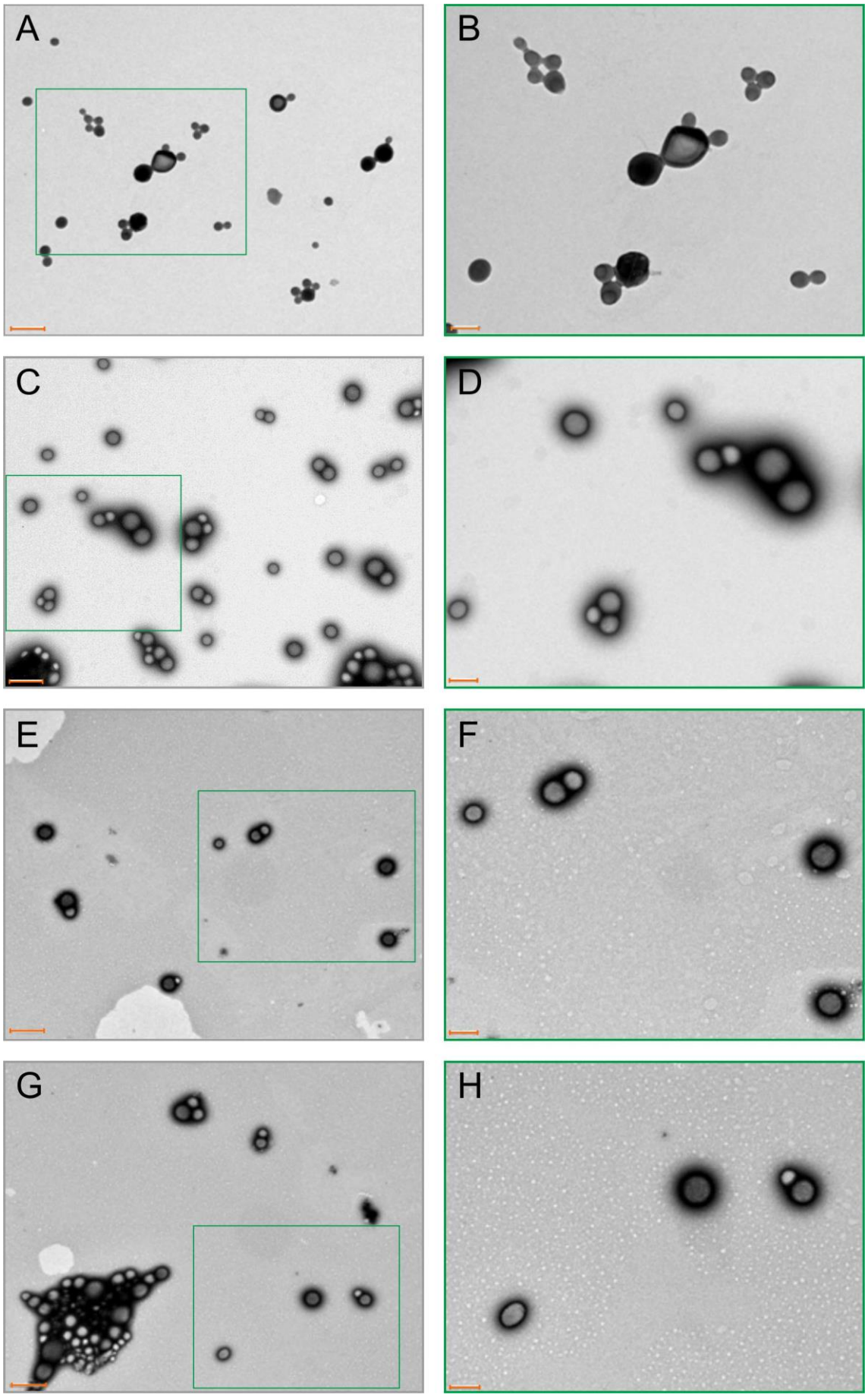

Figure 9 (cont.)

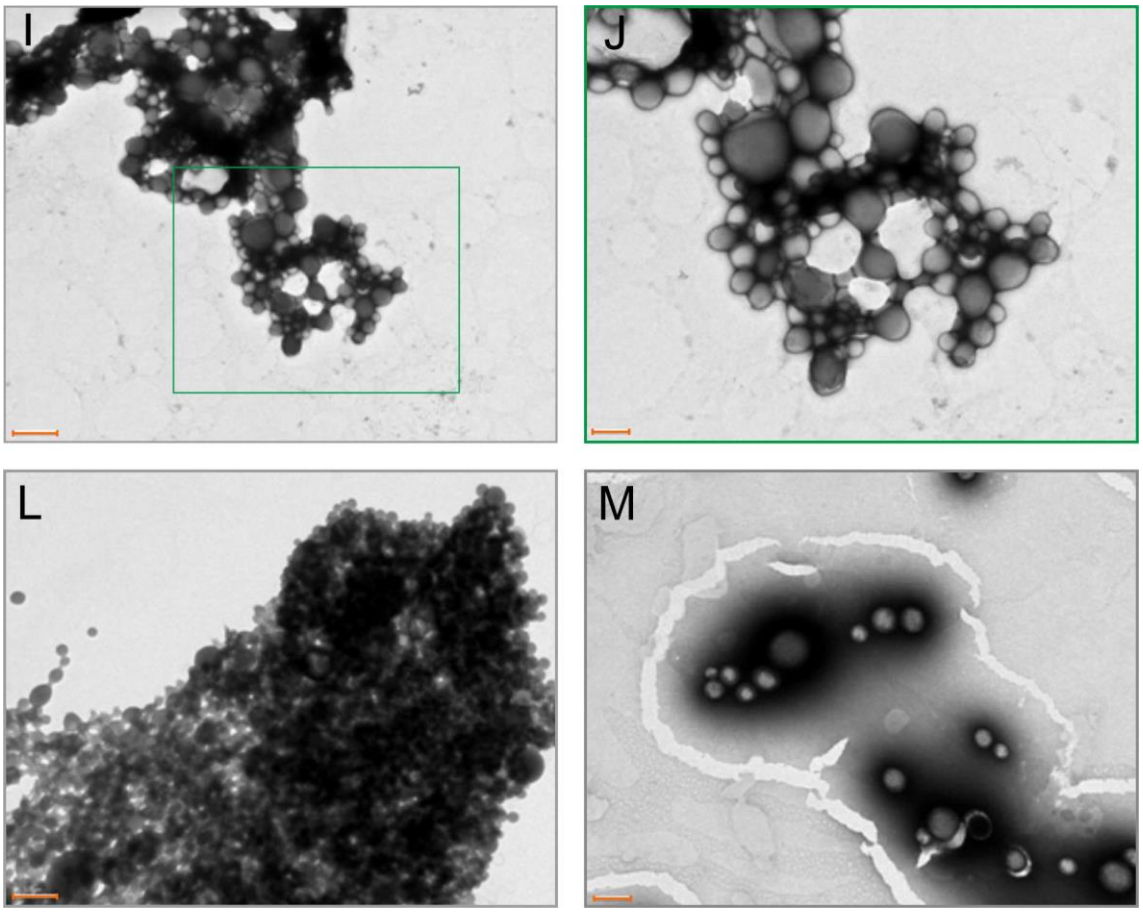

Figure 9 – TEM images of Sp-AcDEX NPs functionalized with different concentrations of HA. (A) Bare NPs; (B) magnification of A; (C) NPs containing 0,01% HA; (D) magnification of C; (E) NPs containing 0,1% HA; (F) magnification of E; (G) NPs containing 0,2% HA; (H) magnification of G; (I) NPs containing 0,3% HA; (J) magnification of I; (L) NPs containing 0,5% HA; (M) magnification of the preparation in L, at a different location. HA percentages are presented in respect to the original polymer's mass. Scale bars represent 500 nm in pictures on the left and 200 nm in pictures on the right.

3.2.5. Functionalization by chemical conjugation

After defining an optimal HA ratio for NP coating, the same functionalization was attempted by chemical conjugation, in the intent of obtaining more stable HA:Sp-AcDEX NPs. Specifically, and considering both the NH_2 groups in the spermine molecules and COOH groups in the HA backbone, a carbodiimide coupling reaction was employed to covalently link the HA motifs to the NPs. In that sense, previously prepared NPs were resuspended in 10 mM MES buffer containing EDC, NHS and 0.2% HA (m/m of NPs) and stirred for two hours, followed by washing by ultracentrifugation as described above. A negative control (without HA) and a positive one (with NPs and HA only) were included; results are presented in Table 6. Particles where EDC-NHS conjugation was performed

presented similar diameter and surface charge to those without HA, although with lower PdI. On the other hand, as previously observed, NPs where only HA adsorption was carried out displayed a significant increase in size and decrease in surface potential; as a result, and since no marked improvements in the particles' quality parameters were gathered from EDC-NHS conjugation, HA adsorption was herein adopted as the strategy to functionalize NPs throughout the rest of the work. The optimized variables are summarized in Box 1.

Table 6 - Physicochemical characterization of Sp-AcDEX NPs upon functionalization with 0.2 % HA (m/m of NPs) via charge-based adsorption and carbodiimide conjugation (EDC-NHS). A control condition without HA but containing EDC and NHS was included. HA percentages are presented in respect to the original polymer's mass. Measurements are displayed as means ± SD (n=5). N.D., not determined.

	Size (nm)	PdI	Zeta Potential (mV)
NPs w/o HA	256 ± 16	0.232 ± 0.046	36.5 ± 2.2
NPs + 0.2% HA (adsorption)	325 ± 29	0.219 ± 0.022	17.7 ± 1.8
NPs + 0.2% HA (EDC-NHS)	245 ± 8	0.189 ± 0.040	33.3 ± 5.3

Box 1 – Optimized variables for the production of HA:Sp-AcDEX NPs:

- ✓ **Functionalization methodology**: Charge-based adsorption;
- ✓ **HA ratio**: 0.2% of the utilized NPs' mass;
- ✓ **Reaction buffer**: MES buffer, at 10 mM concentration and pH 7.2;
- ✓ **Stirring**: 2 hours, at 300 rcf;
- ✓ **Washing**: By ultracentrifugation - 2 washes in HEPES buffer at 10mM concentration and pH 8.0, for 5 minutes, at 11000 rcf, 10 °C;
- ✓ **Storage**: in 1 mL of 10 mM HEPES, pH 8.0, at RT.

3.3. Nut-3a encapsulation

Following the optimization of the functionalization procedure for Sp-AcDEX NPs, Nut-3a encapsulation was performed by dissolving the drug in the organic solvent during the double-emulsion protocol. Its inclusion in the system did not significantly affect the basic properties of either type of particles (bare or HA-coated), as shown in Table 7 and Figure 10.

Table 7 - Physicochemical characterization of bare and HA-functionalized Sp-AcDEX NPs upon encapsulation of Nut-3a. HA percentages are presented in respect to the original polymer's mass. Measurements are displayed as means ± SD (n=6).

Washing protocol	Size (nm)	PdI	Zeta Potential (mV)
Bare NPs	191 ± 2	0.104 ± 0.030	41.7 ± 3.4
0.2% HA-NPs	223 ± 1	0.129 ± 0.010	27.5 ± 1.8
Bare NPs w/ Nut-3a	188 ± 1	0.088 ± 0.015	45.6 ± 1.3
0.2% HA-NPs w/ Nut-3a	206 ± 3	0.101 ± 0.014	34.5 ± 1.6

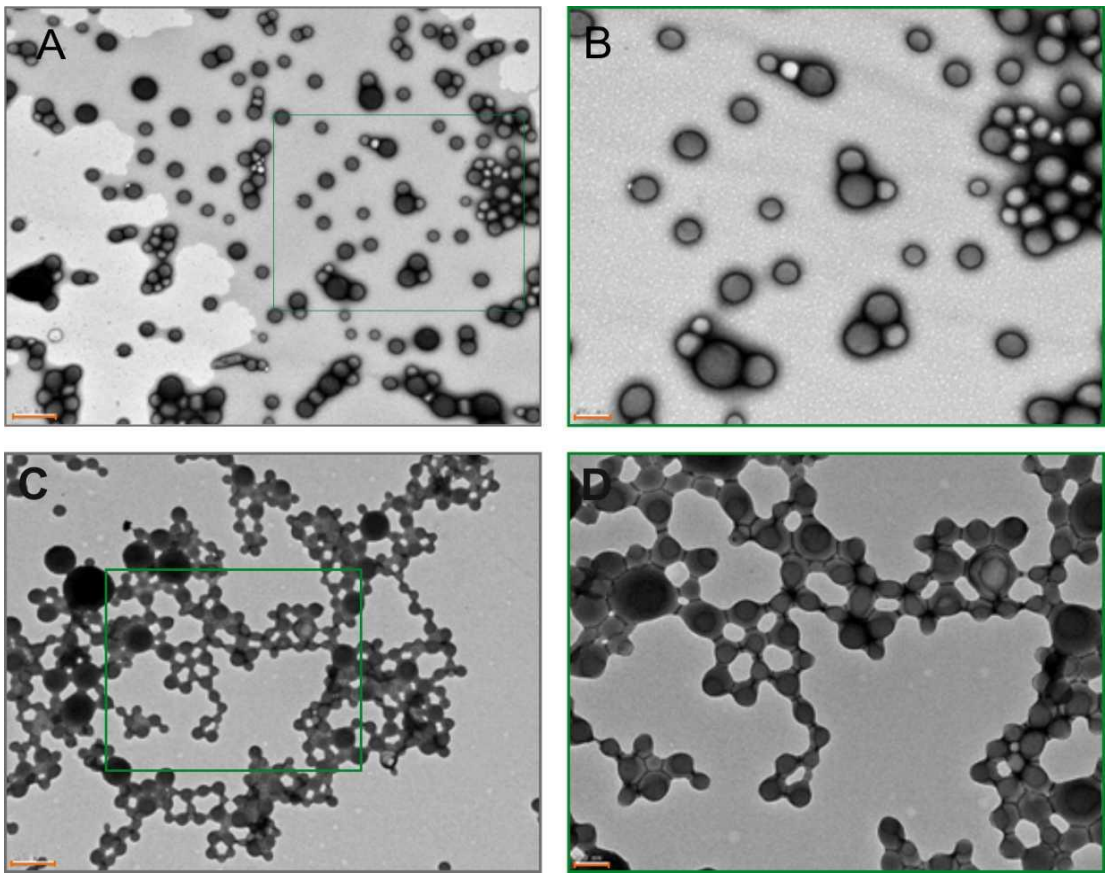

Figure 10 - TEM image of Nut-3a loaded Sp-AcDEX NPs. (A) Uncoated NPs; scale bar is 500 nm. (B) Magnification of A; scale bar is 200 nm. (C) NPs functionalized with 0.2% HA (m/m of NPs); scale bar is 500 nm. (B) Magnification of C; scale bar is 200 nm.

3.4. Cytotoxicity

When devising a nanosystem aimed at interacting with different types of cells in the organism, it is important to firstly safeguard that its elements do not possess any kind of intrinsic toxicity towards the host's own cells. In the specific case of the HA:Sp-AcDEX NPs under study, it is pertinent to assess their cytotoxicity in regard to the cells present in the TME, since a large portion of these consists of populations of non-malignant cells whose role might be vital to delay or suppress tumour progression. Therefore, NPs' cytocompatibility was individually tested in HCT116 colon cancer cells, human intestinal fibroblasts and differentiated human macrophages, as these were the cells later utilized in the construction of the spheroid tumour model. Cells were incubated with bare and HA-coated Sp-AcDEX NPs at different concentrations (50, 100, 200 and 500 μg/mL) and their metabolic activity was monitored for three days via resazurin reduction assays (Figure 11). In the case of HCT116 and macrophages, an additional experimental group where cells were incubated with medium containing free HA (in amounts equal to those of the HA existing in the functionalized NPs at each different concentration) was included. Incubation with both NP formulations did not compromise the survival of HCT116 cells for the first 72h, with these cells showing a percentage of viability above 70% for every NP concentration under test (Figure 11A). Additionally, when incubated with macrophages, NPs showed no significant toxicity at concentrations up to 200 μg/mL. Interestingly, free HA seemed to have a bigger impact on the viability of these cells than both NP formulations.; moreover, both types of NPs led to percentages of viable macrophages significantly superior to those of the untreated control at 72 h. As for HIF, the registered percentages of viable cells were concentration-dependent during the first 24 h for both types of NPs, with values below 60%, though they increased in subsequent days. Overall, the NP were proven safe towards all cell types at concentrations up to 200 μg/mL, although the results may hint at a mild degree of acute toxicity towards HIF and macrophages at 24 h only. Moreover, the inclusion of HA in the NPs did not seem to result in added toxicity towards any of the cells, regardless of day or NP concentration.

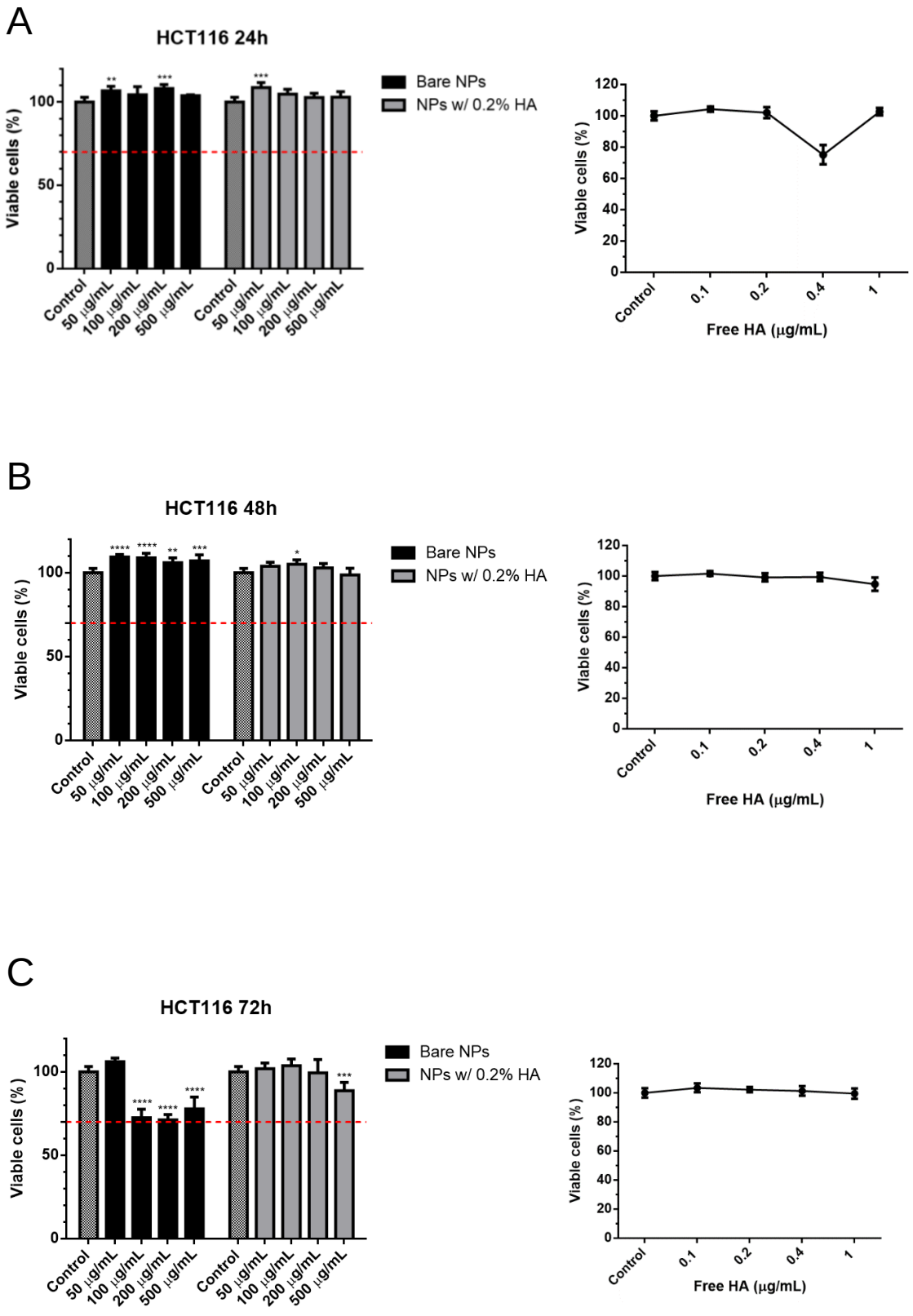

Figure 11 (cont.)

D

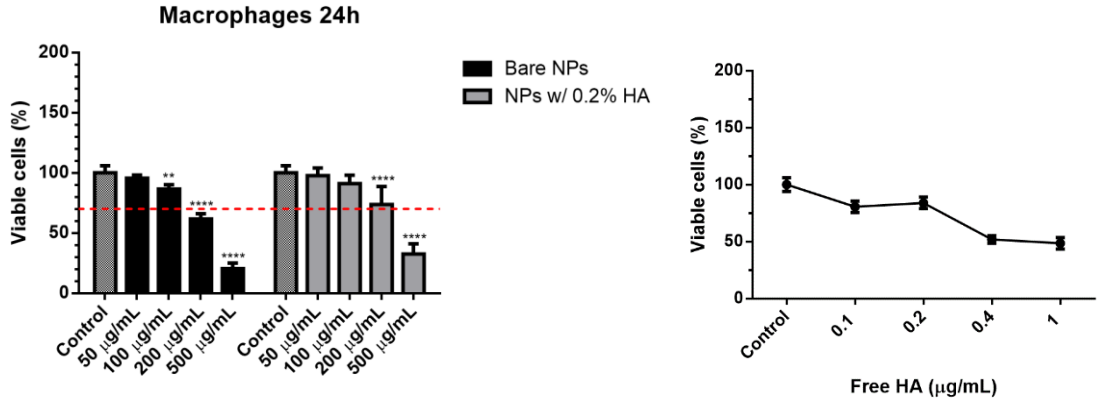

E

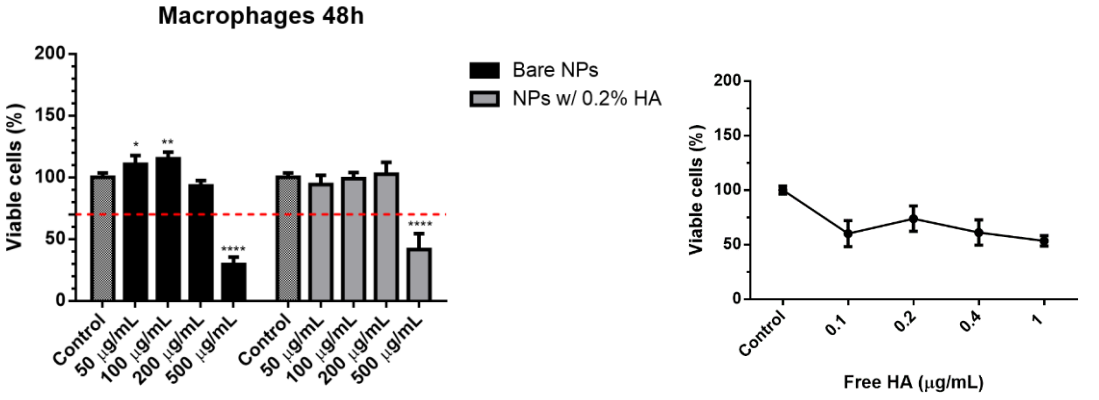

F

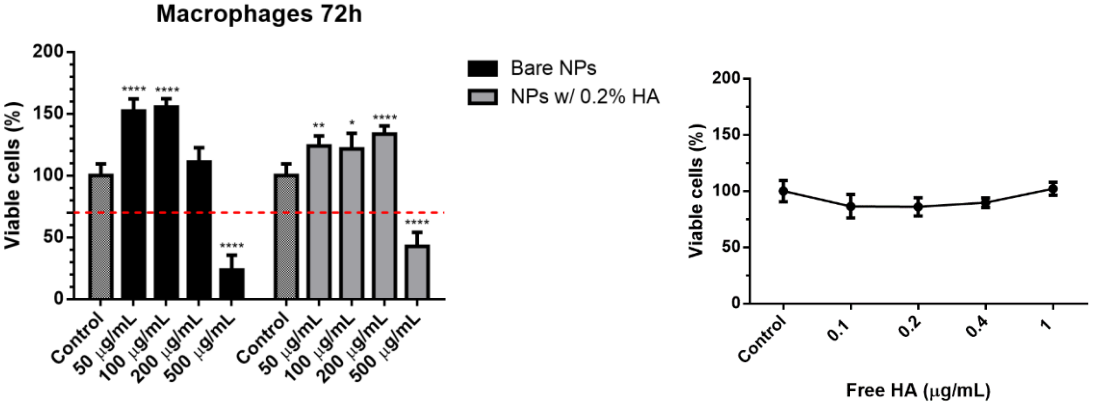

Figure 11 (cont.)

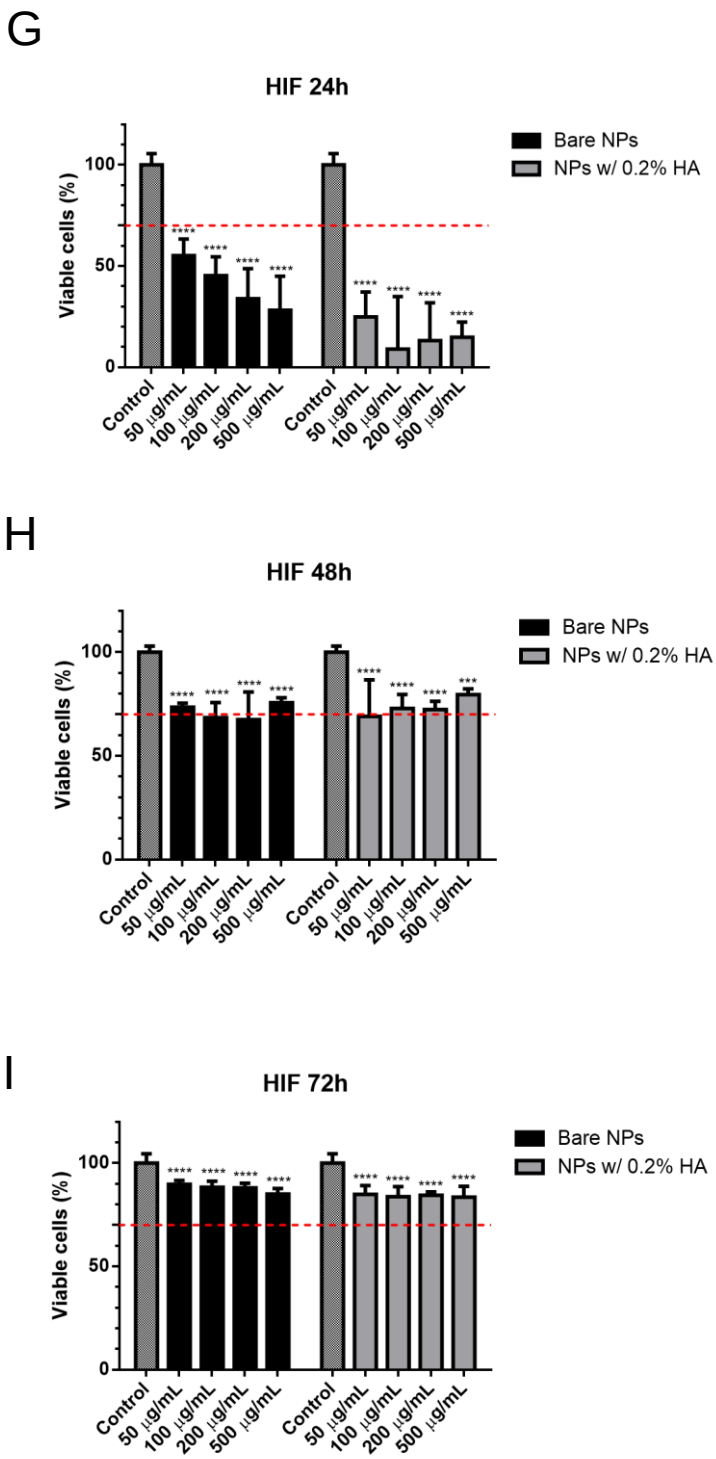

Figure 11 – Cell viability percentages of 2D monocultures of HCT116 cells, HIF and human macrophages after 24h, 48h and 72h of incubation with bare and HA-functionalized Sp-AcDEX NPs. Graphs represent the viability percentages of HCT116 cells at (A) 24 h, (B) 48 h and (C) 72 h, 7-day macrophages at (D) 24 h, (E) 48 h and (F) 72 h, and HIF at (G) 24 h, (H) 48 h and (I) 72 h. For HCT116 cells and macrophages, viability upon incubation with free HA was also evaluated, at HA concentrations matching the total amount of HA adsorbed to the NP in the remaining conditions. All samples were compared with the respective negative control (i.e. cells in culture medium). Results were analysed by two-way ANOVA, followed by Bonferroni's post-hoc test (n=6). Significance levels were defined as follows: *P<0.05, **P<0.01, ***P<0.001, and ****P<0.0001. Error bars represent mean + SD.

3.5. Spheroid production and characterization

Although 2D cultures are a practical and effective way to acquire a primary view of the basic interactions between the cells involved in the TME and the NPs under study, they hardly bear functional resemblance to the dynamics of a tumour in vivo (Cattin et al., 2018; Virgone-Carlotta et al., 2017). Therefore, and to more accurately investigate the therapeutic potential of the HA:Sp-AcDEX NPs, a multicellular spheroid model previously optimized by our group was utilized to simulate the typical cellular microenvironment present in CrC. To this end, HCT116 colon cancer cells, peripheral blood-derived monocytes and HIF were seeded in triple culture atop agarose 3D Petri Dishes® and allowed to settle into spheroid conformation. Each spheroid originally contained 5000 cells, at an established proportion of 4 human monocytes to 1 HCT116 cell to 4 HIF. Spheroids were then grown for 10 days, with their size and metabolic activity being monitored at days 1, 4, 7 and 10 (Figure 12); additional spheroid samples were collected and fixated for histological analysis at these timepoints (Figure 13). Spheroids revealed a steady increase in their average diameter over time (Figure 12A, 12B), accompanied by a similarly paced intensification in metabolic rate (Figure 12C). Interestingly, the obtained spheroids were generally heterogeneous in shape (particularly at days 1 and 4), often displaying cellular protrusions across the borders; an expanding dark region at the core of the formation could also be observed (Figure 12A), corresponding to a body of dead or quiescent cells (Desoize, Gimonet, & Jardiller, 1998) as confirmed upon examination of histological sections of these spheroids (Figure 13).

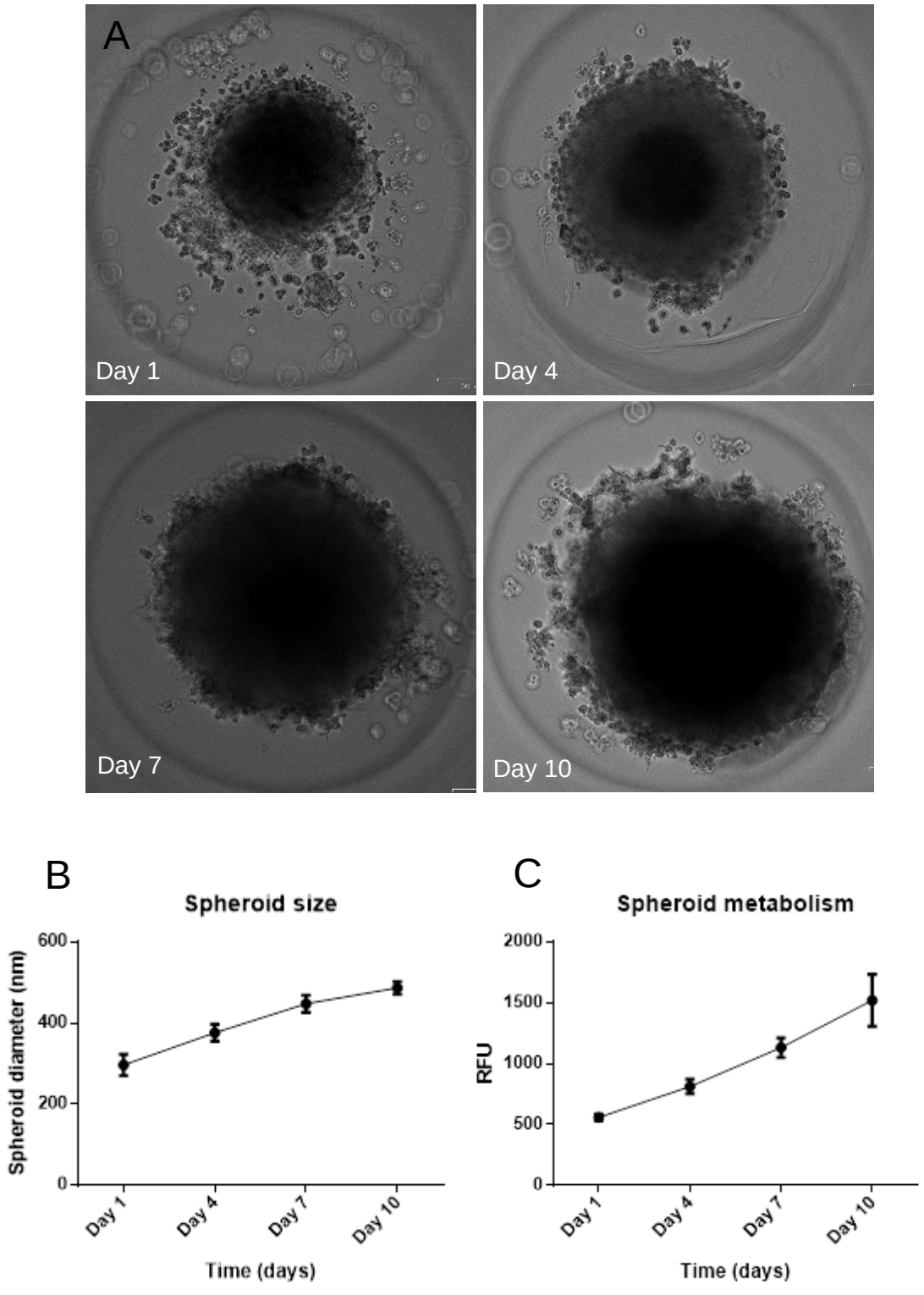

Figure 12 – Characterization of the monocyte: HCT116: HIF spheroid model. Cells were seeded at a density of 5000 cells per spheroid and an initial cell ratio of 4:1:4, and the model was characterized at days 1, 4, 7 and 10. (A) Images of the growing spheroids were captured throughout the 10 days using a ZOE Fluorescent Cell Imager. Spheroids showed positive progression in terms of (B) size (n=9) and (C) metabolic activity (n=10). 7-day spheroids were herein used for further experiments. RFU, relative fluorescence units.

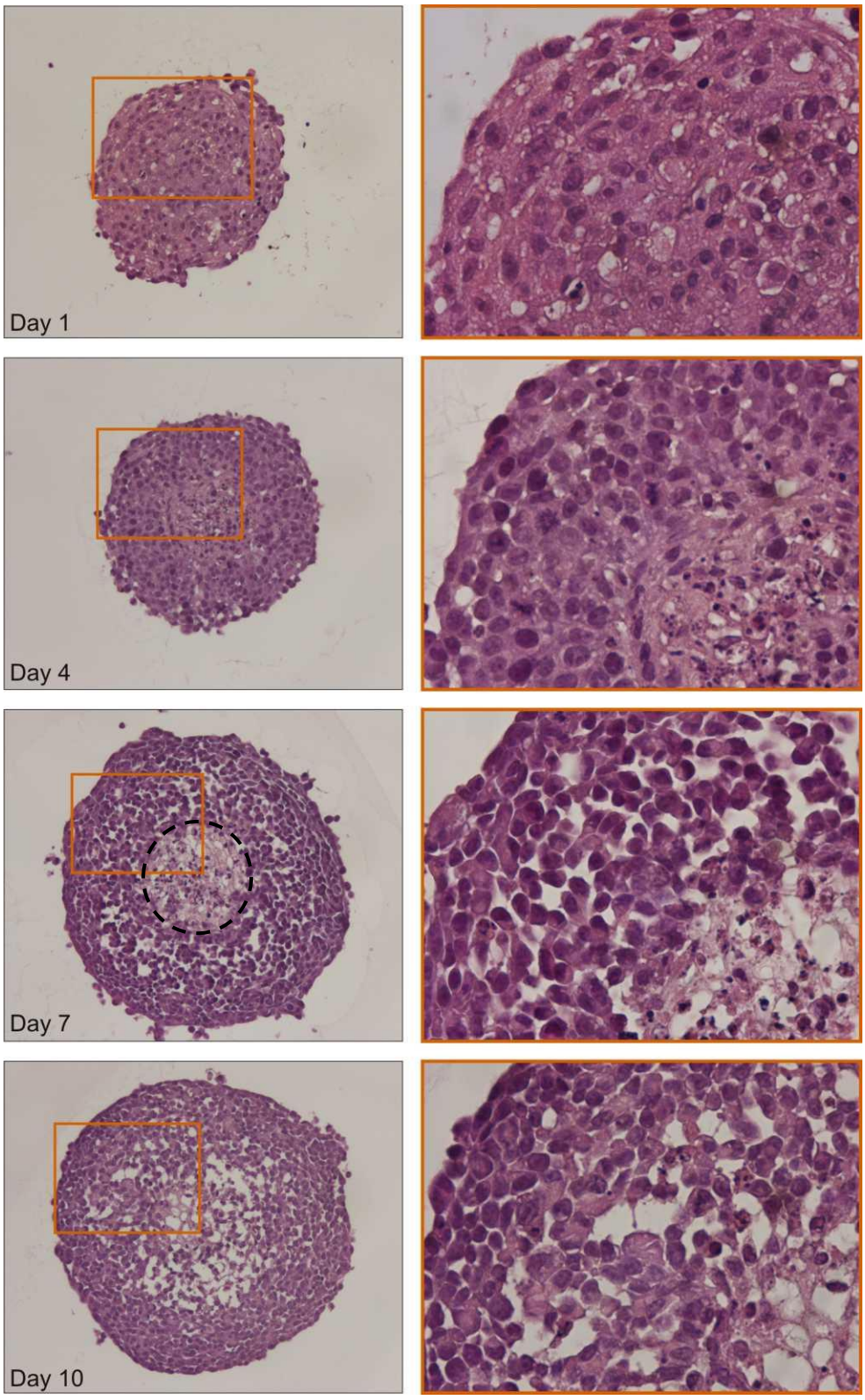

Figure 13 – H&E staining of the monocyte: HCT116: HIF spheroid model at days 1, 4, 7 and 10 post seeding. The formation of an inner, cell-depleted area at the centre of the spheroid can be observed at day 7 (dotted line) and onward, as a result of the intensive cellular necrosis taking place at this region.

3.6. Spheroid viability and antiproliferation assays

Following its characterization, the triple-culture spheroid model was used to comparatively assess the anticancer potential of bare and HA:Sp-AcDEX NPs when loaded with the non-genotoxic drug Nut-3a. In order to allow for both full differentiation and tumour-driven polarization of macrophages, and the formation of the previously observed necrotic cores, all spheroids were utilized for testing 7 days after seeding. These spheroids were individually transferred onto 96-well plates coated with agarose 2%, allowed to settle for one day and then incubated with NPs for 24 h, 48 h and 72 h. The percentage of viable cells was determined in regard to an unstimulated control via resazurin reduction assays, in order to comparatively mirror the testing configuration employed in 2D (Figure 14). The registered percentages of cell viability suffered a marked decrease when compared to the untreated control. The positive safety profile that was obtained for the particles in 2D could not be observed in the spheroid model, as both bare and HA-functionalized NPs not containing Nut-3a generated cell viability values well below the 70% threshold. Similarly, the inclusion of Nut-3a in the system did not significantly increase NPs' toxicity in regard to the remaining conditions, although a slight, consistent tendency to decrease cell survival was observed for HA-NPs containing Nut-3a in respect to bare NPs carrying the same drug. Additionally, the increase in NP concentration did not result in significant added toxicity across the three days and different conditions, and no major changes in the cellular responses were registered either throughout the days. Notwithstanding, the results were considered overall inconclusive, given the unexpectedly low percentages of cellular viability coupled to the wide discrepancies and sizeable standard deviations verified within each condition.

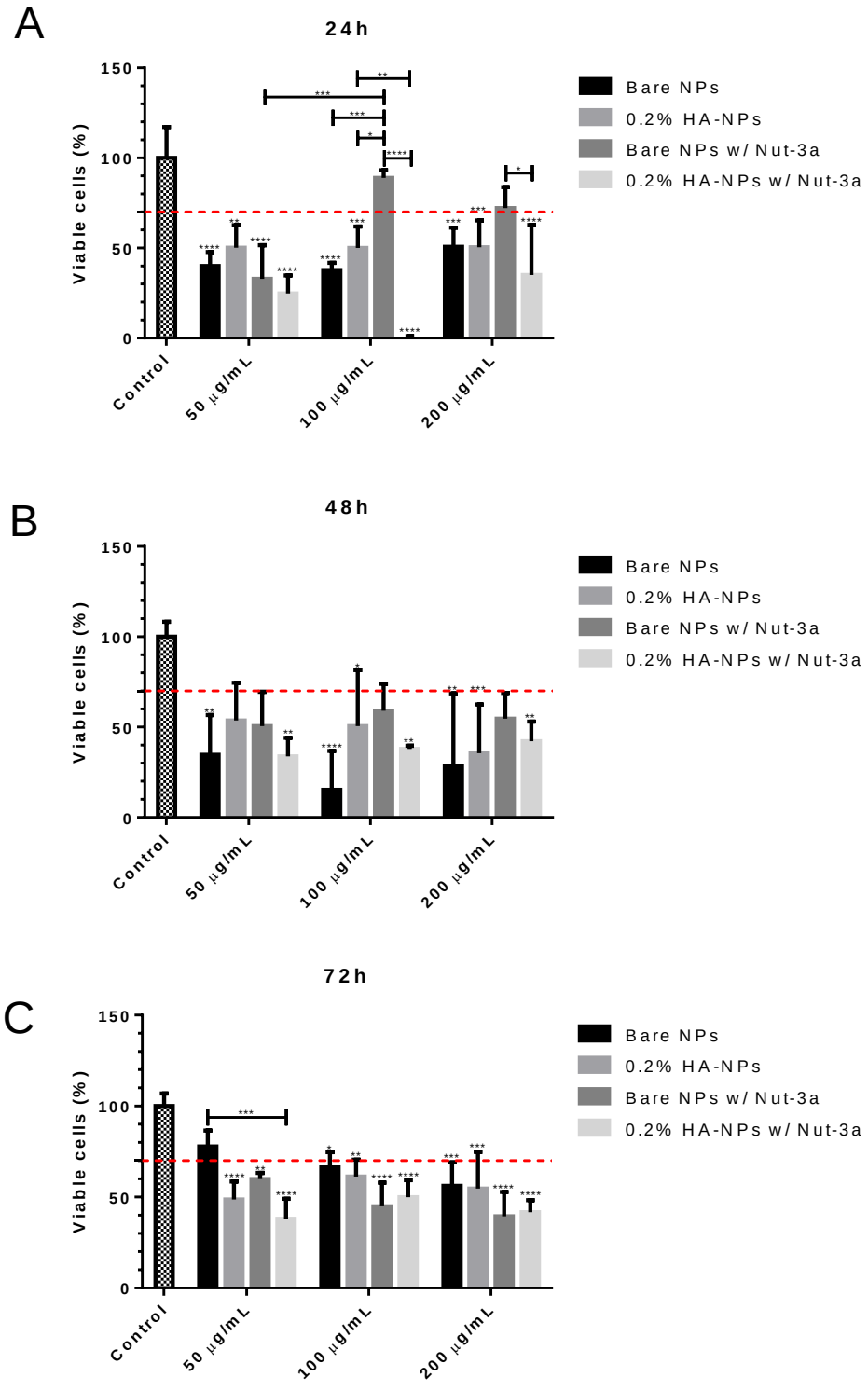

Figure 14 – Cell viability percentages of spheroids incubated with bare and HA-functionalized Sp-AcDEX NPs, with or without Nut-3a, at concentrations of 50, 100 and 200 µg/mL. Cell viability was assessed at (A) 24 h, (B) 48 h and (C) 72 h following NP incubation**.** All samples were compared with the respective negative control (i.e. spheroids in culture medium). Results were analysed by two-way ANOVA, followed by Bonferroni's post-hoc test (n=6). Significance levels were defined as follows: *P<0.05, **P<0.01, ***P<0.001, and ****P<0.0001. Error bars represent mean + SD.

3.7. NP cellular association

To better assess the viability results obtained in 3D, as well as the potential benefit of using HA as a targeting agent for Sp-AcDEX NPs, a flow cytometry assay was devised to measure NP uptake by the cells in the spheroids at different timepoints. To this end, FITC was diluted and dispersed in the organic solvent during particle preparation, in order to fluorescently tag the cells once the NPs in question were internalized. However, while the inclusion of FITC in bare NPs did not impact their physicochemical properties, its presence caused these NPs to once again form dense, insoluble aggregates during the functionalization protocol with HA (as implied by the high values measured for particle diameter and PdI in Table 8). In an attempt to obtain viable FITC-loaded NPs, the percentage of utilized HA was further reduced to 0.1% (m/m of NPs), but such decrease did not avert particle aggregation (*data not shown*). Consequently, it was only possible to test the cellular uptake of bare Sp-AcDEX NPs.

To carry out NP uptake assays, spheroids grown for 7 days were incubated with FITC-loaded Sp-AcDEX NPs at 50 µg/mL, and cellular uptake was evaluated at 3 and 24 hours following incubation. As shown in Figure 15, although there was an increase in the percentage of particles associated with cells in the spheroids between the two timepoints, this association did not exceed 10% of the total NPs at 24h. Bearing in mind that these results do not exclude particles that are merely attached to cells, and not internalized by them, the overall cellular uptake dynamics can be considered poor for the first 24h, suggesting the occurrence of a passive and slow-paced internalization process.

Table 8 – Physicochemical properties of the bare and HA-functionalized FITC-loaded NPs utilized for uptake assays. A regular batch was prepared in parallel to monitor any possible effects of the inclusion of FITC in particle stability. HA percentages are presented in respect to the original polymer mass; measurements are displayed as means ± SD (n=3).

Washing protocol	Size (nm)	PdI	Zeta Potential (mV)
Bare NPs	197 ± 0	0.143 ± 0.028	29.4 ± 1.8
0.2% HA:NPs	246 ± 3	0.176 ± 0.009	25.7 ± 1.3
FITC-Bare NPs	225 ± 1	0.191 ± 0.025	29.0 ± 1.2
FITC-0.2% HA:NPs	1240 ± 261	0.817 ± 0.108	-12.5 ± 3.5

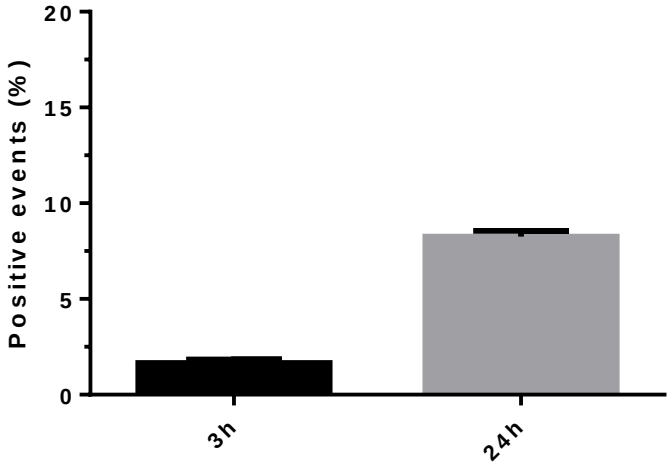

Figure 15 – Quantitative determination of the percentage of association between bare Sp-AcDEX NPs and spheroid cells. Spheroids were incubated with NPs for 3 and 24 h at 37 °C, and cells were dissociated via trypsin emersion prior to flow cytometry analysis. Error bars represent mean + SD.

IV. Discussion

One of the main challenges in CrC treatment is the safe administration of therapeutic drugs that specifically target malignant cells while exerting minimal adverse effects in the host's healthy tissues. In the current work, the therapeutic potential of a targeted nanosystem based on HA-functionalized Sp-AcDEX NPs was evaluated, along with the significance of a triple culture spheroid model as a proxy for *in vitro* drug delivery and therapy screening in the context of CrC.

The advantages of Sp-AcDEX NPs have been described by our group in previous works (Bauleth-Ramos et al., 2017). Given the properties of acetalated dextran, these NPs have the inherent ability of maintaining their conformation at physiological pH, but degrade upon contacting with acidic environments such as those of the tumours - thus promoting a pH-responsive release of their cargos (E. M. Bachelder et al., 2017). The modification of the polymer with cationic spermine bestows the particles with a strongly positive charge, improving their stability and enabling interactions with the negatively charged cell membranes, facilitating internalization. Furthermore, being prepared via a double-emulsion technique, the utilized particles encompass both a hydrophilic core and a hydrophobic body, allowing for the co-encapsulation of therapeutics with diverging physicochemical properties. For instance, the hydrophobic drug Nut-3a acts as a stimulator of the cell cycle inhibitor p53 by sequestering its negative regulator MDM2, and can be incorporated into the hydrophobic phase of these particles. Although only Nut-3a was encapsulated into the particles in the current study, the system harbours the additional potential to co-encapsulate a variety of hydrophilic immune modulators such as IFN-γ or the macrophage stimulator GM-CSF in its inner core (Bauleth-Ramos et al., 2017; Kyle E. Broaders et al., 2009). By formulating these particles for *in situ* cancer vaccination, a powerful combined anticancer effect - guided on the one hand by the induction of apoptosis in cancer cells, and on the other by the stimulation and differentiation of immune cells with an effector function - could be promoted (Bracci et al., 2014). Therefore, said NPs are regarded as a promising agent for specialized chemoimmunotherapy in the context of CrC.

It is important to note however that the therapeutic delivery envisioned by this system relies solely on the EPR effect to promote tumour accumulation, and the acidic environment of the TME as a trigger for particle degradation and drug release. While the favourable uptake of these particles by cancer cells has been previously demonstrated (Bauleth-Ramos et al., 2017), there is still a risk of unspecific uptake by healthy cells, which could generate harmful consequences for the patient. Therefore, in the present work, the known interaction between the polysaccharide HA and the surface receptor CD44 – which is overexpressed in cancer cells (and CSCs in particular), and also present

in macrophages and other immune cells - was exploited as a targeting system. While the main advantage of this strategy rests in specifically directing the aforementioned NPs towards tumoral populations to exert their Nut-3a-mediated cytotoxic action in a more controlled way (negating hazardous side effects on the host's healthy cells), it may also serve the immunostimulatory component of the therapy by delivering designated immune stimulators to macrophage populations within the tumour. Of note, the ability to target CSCs is particularly valuable in anticancer therapies, as the enhanced resistance and self-renewal capacity of these cells usually enable them to circumvent (or simply remain inaccessible to) traditional interventions, while fuelling the growth and dissemination of new tumour cells after a portion of these cells are eliminated by therapeutics or the organism itself (Hanahan & Weinberg, 2011; Reya et al., 2001). CSCs are also believed to be responsible for the sustenance of distant metastasis, which bear critically worse prognosis among typical cases of CrC (Reya et al., 2001).

Functionalization of NPs with HA has been previously reported in the literature through a number of procedures (Salis et al., 2016). However, most protocols tend to carry out these reactions in acidic buffers (such as acetate, at pH 5.5), where both HA and other reagents present increased stability, improving the reaction yield. Conversely, due to AcDEX being pH-sensitive and degrading upon contact with acidic environments, it became necessary to investigate whether the same procedure could be executed under more neutral/alkaline conditions.

As could be expected, the introduction of HA in the previously optimized Sp-AcDEX NPs initially reduced its overall stability by promoting undesirable particle aggregation. Such instability became evident upon detection of significant increases in average size and PdI in newly functionalized NPs. Of note, aggregation seemed to also have an effect in NPs' surface zeta potential, which tended to drop to neutral or negative values when the former was verified at a significant scale. Since stable HA-coated NPs were unobtainable when performing the coupling reaction in 10 mM HEPES at pH 8.0, it was imperative to carefully optimize the procedure in order to create favourable conditions for the adsorption of HA onto these NPs. While it was possible to obtain acceptable values for particle size and PdI when casting the reaction in MES buffer at pH 7.2, working at these conditions represented a clear compromise of effectiveness in HA adsorption in detriment of conserving the stability of the original NPs as much as possible. Nonetheless, even if at lower yield, HA functionalization was ultimately achieved with success under said settings.

Following the rationale of improving the functionalization conditions across all stages of the procedure, it also became necessary to optimize the method for NP washing, where most particle aggregation was taking place. While lowering the centrifugation velocity would be a logical route to this goal, it would be undesirable to risk the loss of higher amounts of NPs in the process. One auspicious strategy to improve this scenario was the use of Amicon® Ultra Centrifugal Filters, allowing for higher rates of sample concentration and recovery at lower centrifugation speeds. While primary assays with these filters offered acceptable results, as shown in Table 4, their reutilization in subsequent functionalization attempts surprisingly contributed to intensify the previously described aggregation phenomena. Moreover, close inspection of these filters revealed accumulations of NP debris that could not be recovered (thus severely decreasing the yield of the process), and which promptly compromised the integrity of the membranes. Considering that ultracentrifugation at lower velocities, despite also lowering the amount of recoverable NPs, was rather successful at averting particle coalescence, higher particle yields were ultimately sacrificed in favour of bypassing NP aggregation. Consequently, washings were thus performed by ultracentrifugation at 11000 rcf henceforth.

The amount of HA used to functionalize the particles was one of the most important and delicate variables to tune, since minor variations in HA concentration often caused dramatic changes in terms of aggregation, as shown in Table 5 and Figure 9. The degree of success in the functionalization protocol was evaluated mainly according to the alterations in the NPs surface charge, since the adsorption of anionic HA chains is expected to decrease this value in comparison to the highly positive zeta potential observed for bare NPs. While this reduction end up not being as flagrant as originally anticipated, it may still represent an overall advantage for the system, as it allows particles to conserve their positive charge, thus favouring their interaction with cell membranes. Interestingly, a clear shifting point in the behaviour of the nanosystem was observed when carrying out HA adsorption at 0.3% of the total polymer mass, as it was consistently impossible to obtain monodisperse particles at superior HA concentrations. Likewise, NP functionalization was eventually implemented at 0.2% HA, with this being the highest tested concentration favouring stable adsorption while still avoiding particle aggregation. Although this adsorption technique is simple and effective, it does not however provide control over the actual amount of HA interacting with the particles or the strength of such interactions. As a result, it was hypothesised that promoting HA linkage through a specific form of chemical conjugation could improve the effectiveness of particle functionalization. One attractive property of this system resides in the fact that

the carboxyl groups present in the side chains of HA could easily bind the primary amines existing in the spermine molecules through a simple carbodiimide conjugation reaction. Therefore, an EDC-NHS mediated carbodiimide conjugation was also attempted as a functionalization strategy in order to investigate whether the same NPs could be produced under a more stable and tuneable reaction. As evidenced in Table 6, the NPs obtained by this methodology showed an approximate size of 250 nm and PdI values lower that 0.2, with no signs of aggregation. However, there was also no tangible indication of successful functionalization, since no significant alterations in respect to the physicochemical properties measured for control particles could be detected. In comparison, NPs functionalized by adsorption in the same assay exhibited a marked increase and decline in size and zeta potential (respectively), as would be expectable for an effective HA coating. Interestingly, passive HA adsorption should still take place when the EDC-NHS conjugation reaction is being carried out, so even if this reaction fails it would be expectable for the NPs in question to acquire similar properties to those where only HA adsorptions were performed. Remarkably, in the present assay, such assessment could not be verified.

One hypothesis to explain the lack of success in this functionalization route is tied to the low amounts of utilized EDC and NHS, which were dosed in accordance to the working masses of the remaining reagents and may not have been sufficient to bind a significant amount of HA. On the contrary, increasing the concentrations of EDC and NHS while maintaining the other conditions resulted in particle aggregation (*data not shown*). Overall, it is conjectured that EDC-NHS coupling reactions are typically more suitable at higher concentrations and working volumes of NPs and respective ligands, as opposed to the small values employed in the present study, which aimed to maximize particle stability. Moreover, and considering the particles' natural tendency to coalesce in the presence of small amounts of HA, it can be reasoned that the ionic forces driving the regular charge-based adsorption of HA to NPs are sufficient to properly guide the desired functionalization, thus dispensing the covalent bonding promoted by the carbodiimide conjugation reaction. Furthermore, when analysing the present reaction more deeply, another characteristic of this particular application that may limit the success of the current functionalization technique is the fact that the carboxyl groups are present as side chains of the HA molecules, and not at their terminus. As a result, not only is it impractical to control the stoichiometry of the reaction (since the number of carboxyl groups available to react equals the number of individual HA residues present in each polymeric chain, whose length varies), but it is also possible for multiple spermine molecules across different NPs to bind a single HA chain along its repetitive residues –

thus establishing covalent bonds between various particles and inadvertently causing them to aggregate. Consequently, considering its demonstrated simplicity and effectiveness, HA adsorption (under the previously optimized conditions) was elected as the functionalization strategy to follow for the rest of the work.

Once adequate values for the quality parameters of HA:Sp-AcDEX NPs were obtained, the optimization procedure was concluded and these particles were submitted to *in vitro* cellular assays. Considering the NPs' original design foreseeing their administration in the TME, it was reasonable to contemplate not only their effect on tumour cells themselves, but also their potential impact on other cell types commonly present at cancer sites. In the current study, primary cultures of both human macrophages and intestinal fibroblasts were thus utilized alongside the HCT116 colon cancer cell line, and these three cell types configured the main testing platforms for the developed particles, both in 2D and 3D.

NP-cell interactions were firstly assessed in flat monocultures, so as to obtain primary insights regarding the eventual toxicity of the utilized materials and techniques. According to Figure 11, both bare and HA-functionalized NPs could be deemed generally safe, with only HIF registering significant declines in respect to the acceptable threshold of viability (established at 70%), at 24h following NP incubation, and macrophages exhibiting similar tendencies at higher NP concentrations. These results were overall expected, as the cytocompatibility of AcDEX and HA has been attested multiple times in past works (E. M. Bachelder et al., 2017; Choi et al., 2009; Mattheolabakis et al., 2015) – thus enabling the safe inclusion of the designated HA:CD44 targeting strategy into the system. It is important to address the fact that the relative percentages of cell viability were quantified according to their metabolic activity, which in turn was determined through a resazurin reduction assay. This test rests on the principle that resazurin, a minimally-toxic blue fluorometric indicator that passively permeates the cell membrane, can be reduced to resorufin, a stable pink compound whose fluorescence can be measured, by metabolically active cells; such reaction can be carried out by mitochondrial or microsomal enzymes, for instance, among others that participate in normal cells' metabolism, generally using NAD(P)H as the electron donor (Präbst, 2017). A higher fluorescence intensity thus represents a globally more intense cell metabolic activity, and can be correlated to higher density in viable cells. However, it is important to stress the fact that it is metabolic activity – and not cell viability itself – that is being measured in this assay; likewise, the connection between these parameters may not be as evident as originally assumed, since a shift in metabolic activity may be associated with a mere response to cellular stress, and not necessarily imply a linearly equivalent

amount of cell death. Moreover, apoptosis is an energetically active process in cells, often taking place at the expense of ATP molecules, with subsequent intensification of metabolic activity (Green, Galluzzi, & Kroemer, 2014).

After safeguarding the globally non-cytotoxic profile of the developed NPs, the interest shifted to evaluating its therapeutic potential in a more reliable and informative model, capable of replicating the geometry, composition and main biological interactions characteristic of the TME. To this end, the previously employed cell types were assembled into spheroid configuration, and the seeding ratio of 4:1:4 (monocytes:HCT116 cells:HIF) was established in order to account for the very low duplication time of the HCT116 cancer cells (~20h), and also to confer higher significance to the biological role of non-tumour cells in the microenvironment. As depicted in Figure 12, these spheroids presented a steady and continuous growth in size that was consistent with the recorded metabolic activity throughout the days. The formation of the aforementioned necrotic cores was previously observed (Figure 13) and is characteristic for spheroids with over 300 μm in diameter. These structures stem both from the poor accessibility of oxygen and nutrients to cells located at the centre of the spheroid, and the accumulation of toxic metabolites in these zones – thus recapitulating the *in vivo* scenario in a pertinent way (Desoize et al., 1998; Wang et al., 2017). Another observed feature was the irregular shape of spheroid borders, coupled to the existence of small cellular populations on the outskirt of the main congregate body. While spheroids tend to be almost perfectly round-shaped when cast in monoculture, these differences can be owed to one of the cellular types not being able to properly integrate the spherical conformation, as previous works with co-culture spheroids reveal that the inclusion of macrophages, for instance, often disrupts the morphology of the spheroids are observed herein (Susanti et al., 2018). Another alternative relates to the early manifestation of metastatic cues prompting cells in the periphery of the tumour to proliferate outwards; fluorescently tagging each cell type with specific markers prior to spheroid analysis through confocal microscopy could shed some light onto this matter.

Another important element contemplated by the present 3D model are the natural interactions between cells and certain environmental aspects that can also be observed within real-life tumours. For instance, the inclusion of fibroblasts is in great part responsible for an augmented secretion of ECM components, which contribute to replicate *in vivo* cellular concatenation and stimulation via mechanoreceptors while conferring mechanical stability to the structure. Another example lies on the utilization of the spheroids at the 7th day post-seeding, allowing for both the formation of the observed necrotic cores (Figure 13) and the full differentiation of monocytes into macrophages

(under the stimuli of M-CSF). By promoting this process in the presence of cancer cells (instead of culturing previously differentiated macrophages, for example), it is expected that these macrophages may be induced by diverse biochemical stimuli to adopt the immunosuppressive phenotype characteristic of TAMs, allowing for a more authentic representation of these cells in the TME (which should be of paramount importance when carrying out immunomodulatory assays, among others).

Overall, and despite not mimicking every intrinsic aspect of the TME, the developed model was initially regarded as a strong, suitable platform to test the nanosystem at hand. However, upon evaluating the antiproliferative effect of Nut-3a-loaded NPs (with and without HA) on the spheroid model, the results attributed these particles a severe degree of toxicity, that was verified across all timepoints, all concentrations and independently of the presence of Nut-3a. Such observations are highly inconsistent with the conclusions provided by 2D studies, which only hinted at NPs toxicity at the highest tested concentration (or, in the exclusive case of HIF, at lower concentrations in the first 24h); moreover, given this possibility of particles manifesting cytotoxicity at 500 μg/mL in 2D, NP concentration was capped at 200 μg/mL for viability studies in 3D. One interpretation for these results follows the hypothesis that HCT116 cells, despite being the population originally cultured at the lowest cell density, are still able to surpass the other cell types in terms of proliferation and eventually dominate the spheroid environment. Considering that Nut-3a acts as an MDM-2 antagonist, thus promoting p53-mediated apoptosis in cancer cells, it would be expectable for particles loaded with this drug to have a marked antiproliferative effect if spheroids were indeed mainly composed of cancer cells (as the drug is normally non-toxic to healthy cells) (H. Janouskova et al., 2013; Vassilev et al., 2004). While such explanation could justify the low percentage in spheroids treated with Nut-3a-containing NPs, as well as the marginal decrease in viability observed for HA-coated particles containing the same drug (indicating the effectiveness of the targeting strategy), it does not explain the low viability observed for unloaded NPs, especially when considering that these particles showed minimal toxicity against HCT116 cells in flat cultures. A more plausible explanation relates instead to the questionable validity of resazurin reduction assays to measure cell viability in spheroids. In truth, this compound is likely unable to penetrate the densely packed and reticulated cell layers of the spheroids, which would in turn explain the massive variability in viability observed between spheroids under the same conditions. While the aforementioned problems with these assays are still valid in 3D, they are further aggravated by the fact that a high number of cells are naturally under stress due to the geometry of the spheroid itself, which deprives the innermost cells of free access

to nutrients and oxygen; therefore, although high ratios of dead or quiescent cells are contemplated by this assay, these percentages cannot be attributed to the action of the drug or the particles alone – hence biasing the implicit correlation between metabolic activity and cell viability.

To further examine the significance of NPs' toxicity towards spheroids, the uptake of these particles was studied and quantified in the same model. To this end, fluorescently tagged NPs were produced after dissolving FITC into the hydrophobic phase of the system, but an intensive particle aggregation problem prevented their further functionalization with HA (Table 8). FITC-loaded Sp-AcDEX NPs were subsequently incubated with spheroids for 3 and 24 hours, but no major shifts in cellular fluorescence intensity were observed in regard to control, with particles showing percentages of internalization inferior to 2% at 3h and 9% at 24h. Such values may express the particles' physical inaccessibility to the majority of the inner cells in the spheroids, owing for instance to the densely reticulated ECM hindering NP penetration in this model (Nyga, Cheema, & Loizidou, 2011). These results also contradict the high degree of particle toxicity revealed in the previous test, since it is not plausible that particles initially regarded as generally safe before all three utilized cell types are able to exert such powerfully cytotoxic effects while bearing minimal internalization rates. Although there is room to question the validity of the techniques utilized to assess the antiproliferative effect of the NPs in the spheroid model (as detailed above), it is equally important to acknowledge the need for further optimization of protocols in the present assay as well. In fact, in order to dissociate the cells prior to FACS analysis, spheroids had to be immersed in trypsin for 30 minutes, so as to overcome the densely reticulated matrix sustaining the spheroid structure. Trypsin is a serine protease that cleaves the amino acids lysine and arginine found at certain cell-cell junctions and focal adhesions, thereby contributing to separate aggregated cells or detach them from ECM components. However, prolonged exposure to trypsin is highly toxic for the cells, and doing so in order to dissociate the spheroids may compromise the viability of their cellular components in an insidious way, possibly distorting the results of this test.

The mechanisms underlying NP uptake by cells are currently poorly understood, but are known to vary between clathrin or caveolae-mediated endocytosis, (macro)pinocytosis and phagocytosis in the case of bigger particles (~ 250-300 nm in diameter) (Foroozandeh & Aziz, 2018); moreover, aspects like particles' size, charge, shape and surface chemistry are preponderant factors in dictating the success of NP uptake and its biological route (Foroozandeh & Aziz, 2018). While the positive surface charge of the particles utilized in this study (both bare and HA-coated) favours their

interaction with the negatively charged cell membranes, their average diameter slightly exceeds the recommended size range for anticancer applications (Peer et al., 2007). In fact, one aspect hindering particle uptake by the spheroid cells is likely to relate to the poor accessibility of these NPs to cells located in inner layers of these structures – a scenario that could possibly be improved upon reducing the size of the particles under study. In light of the poor uptake rates observed for bare particles at 24h, it may be hypothesized that the incorporation of HA onto the surface of particles to promote CD44 targeting would indeed be a valuable asset to include in the present nanosystem, as particle internalization at a whole-tumour scale seems currently lacklustre. However, considering that functionalization of Sp-AcDEX NPs consistently brought about a marginal increase in the particles' average hydrodynamic size, HA-coated particles may still face a bigger challenge in penetrating the spheroid body rather than in entering the cells – which would in turn render the CD44 targeting ineffective. Nevertheless, a recent study using magnetic Fe_3O_4 NPs of different sizes reported greater retention and accumulation of larger sized particles in tumours (mainly due to the reduced migration rate of these NPs, preventing them of exiting the tumour) (Guo et al., 2016). Definitive disclosure regarding the effect of NP size in the current system can therefore only be attained upon further optimization of the functionalization conditions, in order to produce fluorescently-tagged HA:Sp-AcDEX NPs that can be utilized for additional uptake assays.

V. Final Remarks and Future Perspectives

The implementation of a HA:CD44-mediated targeting strategy in the nanosystem described in this work proved to be a challenging task, in virtue of the low colloidal stability attained by the resulting NPs, which frequently caused them to aggregate and precipitate during the coating procedure. In order to avert the persistent aggregation experienced by these NPs, it was ultimately necessary to sacrifice a potentially higher reaction yield, with lower degrees of functionalization and superior losses of NP mass upon washing. Nevertheless, is was possible to successfully produce HA:Sp-AcDEX NPs with consistency upon optimization of the protocol.

Two variables whose meticulous adjustment was vital for the success of this technique were the centrifugation velocity during washes and the amount of utilized HA. Regarding the former, higher velocities, implying more intense centripetal force, naturally predispose NPs to more frequently collide and coalesce; as for the latter, it was evidenced that HA, due to its naturally long anionic chain, is prone to establish electrostatic interactions with the positive bulks of several NPs at once, bringing them together and eventually resulting in their aggregation. It was therefore crucial to determine an ideal concentration of HA that was sufficiently high to display positive association with the NPs, but simultaneously low enough to avoid reticulating numerous NPs through non-specific interactions; such setting was appropriately accomplished upon adjusting the total mass of HA to 0.2% of that of the NPs. Importantly, a pertinent follow-up test to further characterize the HA:Sp-AcDEX NPs would be to formally assess their long term colloidal stability in comparison to bare particles, by for instance monitoring changes in their PdI throughout previously established timepoints. FITC loading severely interfered with the success of functionalization in these NPs, and while the reasons for such interaction remain elusive, additional insight regarding NP stability could be vital for understanding these differences, and even determining the necessity for further particle optimization.

On another note, the differences between the cellular responses elicited by NPs when tested in flat and spheroid cultures highlighted the functional discrepancies between the two models. On the first case, 2D viability assays showed that both bare and HA-functionalized NPs exerted minimal toxicity overall when individually cultured with each of the contemplated cell types – demonstrating that none of the polymers or reagents (or even the nanoparticulate conformation itself) poses any intrinsic risk to these cells. However, flat cell monocultures failed to replicate with fidelity cancer-associated features like cell morphology and physiology, nutrient flow, oxygen perfusion, accumulation of metabolites, tumour geometry, ECM biochemical properties, immune cell priming and metastatic cues, among others - which are essential to properly recapitulate the TME *in vitro*. When integrating all these variables into triple-culture

MCTS on the other hand, the same NPs vastly limited the proliferation of cells in the spheroids (regardless of Nut-3a encapsulation), while displaying residual association rates towards these cells during uptake assays. Following the inherent inconsistency between these observations and the safety profile established for the NPs in 2D, along with the predicament in functionalizing FITC-loaded Sp-AcDEX NPs, it was impossible to determine whether HA functionalization and active CD44 targeting significantly favoured NP uptake and its therapeutic efficiency. As a result, the therapeutic benefit of Nut-3a-loaded HA:Sp-AcDEX NPs could not ultimately be confirmed in this study.

Notwithstanding, the *in vitro* assays with the present nanosystem still provided important insights concerning the biological significance of the utilized spheroid model in regard to traditional flat cultures. In fact, by simultaneously incorporating epithelial cancer cells, intestinal fibroblasts and macrophages previously subjected to alternative polarization, these spheroids reproduce a cellular milieu that qualitatively resembles those of *in vivo* tumours. The natural coexistence of these cells in the same spheroids contributes to recapitulate the intercellular interactions that shape the TME, eventually inciting cancer cell proliferation/dormancy, immune suppression of macrophages or secretion of ECM components by fibroblasts (with the latter possible causing the observed physical hindrance of NP delivery to inner cell layers, for instance). Such multifactorial mimicry, either directly or indirectly, of real cancer-associated elements and processes is what makes these MCTS more appealing in terms of *in vitro* significance relatively to 2D models. Of note, such assessment does not in any way entirely exclude the biological value of 2D assays, as these generally still hold the advantage over 3D cultures in terms of simplicity and time efficiency for elementary studies with simple endpoints.

It is important to stress, however, that despite adequately portraying both the closely packed tri-dimensionality, multiple cellular types and hypoxic regions in the TME, the utilized model does not contemplate certain key features such as tumour vascularization, chemotactic cues and extensive immune landscapes (since only monocytes were represented from the wide spectrum of leucocytes observable in the tumour). Nonetheless, such limitations do not necessarily invalidate eventual inferences regarding NP cellular response or the dynamics of anticancer drug delivery; in truth, achieving complete *in vitro* fidelity to the clinical presentation of CrC would be a daunting task, and likely unfeasible in a practical sense. Instead, the success in designing these models hinges on clearly establishing the purposes of the study and the variables under scrutiny, in order to accordingly determine which aspects should be prioritized in detriment of others and which output variables should be collected to produce comparable and reproducible results. More importantly, this study showed that refining

and adapting suitable protocols and cell culture techniques to the model at hand is just as critical as developing the model itself, as more robust and intricate platforms naturally demand more delicate and sophisticated procedures than the ones employed. For instance, it is unlikely that resazurin reduction assays constitute an appropriate method to assess the proliferation of spheroid cells, or that prolonged trypsinization represents a reliable process to dissociate cells in the spheroid, as was previously pointed out; it is even possible that factors like these can have compromised, at least in part, the results obtained in such assays. Therefore, two ways to improve these tests could entail measuring cell viability through bioluminometric quantification of ATP (which is correlatable to the number of viable cells), in the first case, or utilizing an enzymatic cocktail (composed of collagenases, elastases, etc.) to digest the main components of the ECM holding the spheroids together in the second one (instead of simply targeting cell-cell adhesions via trypsinization).

On a final note, although the reported HA:Sp-AcDEX NPs represent a promising concept as a vehicle for chemoimmunotherapy aiming to halt tumour progression and promote cancer cell death in CrC, much work remains to be done to validate their therapeutic potential. Following further NP optimization in the future (allowing for stable loading of fluorescent probes), it would be interesting to attempt the co-encapsulation of Nut-3a and an immunostimulatory cytokine like IFN-γ in HA-functionalized NPs, as well as evaluating the encapsulation efficiency and release kinetics of both molecules (thereby completing the originally envisioned formulation of targeted, pH-labile NPs with specialized chemoimmunotherapeutic anticancer action). Meanwhile, the described triple-culture spheroid model could also be further characterized through techniques like flow cytometry and confocal microscopy, in order to quantify the individual populations of each cell type within 7-day spheroids. Bearing this knowledge, and upon regularizing and slightly adjusting the model's handling protocols, the effects of these co-loaded NPs could again be tested in the model, along with the efficiency of HA functionalization in contributing to increased NP uptake and tumour-restricted cytotoxicity. Finally, in a later stage, the effectiveness of this strategy in macrophage repolarization and M1 differentiation could also be evaluated in the present model, by assessing cell activation markers and cytokine release.

VI. References

Antoni, D., Burckel, H., Josset, E., & Noël, G. (2015). Three-Dimensional Cell Culture: A Breakthrough in Vivo. *International Journal of Molecular Sciences, 16*, 5517-5527.

Bachelder, E. M., Beaudette, T. T., Broaders, K. E., Dashe, J., & Frechet, J. M. (2008). Acetal-derivatized dextran: an acid-responsive biodegradable material for therapeutic applications. *J Am Chem Soc, 130*(32), 10494-10495.

Bachelder, E. M., Pino, E. N., & Ainslie, K. M. (2016). Acetalated dextran: a tunable and acid-labile biopolymer with facile synthesis and a range of applications. *Chemical reviews, 117*(3), 1915-1926.

Bachelder, E. M., Pino, E. N., & Ainslie, K. M. (2017). Acetalated Dextran: A Tunable and Acid-Labile Biopolymer with Facile Synthesis and a Range of Applications. *Chem Rev, 117*(3), 1915-1926.

Bae, Y. H. (2009). Drug targeting and tumor heterogeneity. *J Control Release, 133*(1), 2-3.

Bajetta, E., Di Bartolomeo, M., Somma, L., Del Vecchio, M., Artale, S., Zunino, F., . . . Buzzoni, R. (1997). Doxifluridine in colorectal cancer patients resistant to 5-fluorouracil (5-FU) containing regimens. *European Journal of Cancer, 33*(4), 687-690.

Baselga, J. (2002). Why the Epidermal Growth Factor Receptor? The Rationale for Cancer Therapy. *The Oncologist, 7*(suppl 4), 2-8.

Bauleth-Ramos, T., Shahbazi, M.-A., Liu, D., Fontana, F., Correia, A., Figueiredo, P., . . . Santos, H. A. (2017). Nutlin-3a and Cytokine Co-loaded Spermine-Modified Acetalated Dextran Nanoparticles for Cancer Chemo-Immunotherapy. *Advanced Functional Materials, 27*(42), 1703303.

Bauleth-Ramos, T., Shahbazi, M. A., Liu, D., Fontana, F., Correia, A., Figueiredo, P., . . . Granja, P. (2017). Nutlin-3a and Cytokine Co-loaded Spermine-Modified Acetalated Dextran Nanoparticles for Cancer Chemo-Immunotherapy. *Advanced functional materials, 27*(42), 1703303.

Bilati, U., Allemann, E., & Doelker, E. (2003). Sonication parameters for the preparation of biodegradable nanocapsules of controlled size by the double emulsion method. *Pharm Dev Technol, 8*(1), 1-9.

Biswas, S. K., & Mantovani, A. (2010). Macrophage plasticity and interaction with lymphocyte subsets: cancer as a paradigm. *Nat Immunol, 11*(10), 889-896.

Bogorad, M. I., DeStefano, J., Karlsson, J., Wong, A. D., Gerecht, S., & Searson, P. C. (2015). Review: in vitro microvessel models. *Lab Chip, 15*(22), 4242-4255.

Bracci, L., Schiavoni, G., Sistigu, A., & Belardelli, F. (2014). Immune-based mechanisms of cytotoxic chemotherapy: implications for the design of novel and rationale-based combined treatments against cancer. *Cell death and differentiation, 21*(1), 15-25.

Bray, F., Ferlay, J., Soerjomataram, I., Siegel, R. L., Torre, L. A., & Jemal, A. (2018). Global cancer statistics 2018: GLOBOCAN estimates of incidence and mortality worldwide for 36 cancers in 185 countries. *CA Cancer Journal for Clinicians, 68*(6), 394-424.

Breitenbach, M., & Hoffmann, J. (2018). Editorial: Cancer Models. *Frontiers in oncology, 8*, 401-401.

Broaders, K. E., Cohen, J. A., Beaudette, T. T., Bachelder, E. M., & Fréchet, J. M. (2009). Acetalated dextran is a chemically and biologically tunable material for particulate immunotherapy. *Proceedings of the National Academy of Sciences, 106*(14), 5497-5502.

Broaders, K. E., Cohen, J. A., Beaudette, T. T., Bachelder, E. M., & Fréchet, J. M. J. (2009). Acetalated dextran is a chemically and biologically tunable material for particulate immunotherapy. *Proceedings of the National Academy of Sciences, 106*(14), 5497-5502.

Budhu, S., Wolchok, J., & Merghoub, T. (2014). The importance of animal models in tumor immunity and immunotherapy. *Curr Opin Genet Dev, 24*, 46-51.

Cai, X., Yin, Y., Li, N., Zhu, D., Zhang, J., Zhang, C. Y., & Zen, K. (2012). Re-polarization of tumor-associated macrophages to pro-inflammatory M1 macrophages by microRNA-155. *J Mol Cell Biol, 4*(5), 341-343.

Casting, Equilibrating and Seeding the 3D Petri Dish®. *microtissues® protocols.* Retrieved from http://ftp.microtissues.com/3DP/3dcellculture_protocols/Casting_Equilibrating_and_Seeding_the_3D_Petri_Dish.pdf

Cattin, S., Ramont, L., & Ruegg, C. (2018). Characterization and In Vivo Validation of a Three-Dimensional Multi-Cellular Culture Model to Study Heterotypic Interactions in Colorectal Cancer Cell Growth, Invasion and Metastasis. *Frontiers in bioengineering and biotechnology, 6*, 97.

Chen, G., & Emens, L. A. (2013). Chemoimmunotherapy: reengineering tumor immunity. *Cancer Immunol Immunother, 62*(2), 203-216.

Cheung, A., Bax, H. J., Josephs, D. H., Ilieva, K. M., Pellizzari, G., Opzoomer, J., . . . Karagiannis, S. N. (2016). Targeting folate receptor alpha for cancer treatment. *Oncotarget, 7*(32), 52553-52574.

Choi, K. Y., Min, K. H., Na, J. H., Choi, K., Kim, K., Park, J. H., . . . Jeong, S. Y. (2009). Self-assembled hyaluronic acid nanoparticles as a potential drug carrier for cancer therapy: synthesis, characterization, and in vivo biodistribution. *Journal of Materials Chemistry, 19*(24), 4102-4107.

Chua, P.-H., Neoh, K.-G., Kang, E.-T., & Wang, W. (2008). Surface functionalization of titanium with hyaluronic acid/chitosan polyelectrolyte multilayers and RGD for promoting osteoblast functions and inhibiting bacterial adhesion. *Biomaterials, 29*(10), 1412-1421.

Clayton, K. N., Salameh, J. W., Wereley, S. T., & Kinzer-Ursem, T. L. (2016). Physical characterization of nanoparticle size and surface modification using particle scattering diffusometry. *Biomicrofluidics, 10*(5), 054107-054107.

Cohen, J. L., Schubert, S., Wich, P. R., Cui, L., Cohen, J. A., Mynar, J. L., & Frechet, J. M. (2011). Acid-degradable cationic dextran particles for the delivery of siRNA therapeutics. *Bioconjug Chem, 22*(6), 1056-1065.

Coulie, P. G., Van den Eynde, B. J., van der Bruggen, P., & Boon, T. (2014). Tumour antigens recognized by T lymphocytes: at the core of cancer immunotherapy. *Nat Rev Cancer, 14*(2), 135-146.

Cox, M. C., Reese, L. M., Bickford, L. R., & Verbridge, S. S. (2015). Toward the Broad Adoption of 3D Tumor Models in the Cancer Drug Pipeline. *ACS Biomaterials Science & Engineering, 1*(10), 877-894.

Crotti, S., Piccoli, M., Rizzolio, F., Giordano, A., Nitti, D., & Agostini, M. (2017). Extracellular Matrix and Colorectal Cancer: How Surrounding Microenvironment Affects Cancer Cell Behavior? *Journal of Cellular Physiology, 232*(5), 967-975.

Danhier, F., Feron, O., & Préat, V. (2010). To exploit the tumor microenvironment: Passive and active tumor targeting of nanocarriers for anti-cancer drug delivery. *Journal of Controlled Release, 148*(2), 135-146.

Daniels, T. R., Delgado, T., Helguera, G., & Penichet, M. L. (2006). The transferrin receptor part II: targeted delivery of therapeutic agents into cancer cells. *Clin Immunol, 121*(2), 159-176.

Davis, M. E., Chen, Z., & Shin, D. M. (2008). Nanoparticle therapeutics: an emerging treatment modality for cancer. *Nature Reviews Drug Discovery, 7*, 771.

de Visser, K. E., Eichten, A., & Coussens, L. M. (2006). Paradoxical roles of the immune system during cancer development. *Nature Reviews Cancer, 6*(1), 24-37.

Desoize, B., Gimonet, D., & Jardiller, J. C. (1998). Cell culture as spheroids: an approach to multicellular resistance. *Anticancer research, 18*(6A), 4147-4158.

Devi, K. S. P., Mishra, D., Roy, B., Ghosh, S. K., & Maiti, T. K. (2015). Assessing the immunomodulatory role of heteroglycan in a tumor spheroid and macrophage co-culture model system. *Carbohydrate Polymers, 127*, 1-10.

Dolcetti, R., Viel, A., Doglioni, C., Russo, A., Guidoboni, M., Capozzi, E., . . . Boiocchi, M. (1999). High prevalence of activated intraepithelial cytotoxic T lymphocytes and increased

neoplastic cell apoptosis in colorectal carcinomas with microsatellite instability. *The American journal of pathology, 154*(6), 1805-1813.

Duluc, D., Corvaisier, M., Blanchard, S., Catala, L., Descamps, P., Gamelin, E., . . . Jeannin, P. (2009). Interferon-gamma reverses the immunosuppressive and protumoral properties and prevents the generation of human tumor-associated macrophages. *Int J Cancer, 125*(2), 367-373.

Dunn, G. P., Old, L. J., & Schreiber, R. D. (2004). The three Es of cancer immunoediting. *Annu Rev Immunol, 22*, 329-360.

Duval, K., Grover, H., Han, L.-H., Mou, Y., Pegoraro, A. F., Fredberg, J., & Chen, Z. (2017). Modeling Physiological Events in 2D vs. 3D Cell Culture. *Physiology, 32*(4), 266-277.

Edler, D., Glimelius, B., Hallström, M., Jakobsen, A., Johnston, P. G., Magnusson, I., . . . Blomgren, H. (2002). Thymidylate synthase expression in colorectal cancer: a prognostic and predictive marker of benefit from adjuvant fluorouracil-based chemotherapy. *Journal of Clinical Oncology, 20*(7), 1721-1728.

el-Deiry, W. S., Tokino, T., Velculescu, V. E., Levy, D. B., Parsons, R., Trent, J. M., . . . Vogelstein, B. (1993). WAF1, a potential mediator of p53 tumor suppression. *Cell, 75*(4), 817-825.

Elgert, K. D., Alleva, D. G., & Mullins, D. W. (1998). Tumor-induced immune dysfunction: the macrophage connection. *Journal of leukocyte biology, 64*(3), 275-290.

Emens, L. A. (2010). Chemoimmunotherapy. *Cancer J, 16*(4), 295-303.

Esparis-Ogando, A., Zurzolo, C., & Rodriguez-Boulan, E. (1994). Permeabilization of MDCK cells with cholesterol binding agents: Dependence on substratum and confluency. *American Journal of Physiology - Cell Physiology, 267*(1 36-1), C166-C176.

Fearon, E. R. (2011). Molecular genetics of colorectal cancer. *Annu Rev Pathol, 6*, 479-507.

Ferlay, J., Colombet, M., Soerjomataram, I., Mathers, C., Parkin, D. M., Pineros, M., . . . Bray, F. (2019). Estimating the global cancer incidence and mortality in 2018: GLOBOCAN sources and methods. *Int J Cancer, 144*(8), 1941-1953.

Fernandes, E., Ferreira, J. A., Andreia, P., Luís, L., Barroso, S., Sarmento, B., & Santos, L. L. (2015). New trends in guided nanotherapies for digestive cancers: A systematic review. *Journal of Controlled Release, 209*, 288-307.

Feron, O. (2009). Pyruvate into lactate and back: from the Warburg effect to symbiotic energy fuel exchange in cancer cells. *Radiother Oncol, 92*(3), 329-333.

Ferrara, N., Hillan, K. J., & Novotny, W. (2005). Bevacizumab (Avastin), a humanized anti-VEGF monoclonal antibody for cancer therapy. *Biochemical and Biophysical Research Communications, 333*(2), 328-335.

Ferreira, L. P., Gaspar, V. M., & Mano, J. F. (2018). Design of spherically structured 3D in vitro tumor models -Advances and prospects. *Acta Biomaterialia, 75*, 11-34.

Fidler, M. M., Soerjomataram, I., & Bray, F. (2016). A global view on cancer incidence and national levels of the human development index. *Int J Cancer, 139*(11), 2436-2446.

Fontana, F., Figueiredo, P., Bauleth-Ramos, T., Correia, A., & Santos, H. A. (2018). Immunostimulation and Immunosuppression: Nanotechnology on the Brink. *Small Methods, 2*(5), 1700347.

Fontana, F., Shahbazi, M. A., Liu, D., Zhang, H., Mäkilä, E., Salonen, J., . . . Santos, H. A. (2017). Multistaged nanovaccines based on porous silicon@ acetalated dextran@ cancer cell membrane for cancer immunotherapy. *Advanced Materials, 29*(7), 1603239.

Foroozandeh, P., & Aziz, A. A. (2018). Insight into Cellular Uptake and Intracellular Trafficking of Nanoparticles. *Nanoscale research letters, 13*(1), 339-339.

Franco, O. E., Shaw, A. K., Strand, D. W., & Hayward, S. W. (2010). Cancer associated fibroblasts in cancer pathogenesis. *Seminars in Cell & Developmental Biology, 21*(1), 33-39.

Friedrich, J., Seidel, C., Ebner, R., & Kunz-Schughart, L. A. (2009). Spheroid-based drug screen: considerations and practical approach. *Nat Protoc, 4*(3), 309-324.

Gevaert, M. (2013). Engineering 3D Tissue Systems to Better Mimic Human Biology (Vol. 42, pp. 48-55).

Goswami, K. K., Ghosh, T., Ghosh, S., Sarkar, M., Bose, A., & Baral, R. (2017). Tumor promoting role of anti-tumor macrophages in tumor microenvironment. *Cellular immunology, 316*, 1-10.

Goydos, J. S., Elder, E., Whiteside, T. L., Finn, O. J., & Lotze, M. T. (1996). A phase I trial of a synthetic mucin peptide vaccine. Induction of specific immune reactivity in patients with adenocarcinoma. *J Surg Res, 63*(1), 298-304.

Green, D. R., Galluzzi, L., & Kroemer, G. (2014). Cell biology. Metabolic control of cell death. *Science (New York, N.Y.), 345*(6203), 1250256-1250256.

Guo, X., Wu, Z., Li, W., Wang, Z., Li, Q., Kong, F., . . . You, J. (2016). Appropriate Size of Magnetic Nanoparticles for Various Bioapplications in Cancer Diagnostics and Therapy. *ACS Appl Mater Interfaces, 8*(5), 3092-3106.

Haenszel, W., & Kurihara, M. (1968). Studies of Japanese migrants. I. Mortality from cancer and other diseases among Japanese in the United States. *Journal of the National Cancer Institute, 40*(1), 43-68.

Haggar, F. A., & Boushey, R. P. (2009). Colorectal Cancer Epidemiology: Incidence, Mortality, Survival, and Risk Factors. *Clinics in Colon and Rectal Surgery, 22*(04), 191-197.

Hanahan, D., & Weinberg, R. A. (2000). The Hallmarks of Cancer. *Cell, 100*(1), 57-70.

Hanahan, D., & Weinberg, R. A. (2011). Hallmarks of cancer: the next generation. *Cell, 144*(5), 646-674.

Hirschhaeuser, F., Menne, H., Dittfeld, C., West, J., Mueller-Klieser, W., & Kunz-Schughart, L. A. (2010). Multicellular tumor spheroids: an underestimated tool is catching up again. *J Biotechnol, 148*(1), 3-15.

Horig, H., Lee, D. S., Conkright, W., Divito, J., Hasson, H., LaMare, M., . . . Kaufman, H. L. (2000). Phase I clinical trial of a recombinant canarypoxvirus (ALVAC) vaccine expressing human carcinoembryonic antigen and the B7.1 co-stimulatory molecule. *Cancer Immunol Immunother, 49*(9), 504-514.

Hull, L., Farrell, D., & Grodzinski, P. (2014). Highlights of recent developments and trends in cancer nanotechnology research—View from NCI Alliance for nanotechnology in cancer. *Biotechnology advances, 32*(4), 666-678.

Irvine, D. J., Hanson, M. C., Rakhra, K., & Tokatlian, T. (2015). Synthetic nanoparticles for vaccines and immunotherapy. *Chemical reviews, 115*(19), 11109-11146.

Jackson-Thompson, J., Ahmed, F., German, R. R., Lai, S. M., & Friedman, C. (2006). Descriptive epidemiology of colorectal cancer in the United States, 1998-2001. *Cancer, 107(5, Suppl)*, 1103-1111.

Janouskova, H., Ray, A.-M., Noulet, F., Lelong-Rebel, I., Choulier, L., Schaffner, F., . . . Dontenwill, M. (2013). Activation of p53 pathway by Nutlin-3a inhibits the expression of the therapeutic target α5 integrin in colon cancer cells. *Cancer letters, 336*(2), 307-318.

Janouskova, H., Ray, A. M., Noulet, F., Lelong-Rebel, I., Choulier, L., Schaffner, F., . . . Dontenwill, M. (2013). Activation of p53 pathway by Nutlin-3a inhibits the expression of the therapeutic target alpha5 integrin in colon cancer cells. *Cancer Lett, 336*(2), 307-318.

Janout, V., & Kollárová, H. (2001). EPIDEMIOLOGY OF COLORECTAL CANCER. *Biomedical papers, 145*(1), 5-10.

Jocham, D., Richter, A., Hoffmann, L., Iwig, K., Fahlenkamp, D., Zakrzewski, G., . . . von Wietersheim, J. (2004). Adjuvant autologous renal tumour cell vaccine and risk of tumour progression in patients with renal-cell carcinoma after radical nephrectomy: phase III, randomised controlled trial. *The Lancet, 363*(9409), 594-599.

Johnson, I. T., & Lund, E. K. (2007). Review article: nutrition, obesity and colorectal cancer. *Alimentary Pharmacology & Therapeutics, 26*(2), 161-181.

Jones, J. A., Avritscher, E. B., Cooksley, C. D., Michelet, M., Bekele, B. N., & Elting, L. S. (2006). Epidemiology of treatment-associated mucosal injury after treatment with newer regimens for lymphoma, breast, lung, or colorectal cancer. *Support Care Cancer, 14*(6), 505-515.

Justus, C. R., Leffler, N., Ruiz-Echevarria, M., & Yang, L. V. (2014). In vitro cell migration and invasion assays. *Journal of visualized experiments : JoVE*(88), 51046.

Kabbinavar, F., Hurwitz, H. I., Fehrenbacher, L., Meropol, N. J., Novotny, W. F., Lieberman, G., . . . Bergsland, E. (2003). Phase II, randomized trial comparing bevacizumab plus fluorouracil (FU)/leucovorin (LV) with FU/LV alone in patients with metastatic colorectal cancer. *Journal of Clinical Oncology, 21*(1), 60-65.

Kandoth, C., McLellan, M. D., Vandin, F., Ye, K., Niu, B., Lu, C., . . . Ding, L. (2013). Mutational landscape and significance across 12 major cancer types. *Nature, 502*(7471), 333-339.

Katt, M. E., Placone, A. L., Wong, A. D., Xu, Z. S., & Searson, P. C. (2016). In Vitro Tumor Models: Advantages, Disadvantages, Variables, and Selecting the Right Platform. *Frontiers in bioengineering and biotechnology, 4*, 12-12.

Kline, C. L. B., Schiccitano, A., Zhu, J., Beachler, C., Sheikh, H., Harvey, H. A., . . . El-Deiry, W. S. (2014). Personalized Dosing via Pharmacokinetic Monitoring of 5-Fluorouracil Might Reduce Toxicity in Early- or Late-Stage Colorectal Cancer Patients Treated With Infusional 5–Fluorouracil-Based Chemotherapy Regimens. *Clinical Colorectal Cancer, 13*(2), 119-126.

Koido, S., Ohkusa, T., Homma, S., Namiki, Y., Takakura, K., Saito, K., . . . Tajiri, H. (2013). Immunotherapy for colorectal cancer. *World journal of gastroenterology, 19*(46), 8531-8542.

Komiya, Y., & Habas, R. (2008). Wnt signal transduction pathways. *Organogenesis, 4*(2), 68-75.

Konstantopoulos, K., Wu, P.-H., & Wirtz, D. (2013). Dimensional control of cancer cell migration. *Biophysical journal, 104*(2), 279.

Langer, R. (1998). Drug delivery and targeting. *Nature, 392*(6679 Suppl), 5-10.

Larocca, C., & Schlom, J. (2011). Viral vector-based therapeutic cancer vaccines. *Cancer J, 17*(5), 359-371.

Lazzari, G., Nicolas, V., Matsusaki, M., Akashi, M., Couvreur, P., & Mura, S. (2018). Multicellular spheroid based on a triple co-culture: A novel 3D model to mimic pancreatic tumor complexity. *Acta Biomater, 78*, 296-307. doi:10.1016/j.actbio.2018.08.008

Lenz, H.-J. (2007). Cetuximab in the management of colorectal cancer. *Biologics : targets & therapy, 1*(2), 77-91.

Levine, A. J. (1997). p53, the Cellular Gatekeeper for Growth and Division. *Cell, 88*(3), 323-331.

Levine, A. J., & Oren, M. (2009). The first 30 years of p53: growing ever more complex. *Nat Rev Cancer, 9*(10), 749-758.

Lewis, C. E., & Pollard, J. W. (2006). Distinct Role of Macrophages in Different Tumor Microenvironments. *Cancer Research, 66*(2), 605.

Li, W. A., & Mooney, D. J. (2013). Materials based tumor immunotherapy vaccines. *Current Opinion in Immunology, 25*(2), 238-245.

Li, X.-L., Zhou, J., Chen, Z.-R., & Chng, W.-J. (2015a). P53 mutations in colorectal cancer-molecular pathogenesis and pharmacological reactivation. *World journal of gastroenterology: WJG, 21*(1), 84.

Li, X.-L., Zhou, J., Chen, Z.-R., & Chng, W.-J. (2015b). P53 mutations in colorectal cancer - molecular pathogenesis and pharmacological reactivation. *World journal of gastroenterology, 21*(1), 84-93.

Liu, W., Li, L., Wang, X., Ren, L., Wang, X., Wang, J., . . . Wang, J. (2010). An integrated microfluidic system for studying cell-microenvironmental interactions versatilely and dynamically. *Lab Chip, 10*(13), 1717-1724.

Lopez, I., L, P. O., Tucci, P., Alvarez-Valin, F., R, A. C., & Marin, M. (2012). Different mutation profiles associated to P53 accumulation in colorectal cancer. *Gene, 499*(1), 81-87.

Lu, P., Weaver, V. M., & Werb, Z. (2012). The extracellular matrix: A dynamic niche in cancer progression. *The Journal of Cell Biology, 196*(4), 395-406.

Lurje, G., & Lenz, H. J. (2009). EGFR signaling and drug discovery. *Oncology, 77*(6), 400-410.

Maeda, H., Wu, J., Sawa, T., Matsumura, Y., & Hori, K. (2000). Tumor vascular permeability and the EPR effect in macromolecular therapeutics: a review. *J Control Release, 65*(1-2), 271-284.

Maishi, N., & Hida, K. (2017). Tumor endothelial cells accelerate tumor metastasis. *Cancer Science, 108*(10), 1921-1926.

Mann, B., Gelos, M., Siedow, A., Hanski, M. L., Gratchev, A., Ilyas, M., . . . Hanski, C. (1999). Target genes of beta-catenin-T cell-factor/lymphoid-enhancer-factor signaling in human colorectal carcinomas. *Proc Natl Acad Sci U S A, 96*(4), 1603-1608.

Mantovani, A., Sozzani, S., Locati, M., Allavena, P., & Sica, A. (2002). Macrophage polarization: tumor-associated macrophages as a paradigm for polarized M2 mononuclear phagocytes. *Trends in immunology, 23*(11), 549-555.

Matos, A. I., Carreira, B., Peres, C., Moura, L. I. F., Conniot, J., Fourniols, T., . . . Florindo, H. F. (2019). Nanotechnology is an important strategy for combinational innovative chemo-immunotherapies against colorectal cancer. *J Control Release, 307*, 108-138.

Mattheolabakis, G., Milane, L., Singh, A., & Amiji, M. M. (2015). Hyaluronic acid targeting of CD44 for cancer therapy: from receptor biology to nanomedicine. *Journal of Drug Targeting, 23*(7-8), 605-618.

Maule, M., & Merletti, F. (2012). Cancer transition and priorities for cancer control. *Lancet Oncol, 13*(8), 745-746.

Meyerhardt, J. A., & Mayer, R. J. (2005). Systemic Therapy for Colorectal Cancer. *New England Journal of Medicine, 352*(5), 476-487.

Mikhail, A. S., Eetezadi, S., & Allen, C. (2013). Multicellular tumor spheroids for evaluation of cytotoxicity and tumor growth inhibitory effects of nanomedicines in vitro: a comparison of docetaxel-loaded block copolymer micelles and Taxotere®. *PLoS One, 8*(4), e62630.

Morse, M. A., Deng, Y., Coleman, D., Hull, S., Kitrell-Fisher, E., Nair, S., . . . Lyerly, H. K. (1999). A Phase I study of active immunotherapy with carcinoembryonic antigen peptide (CAP-1)-pulsed, autologous human cultured dendritic cells in patients with metastatic malignancies expressing carcinoembryonic antigen. *Clin Cancer Res, 5*(6), 1331-1338.

Morson, B. (1974). President's address. The polyp-cancer sequence in the large bowel. *Proceedings of the Royal Society of Medicine, 67*(6 Pt 1), 451-457.

Nazemalhosseini Mojarad, E., Kuppen, P. J., Aghdaei, H. A., & Zali, M. R. (2013). The CpG island methylator phenotype (CIMP) in colorectal cancer. *Gastroenterology and hepatology from bed to bench, 6*(3), 120-128.

Necas, J., Bartosikova, L., Brauner, P., & Kolář, J. (2008). Hyaluronic acid (Hyaluronan): A review. *Veterinarni Medicina, 53*.

Nguyen-Ngoc, K.-V., Cheung, K. J., Brenot, A., Shamir, E. R., Gray, R. S., Hines, W. C., . . . Ewald, A. J. (2012). ECM microenvironment regulates collective migration and local dissemination in normal and malignant mammary epithelium. *Proceedings of the National Academy of Sciences, 109*(39), E2595-E2604.

Noy, R., & Pollard, Jeffrey W. (2014). Tumor-Associated Macrophages: From Mechanisms to Therapy. *Immunity, 41*(1), 49-61.

Nyga, A., Cheema, U., & Loizidou, M. (2011). 3D tumour models: novel in vitro approaches to cancer studies. *Journal of Cell Communication and Signaling, 5*(3), 239.

O'Sullivan, T., Saddawi-Konefka, R., Vermi, W., Koebel, C. M., Arthur, C., White, J. M., . . . Bui, J. D. (2012). Cancer immunoediting by the innate immune system in the absence of adaptive immunity. *The Journal of experimental medicine, 209*(10), 1869-1882.

Okuno, K., Sugiura, F., Hida, J. I., Tokoro, T., Ishimaru, E., Sukegawa, Y., & Ueda, K. (2011). Phase I clinical trial of a novel peptide vaccine in combination with UFT/LV for metastatic colorectal cancer. *Exp Ther Med, 2*(1), 73-79.

Oliveira, M. I., Santos, S. G., Oliveira, M. J., Torres, A. L., & Barbosa, M. A. (2012). Chitosan drives anti-inflammatory macrophage polarisation and pro-inflammatory dendritic cell stimulation. *Eur Cell Mater, 24*, 136-152; discussion 152-133.

OMRAN, A. R. (2005). The Epidemiologic Transition: A Theory of the Epidemiology of Population Change. *The Milbank Quarterly, 83*(4), 731-757.

Östman, A., & Augsten, M. (2009). Cancer-associated fibroblasts and tumor growth – bystanders turning into key players. *Current Opinion in Genetics & Development, 19*(1), 67-73.

Parayath, N. N., Parikh, A., & Amiji, M. M. (2018). Repolarization of Tumor-Associated Macrophages in a Genetically Engineered Nonsmall Cell Lung Cancer Model by Intraperitoneal Administration of Hyaluronic Acid-Based Nanoparticles Encapsulating MicroRNA-125b. *Nano Lett, 18*(6), 3571-3579.

Park, S., Park, H., Jeong, S., Yi, B. G., Park, K., & Key, J. (2019). Hyaluronic Acid-Conjugated Mesoporous Silica Nanoparticles Loaded with Dual Anticancer Agents for Chemophotodynamic Cancer Therapy. *Journal of Nanomaterials, 2019*, 11.

Passardi, A., Nanni, O., Tassinari, D., Turci, D., Cavanna, L., Fontana, A., . . . Amadori, D. (2015). Effectiveness of bevacizumab added to standard chemotherapy in metastatic colorectal cancer: final results for first-line treatment from the ITACa randomized clinical trial. *Ann Oncol, 26*(6), 1201-1207.

Peer, D., Karp, J. M., Hong, S., Farokhzad, O. C., Margalit, R., & Langer, R. (2007). Nanocarriers as an emerging platform for cancer therapy. *Nature Nanotechnology, 2*, 751.

Perche, F., Patel, N. R., & Torchilin, V. P. (2012). Accumulation and toxicity of antibody-targeted doxorubicin-loaded PEG-PE micelles in ovarian cancer cell spheroid model. *J Control Release, 164*(1), 95-102.

Petty, A. J., & Yang, Y. (2017). Tumor-associated macrophages: implications in cancer immunotherapy. *Immunotherapy, 9*(3), 289-302.

Pino, M. S., & Chung, D. C. (2010). The chromosomal instability pathway in colon cancer. *Gastroenterology, 138*(6), 2059-2072.

Porru, M., Pompili, L., Caruso, C., Biroccio, A., & Leonetti, C. (2018). Targeting KRAS in metastatic colorectal cancer: current strategies and emerging opportunities. *Journal of experimental & clinical cancer research : CR, 37*(1), 57-57.

Prabha, S., Zhou, W.-Z., Panyam, J., & Labhasetwar, V. (2002). Size-dependency of nanoparticle-mediated gene transfection: studies with fractionated nanoparticles. *International Journal of Pharmaceutics, 244*(1), 105-115.

Prabst, K., Engelhardt, H., Ringgeler, S., & Hubner, H. (2017). Basic Colorimetric Proliferation Assays: MTT, WST, and Resazurin. *Methods Mol Biol, 1601*, 1-17.

Präbst, K., Engelhardt, H., Ringgeler, S., Hübner, H. (2017). *Basic Colorimetric Proliferation Assays: MTT, WST, and Resazurin* (Vol. 1601).

Reya, T., Morrison, S. J., Clarke, M. F., & Weissman, I. L. (2001). Stem cells, cancer, and cancer stem cells. *Nature, 414*(6859), 105-111.

Rezvantalab, S., Drude, N. I., Moraveji, M. K., Güvener, N., Koons, E. K., Shi, Y., . . . Kiessling, F. (2018). PLGA-Based Nanoparticles in Cancer Treatment. *Frontiers in Pharmacology, 9*(1260).

Robert, C., Wilson, C. S., Venuta, A., Ferrari, M., & Arreto, C. D. (2017). Evolution of the scientific literature on drug delivery: A 1974-2015 bibliometric study. *J Control Release, 260*, 226-233.

Saha, M. N., Qiu, L., & Chang, H. (2013). Targeting p53 by small molecules in hematological malignancies. *Journal of hematology & oncology, 6*, 23-23.

Salis, A., Fanti, M., Medda, L., Nairi, V., Cugia, F., Piludu, M., . . . Monduzzi, M. (2016). Mesoporous Silica Nanoparticles Functionalized with Hyaluronic Acid and Chitosan Biopolymers. Effect of Functionalization on Cell Internalization. *ACS Biomaterials Science & Engineering, 2*(5), 741-751.

Salonga, D., Danenberg, K. D., Johnson, M., Metzger, R., Groshen, S., Tsao-Wei, D. D., . . . Diasio, R. B. (2000). Colorectal tumors responding to 5-fluorouracil have low gene expression levels of dihydropyrimidine dehydrogenase, thymidylate synthase, and thymidine phosphorylase. *Clinical Cancer Research, 6*(4), 1322-1327.

Schuster, M., Nechansky, A., & Kircheis, R. (2006). Cancer immunotherapy. *Biotechnology Journal, 1*(2), 138-147.

Senft, D., Leiserson, M. D. M., Ruppin, E., & Ronai, Z. e. A. (2017). Precision Oncology: The Road Ahead. *Trends in Molecular Medicine, 23*(10), 874-898.

Senturk, E., & Manfredi, J. J. (2012). Mdm2 and tumorigenesis: evolving theories and unsolved mysteries. *Genes & cancer, 3*(3-4), 192-198.

Sharma, M. (2019). Chapter 18 - Transdermal and Intravenous Nano Drug Delivery Systems: Present and Future. In S. S. Mohapatra, S. Ranjan, N. Dasgupta, R. K. Mishra, & S. Thomas (Eds.), *Applications of Targeted Nano Drugs and Delivery Systems* (pp. 499-550): Elsevier.

Sica, A., Larghi, P., Mancino, A., Rubino, L., Porta, C., Totaro, M. G., . . . Mantovani, A. (2008). Macrophage polarization in tumour progression. *Semin Cancer Biol, 18*(5), 349-355.

Siegel, R. L., Miller, K. D., & Jemal, A. (2018). Cancer statistics, 2018. *CA: A Cancer Journal for Clinicians, 68*(1), 7-30.

Singh, Y., Pawar, V. K., Meher, J. G., Raval, K., Kumar, A., Shrivastava, R., . . . Chourasia, M. K. (2017). Targeting tumor associated macrophages (TAMs) via nanocarriers. *J Control Release, 254*, 92-106.

Sousa, F., Cruz, A., Pinto, I. M., & Sarmento, B. (2018). Nanoparticles provide long-term stability of bevacizumab preserving its antiangiogenic activity. *Acta Biomaterialia, 78*, 285-295.

Susanti, S., Raposo, T., Arsalan, A., Tchoryk, A., Martinez-Pomares, L., Grabowska, A., & Ilyas, M. (2018). PO-304 Three-dimensional co-culture of colorectal cancer spheroid with cancer-associated fibroblast as a model to study immune cell modulation. *ESMO Open, 3*(Suppl 2), A347-A347.

Tang, A. S., Chikhale, P. J., Shah, P. K., & Borchardt, R. T. (1993). Utilization of a Human Intestinal Epithelial Cell Culture System (Caco-2) for Evaluating Cytoprotective Agents. *Pharmaceutical Research: An Official Journal of the American Association of Pharmaceutical Scientists, 10*(11), 1620-1626.

Tariq, K., & Ghias, K. (2016). Colorectal cancer carcinogenesis: a review of mechanisms. *Cancer biology & medicine, 13*(1), 120.

Teodoro, J. G., Evans, S. K., & Green, M. R. (2007). Inhibition of tumor angiogenesis by p53: a new role for the guardian of the genome. *J Mol Med (Berl), 85*(11), 1175-1186.

Toshiyuki, M., & Reed, J. C. (1995). Tumor suppressor p53 is a direct transcriptional activator of the human bax gene. *Cell, 80*(2), 293-299.

Vassilev, L. T., Vu, B. T., Graves, B., Carvajal, D., Podlaski, F., Filipovic, Z., . . . Liu, E. A. (2004). In vivo activation of the p53 pathway by small-molecule antagonists of MDM2. *Science (New York, N.Y.), 303*(5659), 844-848.

Ventura, A., Kirsch, D. G., McLaughlin, M. E., Tuveson, D. A., Grimm, J., Lintault, L., . . . Jacks, T. (2007). Restoration of p53 function leads to tumour regression in vivo. *Nature, 445*(7128), 661-665.

Vinothini, K., & Rajan, M. (2019). Chapter 9 - Mechanism for the Nano-Based Drug Delivery System. In S. S. Mohapatra, S. Ranjan, N. Dasgupta, R. K. Mishra, & S. Thomas (Eds.), *Characterization and Biology of Nanomaterials for Drug Delivery* (pp. 219-263): Elsevier.

Virgone-Carlotta, A., Lemasson, M., Mertani, H. C., Diaz, J. J., Monnier, S., Dehoux, T., . . . Rieu, J. P. (2017). In-depth phenotypic characterization of multicellular tumor spheroids: Effects of 5-Fluorouracil. *PLoS One, 12*(11), e0188100.

Vogelstein, B., & Kinzler, K. W. (2004). Cancer genes and the pathways they control. *Nature Medicine, 10*(8), 789-799.

Vogelstein, B., Lane, D., & Levine, A. J. (2000). Surfing the p53 network. *Nature, 408*(6810), 307-310.

Walker, C., Mojares, E., & Del Río Hernández, A. (2018). Role of Extracellular Matrix in Development and Cancer Progression. *International Journal of Molecular Sciences, 19*(10), 3028.

Walsh, E., Ueda, Y., Nakanishi, H., & Yoshida, K. (1992). Neuronal survival and neurite extension supported by astrocytes co-cultured in transwells. *Neuroscience Letters, 138*(1), 103-106.

Wang, M., Zhao, J., Zhang, L., Wei, F., Lian, Y., Wu, Y., . . . Guo, C. (2017). Role of tumor microenvironment in tumorigenesis. *Journal of Cancer, 8*(5), 761-773.

Wang, Q., Cheng, F., Ma, T. T., Xiong, H. Y., Li, Z. W., Xie, C. L., . . . Tu, Z. G. (2016). Interleukin-12 inhibits the hepatocellular carcinoma growth by inducing macrophage polarization to the M1-like phenotype through downregulation of Stat-3. *Mol Cell Biochem, 415*(1-2), 157-168.

Wang, Z., Tian, Y., Zhang, H., Qin, Y., Li, D., Gan, L., & Wu, F. (2016). Using hyaluronic acid-functionalized pH stimuli-responsive mesoporous silica nanoparticles for targeted delivery to CD44-overexpressing cancer cells. *Int J Nanomedicine, 11*, 6485-6497.

Wculek, S. K., Cueto, F. J., Mujal, A. M., Melero, I., Krummel, M. F., & Sancho, D. (2019). Dendritic cells in cancer immunology and immunotherapy. *Nature Reviews Immunology*.

Wei, E. K., Ma, J., Pollak, M. N., Rifai, N., Fuchs, C. S., Hankinson, S. E., & Giovannucci, E. (2005). A prospective study of C-peptide, insulin-like growth factor-I, insulin-like growth factor binding protein-1, and the risk of colorectal cancer in women. *Cancer Epidemiol Biomarkers Prev, 14*(4), 850-855.

Willett, W. C., Stampfer, M. J., Colditz, G. A., Rosner, B. A., & Speizer, F. E. (1990). Relation of Meat, Fat, and Fiber Intake to the Risk of Colon Cancer in a Prospective Study among Women. *New England Journal of Medicine, 323*(24), 1664-1672.

Wirtz, D., Konstantopoulos, K., & Searson, P. C. (2011). The physics of cancer: the role of physical interactions and mechanical forces in metastasis. *Nature Reviews Cancer, 11*(7), 512.

Xiang, B., Snook, A. E., Magee, M. S., & Waldman, S. A. (2013). Colorectal cancer immunotherapy. *Discovery medicine, 15*(84), 301-308.

Zhang, W., Xu, W., Lan, Y., He, X., Liu, K., & Liang, Y. (2019). Antitumor effect of hyaluronic-acid-modified chitosan nanoparticles loaded with siRNA for targeted therapy for non-small cell lung cancer. *Int J Nanomedicine, 14*, 5287-5301.

Zheng, X., Turkowski, K., Mora, J., Brune, B., Seeger, W., Weigert, A., & Savai, R. (2017). Redirecting tumor-associated macrophages to become tumoricidal effectors as a novel strategy for cancer therapy. *Oncotarget, 8*(29), 48436-48452.

Zheng, X., Turkowski, K., Mora, J., Brüne, B., Seeger, W., Weigert, A., & Savai, R. (2017). Redirecting tumor-associated macrophages to become tumoricidal effectors as a novel strategy for cancer therapy. *Oncotarget, 8*(29), 48436.

Zhong, X., Chen, B., & Yang, Z. (2018). The role of tumor-associated macrophages in colorectal carcinoma progression. *Cellular Physiology and Biochemistry, 45*(1), 356-365.

Zietarska, M., Maugard, C. M., Filali-Mouhim, A., Alam-Fahmy, M., Tonin, P. N., Provencher, D. M., & Mes-Masson, A. M. (2007). Molecular description of a 3D in vitro model for the study of epithelial ovarian cancer (EOC). *Mol Carcinog, 46*(10), 872-885.

Zitvogel, L., Kepp, O., Senovilla, L., Menger, L., Chaput, N., & Kroemer, G. (2010). Immunogenic tumor cell death for optimal anticancer therapy: the calreticulin exposure pathway. *Clin Cancer Res, 16*(12), 3100-3104.

Zugazagoitia, J., Guedes, C., Ponce, S., Ferrer, I., Molina-Pinelo, S., & Paz-Ares, L. (2016). Current Challenges in Cancer Treatment. *Clinical Therapeutics, 38*(7), 1551-1566.